Distribution Agreement

In presenting this dissertation as a partial fulfillment of the requirements for an advanced degree from Emory University, I hereby grant to Emory University and its agents the non-exclusive license to archive, make accessible, and display my dissertation in whole or in part in all forms of media, now or hereafter known, including display on the world wide web. I understand that I may select some access restrictions as part of the online submission of this dissertation. I retain all ownership rights to the copyright of the dissertation. I also retain the right to use in future works (such as articles or books) all or part of this dissertation.

Signature:

_____ _____

Jonathan Joseph Havel Date

PRAS40 and mTOR Signaling: A Paradigm for Crosstalk Among Proliferation, Growth, and Stress Signaling

By

Jonathan Joseph Havel
Doctor of Philosophy

Graduate Division of Biological and Biomedical Sciences
Molecular and Systems Pharmacology

_____
Haian Fu, Ph.D.
Advisor

_____
Kathy Griendling, Ph.D.
Committee Member

_____
John Hepler, Ph.D.
Committee Member

_____
Edward Morgan, Ph.D.
Committee Member

Accepted:

_____
Lisa A. Tedesco, Ph.D.
Dean of the James T. Laney School of Graduate Studies

_____
Date

PRAS40 and mTOR Signaling: A Paradigm for Crosstalk Among Proliferation, Growth, and Stress Signaling

By

Jonathan Joseph Havel
B.S., Lehigh University, 2005

Advisor: Haian Fu, Ph.D.

An ***abstract*** of
A dissertation submitted to the Faculty of the
James T. Laney School of Graduate Studies of Emory University
in partial fulfillment of the requirements for the degree of
Doctor of Philosophy

Graduate Division of Biological and Biomedical Sciences
Molecular and Systems Pharmacology

2013

Abstract

PRAS40 and mTOR Signaling: A Paradigm for Crosstalk Among Proliferation, Growth, and Stress Signaling

By Jonathan Joseph Havel

The Proline-Rich Akt Substrate of 40 kDA (PRAS40) has recently been identified as a binding partner and inhibitor of the mechanistic Target of Rapamycin Complex 1 (mTORC1), a growth factor- and nutrient-sensitive kinase whose activity promotes protein synthesis and cell growth. Despite its inhibitory effect on mTORC1, PRAS40 has been shown to promote cell survival in rodent models of spinal cord injury and tumorigenesis. PRAS40 levels have also been found to correlate with poor prognosis in lung cancer patients, an effect not readily explained by mTORC1 inhibition. Here we demonstrate that in addition to its known cytoplasmic role in inhibiting mTORC1, PRAS40 dynamically shuttles to the nucleus, where it exists in a high-molecular weight complex void of mTORC1 components. Mass spectrometry and immunoprecipitation analyses identify ribosomal protein L11 (RPL11) as a nuclear-specific PRAS40-associated protein. This association is dependent upon both mTORC1- and Akt-mediated phosphorylation of PRAS40 residues S221 and T246, respectively. In addition to its canonical role as a member of the ribosome, RPL11 is known to stabilize the tumor suppressor p53 in response to nucleolar stress by binding and inhibiting the p53-directed E3 ubiquitin ligase HDM2. Interestingly, knock-down (KD) of PRAS40 induces p53 protein stabilization and transcriptional activation in an RPL11-dependent manner. As demonstrated by increased senescence-associated beta-galactosidase activity, PRAS40 KD also induces cellular senescence in a p53-dependent manner. In summary, PRAS40 is identified as a novel effector of Akt and mTORC1 signaling that regulates the RPL11-HDM2-p53 nucleolar stress response pathway to suppress the induction of cellular senescence. These findings may help to explain the pro-tumorigenic effects of PRAS40 and identify the PRAS40- and RPL11-containing complex as a promising target for p53-restorative anti-cancer drug discovery.

PRAS40 and mTOR Signaling: A Paradigm for Crosstalk Among Proliferation, Growth, and Stress Signaling

By

Jonathan Joseph Havel
B.S., Lehigh University, 2005

Advisor: Haian Fu, Ph.D.

A ***dissertation*** submitted to the Faculty of the
James T. Laney School of Graduate Studies of Emory University
in partial fulfillment of the requirements for the degree of
Doctor of Philosophy

Graduate Division of Biological and Biomedical Sciences
Molecular and Systems Pharmacology

2013

ACKNOWLEDGEMENTS

I would like to thank my advisor, Haian Fu, for his unwavering dedication to graduate training. He is an exemplary academic in every sense of the word – a brilliant scientist, a caring mentor, and an active contributor of service to the scientific community. I thank him especially for his remarkable patience in allowing me to develop the projects described herein. My growth as an independent scientist has been bolstered exponentially by Haian's eagerness and keen ability to discern the specific and unique needs of every student. The end products of Haian's devotion to training are confidence and critical thought. For these, I will always be grateful. I also thank Yuhong Du for selflessly sharing her time and extensive expertise whenever assistance was needed. I also thank my committee members for their invaluable scientific input and also for their kind words of support and encouragement. I am grateful to my parents and grandparents for instilling a lifelong love of learning in me and for teaching me the value of persistence. I especially thank my grandfather, "Dedo," who sparked my interest in science in the first place. Finally, I am grateful to my wife, Lauren, for believing in me more than I believed in myself, for making challenges bearable, for making joys brighter, and for making everything worthwhile.

TABLE OF CONTENTS

FIGURES AND TABLES

CHAPTER 1

General Introduction

1.1 Overview of Signaling Crosstalk and Scope of Dissertation

In order to maintain homeostasis, cells must properly integrate and respond to a variety of stimuli including growth factors, nutrient levels, and environmental stress cues. The intracellular signaling pathways that respond to these stimuli must be tightly regulated and able to communicate with one another to ensure the execution of appropriate cellular responses. In humans, failure of these molecular pathways to coordinate with one another and properly respond to dynamic environmental conditions at the nanoscale level can result in devastating macroscopic consequences such as cancer, neurodegeneration, and diabetes. Therefore, it is critical to understand the molecular mechanisms through which established cellular signaling pathways interact. Intracellular signal transduction mechanisms are predicated upon the ability of biomolecules to interact and affect one another as governed by their physical and chemical properties. In this dissertation I highlight the importance of protein-protein interactions in signal transduction through a detailed examination of signaling governed by the Proline-Rich Akt Substrate of 40 kDa (PRAS40). Naturally, the ability to study protein-protein interactions in a meaningful way depends on the availability of appropriate technology and reagents. As such, I also describe the development of a novel technology combining the protein-fragment complementation assay (PCA) and bioluminescence resonance energy transfer (BRET) for the study of ternary protein complex dynamics in living cells. Additionally, I describe the design of a time-resolved fluorescence resonance energy transfer (TR-FRET) assay for the discovery of small molecule protein-protein interaction probes by high-throughput screening. Taken together, these studies reveal novel insights into the signaling function of PRAS40, identify the nuclear PRAS40- and RPL11-

containing complex as a potential target for disease therapy, and provide new methodology for the continued study of protein-protein interactions in health and disease.

1.2 Proliferation and Survival Signaling – The PI3K-Akt Pathway

Under homeostatic or pro-proliferative conditions, cells must coordinate growth and proliferation with the inhibition of pro-apoptotic programs. The phosphoinositide 3-kinase (PI3K)-Akt signaling axis is a prominent mechanism responsible for relaying extracellular survival and growth factor signals to a cell's apoptotic and proliferation machinery (1-3).

When growth factors such as insulin-like growth factor-1 (IGF-1), platelet-derived growth factor (PDGF), epidermal growth factor (EGF), or nerve growth factor (NGF) bind their respective transmembrane tyrosine kinase cell-surface receptors, this triggers dimerization of two receptor subunits and subsequent intermolecular autophosphorylation of tyrosine residues in the intracellular domains of the receptor subunits. These phosphorylated tyrosine residues serve as docking sites for Src Homology 2 (SH2)-domain-containing adaptor proteins such as insulin receptor substrate-1 (IRS-1) or growth factor receptor-bound protein 2 (GRB2), which subsequently recruit PI3K to the plasma membrane where it is activated either directly by IRS-1 or through interaction with active Ras. Membrane-docked and activated PI3K catalyzes transfer of a gamma-phosphate of ATP to a 3' hydroxyl of plasma membrane-incorporated phosphatidylinositol-4,5-bisphosphate (PIP2) to generate phosphatidylinositol-3,4,5-trisphosphate (PIP3). PIP3 serves as a docking site for the Pleckstrin Homology (PH) domain of the serine/threonine protein kinase Akt. Once

recruited to the plasma membrane, Akt is phosphorylated at T308, located in the activation loop of Akt's kinase domain, by another membrane-localized PH domain-containing kinase, 3-phosphoinositide dependent protein kinase-1 (PDK-1). T308 phosphorylation results in activation of Akt, enabling it to phosphorylate downstream effectors and thereby relay growth and survival signals to the cell's core regulatory machinery (**Figure 1-1**) (1; 2; 4).

In response to growth factor stimulation, Akt phosphorylates a wide array of substrates to promote and regulate survival, proliferation, growth, angiogenesis, metabolism, and migration (2). For the purposes of this dissertation, I will focus only on the roles of Akt in survival, proliferation, and growth signaling. Akt-mediated phosphorylation events can inhibit apoptotic cell death, i.e. promote survival, through inhibition of the core apoptotic machinery components, inhibition of pro-apoptotic transcription factors and kinases, or activation of anti-apoptotic transcriptional programs (1; 2). The first direct mechanistic link of Akt to apoptosis suppression came with the observation that growth factor-stimulated Akt phosphorylates and inhibits the pro-apoptotic protein BAD (5; 6). Under pro-apoptotic conditions BAD binds and inhibits the anti-apoptotic protein BCL-X_L, thus allowing BAX to dimerize and initiate apoptosis at the mitochondrial membrane by permitting cytochrome c release (7; 8). Growth factor stimulated Akt phosphorylates BAD at S136, inducing binding of the adaptor protein 14-3-3, which subsequently sequesters BAD away from BCL-X_L (9). This frees BCL-X_L to bind BAX, thereby inhibiting apoptosis (**Figure 1-1**) (10). Akt has also been shown to inhibit apoptosis downstream of the BCL family proteins via phosphorylation and catalytic inactivation of Caspase 9 (**Figure 1-1**) (11). In addition to intercepting the core

apoptotic machinery, Akt can also inhibit the function of pro-apoptotic transcription factors such as the FOXO family proteins and p53. As with BAD, Akt-mediated phosphorylation causes binding of FOXO proteins to 14-3-3, resulting in translocation of the FOXO transcription factors from the nucleus to the cytoplasm (1; 12; 13). This cytoplasmic sequestration effectively prevents induction of the pro-apoptotic transcription programs of the FOXO proteins (**Figure 1-1**) (1; 2). Conversely, Akt phosphorylation of the E3 ubiquitin ligase HDM2 induces its translocation from the cytoplasm to the nucleus, where it mediates the ubiquitination and subsequent proteasomal degradation of p53 (14; 15). This serves to prevent the induction of proapoptotic and anti-proliferative p53 targets such as BAX, PUMA, NOXA, and p21. Akt can also inhibit the pro-apoptotic kinase apoptosis signal-regulating kinase 1 (ASK1) via direct phosphorylation (16). Finally, in addition to inhibiting pro-apoptotic events, Akt activity can also stimulate the transcription of anti-apoptotic factors. Specifically, Akt can phosphorylate and activate IKKα (17), leading to NFκB-mediated transcription of anti-apoptotic proteins such as BCL-2 and the caspase inhibitors c-IAP1 and c-IAP2.

In addition to its integral role in cell survival, Akt is also a key mediator of proliferation. This is achieved via the phosphorylation of various cell cycle regulatory proteins. Specifically, Akt can phosphorylate the cyclin-dependent kinase inhibitors p27 and p21, resulting in their cytoplasmic sequestration and inactivation (18-22). Notably, Akt also controls p21 expression via inhibition of p53, as described above. While these events control cell cycle progression at the G1/S phase transition, Akt can also promote progression through the G2/M transition by phosphorylating the DNA damage checkpoint kinase Chk1, thereby causing its inhibition through cytoplasmic sequestration

(23-25). Thus, aberrant Akt hyperactivation is capable of overriding the Chk1-mediated DNA damage checkpoint, allowing proliferation to occur regardless of DNA integrity.

Akt is also a potent inducer of protein translation and cell growth. The mechanistic details of this Akt function will be discussed at length section 1.2 on mTOR signaling below.

The ability of Akt to override the DNA damage checkpoint hints at its oncogenic potential. Indeed, in addition to being discovered as a homolog of Protein Kinases A and C (26), Akt was simultaneously identified as the cellular component of the transforming oncogene generated by the AKT8 murine leukemia retrovirus (27; 28). Gene amplification of PI3K and Akt, as well as activating mutations of PI3K subunits have been identified in many human tumors (3). Furthermore, Akt activation has been shown to be a prognostic marker of poor patient survival (29; 30). However, the most compelling evidence for involvement of the PI3K-Akt pathway in tumorigenesis comes from loss-of-function studies of the PI3K negative regulator phosphatase and tensin homolog (PTEN). PTEN is a lipid phosphatase that dephosphorylates PIP3 to produce PIP2, thereby inhibiting the PI3K signaling cascade (3). PTEN loss occurs in many human cancers, and mice with a heterozygous PTEN deletion have a high incidence of spontaneously occurring tumors. Homozygous PTEN deletion is embryonic lethal (31-34). Considering these findings, the PI3K-Akt pathway is an attractive target for novel cancer therapeutics. Indeed, a number of PI3K or Akt-specific inhibitors have entered clinical trials (35). Notably, Perifosine, a lipid-based Akt inhibitor that prevents Akt translocation to the plasma membrane, has entered phase III clinical trials for colorectal cancer and multiple myeloma. In these studies, Perifosine is being used in combination

with other targeted therapies (35). Promising activity has been observed from Phase II studies of Perifosine in hematological malignancies, melanoma, renal cell carcinoma, non-small cell lung cancer, and hormone-sensitive prostate cancer. However, other Phase II trials in metastatic pancreatic cancer and melanoma showed no significant effect (35; 36). Original attempts to target PI3K clinically using wortmannin or LY294002 were unsuccessful due to poor solubility and high toxicity of the drugs (35; 36). More recently PX-866, a novel irreversible inhibitor of the p110 catalytic subunit of PI3K has undergone a Phase I clinical trial with promising results. The drug was well tolerated and resulted in stable disease in 22%, 53%, or 11% of patients with incurable cancers in the three arms of the study, respectively (37; 38). Taken together, the current body of knowledge concerning the PI3K-Akt pathway suggests that it is a critical mediator of oncogenesis. Further elucidation of its regulation and downstream effects will inform the rational design of improved targeted cancer therapeutics.

1.3 Growth Signaling – The mTOR Pathway

The mechanistic (previously referred to as mammalian) Target of Rapamycin (mTOR) is a large multi-functional atypical serine/threonine protein kinase that serves as a master-regulator of cell growth and proliferation. mTOR is a member of the PI3K-related kinase family and serves as the catalytic subunit of two distinct multi-protein complexes – mTOR Complex 1 (mTORC1) and Complex 2 (mTORC2). These two protein complexes are differentially sensitive to the macrolide small molecule rapamycin, have distinct protein substrates, and serve unique functions in cellular signaling (39-41). Most functions of mTORC1 are potently and acutely sensitive to inhibition by

rapamycin, whereas mTORC2 is largely insensitive to the drug; however, mTORC2 can be inhibited by long-term rapamycin exposure in a cell context-dependent manner. Importantly, rapamycin is an allosteric inhibitor of mTORC1. When rapamycin enters a cell it binds directly to the prolyl isomerase FKBP12. It is the rapamycin-FKBP12 complex that binds and inhibits mTORC1. Rapamycin-FKBP12 is not known to bind mTORC2; however, the precise molecular determinants of this selectivity are not fully understood (39-41).

mTORC1 is a pro-growth/pro-survival kinase that is responsive to nutrient and energy supply, growth factors, and oxygen levels. mTORC1 consists of mTOR, Raptor (the defining component of mTORC1), mLST8 (also known as GβL), Deptor, and PRAS40. Once activated, mTORC1 phosphorylates a handful of well-defined effector substrates to promote cap-dependent translation and cell growth, inhibit autophagy, and regulate metabolism (**Figure 1-2**) (39-41).

As noted above, mTORC1 is a nutrient-sensitive kinase that requires an ample supply of extracellular amino acids and glucose (i.e. energy or ATP) in order to become fully active. The mechanism of amino acid sensing by mTORC1 is not yet fully understood, but appears to involve "inside-out" signaling wherein lysosomal amino acid content is thought to parallel extracellular levels due to constant "sampling" by endocytotic vesicles that deliver their contents to lysosomes. In this model, it is thought that the vacuolar ATPase (v-ATPase) localized on lysosomal membranes communicates intra-lysosomal amino acid content to cytoplasmic signaling machinery (42). Through an unknown mechanism involving v-ATPase, amino acids activate the guanine nucleotide exchange factor (GEF) activity of a multiprotein complex on the surface of lysosomes

known as the Ragulator Complex (43). The Ragulator GEF activity causes GTP loading of the Rag GTPase proteins, which are tethered to the cytoplasmic side of the lysosomal membrane via the Ragulator Complex (43; 44). The GTP-loaded Rag proteins are then able to recruit mTORC1 to the lysosomal membrane via interaction with Raptor. Once localized at the lysosome membrane surface, mTORC1 is potently activated by Rheb, a small GTPase Ras homolog that is localized throughout the endomembrane system. However, Rheb is also subject to upstream regulation by glucose/energy and growth factors. Therefore, full activation of mTORC1 requires simultaneous abundance of amino acids, glucose, and growth factors (40; 41).

Glucose and energy sensing of mTORC1 is achieved through the AMP-activated protein kinase (AMPK) (45; 46). AMPK is a serine/threonine protein kinase that requires phosphorylation in the activation loop of its kinase domain to become active. This phosphorylation is achieved by the constitutively active upstream kinase LKB1; however, when the cellular ratio of ATP to AMP is high, AMPK is quickly de-phosphorylated by phosphatases. Under low energy conditions, when cellular AMP levels are high, AMP binds to AMPK and stabilizes it in its active, LKB1-phosphorylated state (47; 48). Once activated, AMPK impinges upon mTORC1 signaling through at least two separate mechanisms. AMPK can directly phosphorylate and activate the GTPase-activating protein (GAP) Tuberous Sclerosis Complex 2 (TSC2). This enables the TSC1/2 complex to directly inhibit the mTORC1-stimulatory function of Rheb (**Figure 1-2**) (45; 49). AMPK can also directly phosphorylate mTORC1 on Raptor, leading to 14-3-3 binding and subsequent inhibition of mTORC1 (46). Thus, mTORC1 activity is inhibited at multiple levels in response to energetic stress through the activity of AMPK.

Growth factor-induced stimulation of mTORC1 is achieved through at least two divergent pathways. The first and more widely studied mechanism involves the ability of Rheb to potently activate mTORC1 when bound to GTP. The mTORC1 stimulatory activity of Rheb is negatively regulated by the GAP complex TSC1/2. In response to growth factors, Akt phosphorylates and inhibits TSC2, thereby relieving inhibition of Rheb and allowing Rheb to activate mTORC1 (**Figure 1-2**) (39-41; 50). A second mechanism of growth factor-mediated mTORC1 regulation depends upon the Proline-Rich Akt Substrate of 40kDa (PRAS40). When in its non-phosphorylated form, PRAS40 binds mTORC1 through the mTORC1 component Raptor and is believed to inhibit mTORC1 kinase activity by competing for substrate binding. In response to growth factors, PRAS40 binds the scaffolding protein 14-3-3 in a phosphorylation-dependent manner and dissociates from Raptor, thereby allowing mTORC1 access to its downstream effector substrates (**Figure 1-2**) (51-56). Interestingly, both Akt- and mTORC1-mediated phosphorylation of PRAS40 are required for 14-3-3 binding and dissociation of PRAS40 from mTORC1 in response to growth factors (51; 55-57). The fate or function, if any, of mTORC1-dissociated, 14-3-3-bound phospho-PRAS40 remains unknown (**Figure 1-3**). Notably, when compared to their other known substrates, PRAS40 is a major target of both Akt and mTORC1 (2; 58-61). In fact, PRAS40 phosphorylation is used extensively as a biomarker for pre-clinical and clinical trials of PI3K-Akt and mTOR pathway inhibitors (62-68). Taken together, these findings place PRAS40 at a critical juncture of Akt and mTORC1 signaling, indicating that PRAS40 may play a key role in the intracellular integration of extracellular signaling cues (**Figure 1-3**).

The fact that mTORC1 is so tightly regulated by multiple signaling inputs is indicative of its critical functions in controlling cell growth and maintaining homeostasis. Activation of mTORC1 has three primary downstream effects – promotion of cap-dependent translation in support of cell growth and proliferation, inhibition of autophagy, and regulation of cellular metabolism (**Figure 1-2**). The best-characterized substrates of mTORC1 are $p70^{S6K1}$ and 4EBP. mTORC1 phosphorylation activates p70, which goes on to phosphorylate downstream substrates such as Ribosomal Protein S6 and elongation factor 2 kinase (eEF-2K), leading to increased translation. When in its non-phosphorylated state, 4EBP binds and sequesters the eIF-4E elongation initiation factor away from the eIF-4F cap-binding complex, thus preventing cap-dependent translation. Phosphorylation of 4EBP by mTORC1 relieves this inhibition, thereby allowing cap-dependent translation to proceed (39-41). The mechanism of mTORC1-mediated control of autophagy remains largely unknown; however, it is thought that mTORC1 activity inhibits autophagy at least in part through phosphorylation and inhibition of the kinase ULK1 (69; 70). Finally, mTORC1 can control cellular metabolism through various mechanisms, including upregulation of glycolytic enzymes through increased translation of their mRNAs and activation of the SREBP-1 transcription factor through $p70S^{6K1}$ to promote lipid and sterol biosynthesis (**Figure 1-2**) (39-41; 71).

Compared to mTORC1, relatively little is known about the regulation and function of mTORC2. mTORC2 consists of mTOR, Rictor (the defining component of mTORC2), mLST8 (also known as GβL), mSIN1, Deptor, and Protor. The main function ascribed to mTORC2 is that of phosphorylating the secondary activating site S473 in the hydrophobic domain of Akt (this function is sometimes referred to as "PDK-

2" activity). Thus, the mTOR kinase itself functions both downstream and upstream of Akt. Little is known about the upstream regulation of mTORC2 other than it is growth factor sensitive and its activation seems to involve direct interaction with ribosomes in the cytoplasm (39; 41). While studies utilizing Rictor depletion have revealed some mTORC2-specific cellular functions, the relative paucity of insight into mTORC2 function is due in large part to the lack of a specific pharmacological mTORC2 inhibitor (39; 72). Rapamycin is a potent and specific inhibitor of mTORC1, but mTORC2 is generally insensitive to its effects. Although second generation ATP-competitive mTOR inhibitors that block the kinase activity of both mTORC1 and mTORC2 can provide useful insight into mTORC2 function when compared with rapamycin effects, the most tractable and versatile approach to probing mTORC2 function would be the use of a selective small molecule mTORC2 inhibitor. As part of this dissertation, I describe the early development of an assay to screen for small molecule inhibitors of the Rictor-mTOR interaction that could potentially serve this purpose.

As would be expected for a protein with such pleiotropic effects, mTOR dysregulation is known to be a driving force in many human diseases. For the purposes of this dissertation I will focus only on the roles of mTOR pathway dysregulation in cancer and cancer predisposition disorders.

Although mTOR itself is not a *bona fide* transforming oncogene, its upstream regulators include a number of oncogenes and tumor suppressors. Specifically PI3K and Akt are known oncogenes, while PTEN, LKB1, and TSC2 are all *bona fide* tumor suppressors. The most obvious molecular link between mTOR signaling and cancer is found in the hamartoma syndromes. These heritable cancer predisposition syndromes,

including Cowden Disease (CD), Peutz-Jeghers Syndrome (PJS), and Tuberous Sclerosis Complex (TSC), are caused by loss-of-function mutations in the tumor suppressors PTEN, LKB1, and TSC2, respectively (39; 41; 73). As a consequence, these diseases all involve constitutively activated mTORC1 signaling and manifest as benign tumors in multiple organs. Based on their molecular etiology, these diseases are prime candidates for sensitivity to rapamycin treatment (39; 41; 73). Indeed, a Phase II clinical trial found that rapamycin treatment led to a 50% reduction in angiomyolipomas (AML) tumor size in TSC patients; however, this effect was reversed when treatment ended (74). Several *in vitro* and mouse model studies have suggested that many PI3K-Akt driven cancers are actually dependent upon downstream mTORC1 activity. Thus, rapamycin, already approved by the FDA as an immunosuppressant drug for use in transplant therapy, has been studied in many clinical trials targeting various types of cancer. Despite the high expectations of these studies, rapamycin analogues were found to be effective in treating only a few types of cancer, including Kaposi's sarcoma, mantle cell lymphoma, endometrial cancer, and renal cell carcinoma (39; 41; 75). One area in which rapamycin is particularly effective is in treating cancers displaying increased vascular endothelial growth factor (VEGF) signaling and angiogenesis resulting from loss of the Von Hippel-Lindau (VHL) tumor suppressor. VHL is an E3 ubiquitin ligase that negatively controls the protein stability of the VEGF-inducing transcription factor Hypoxia Inducible Factor 1α (HIF1α). It is believed that such tumors are highly dependent upon VEGF signaling and that rapamycin blocks the translation of HIF1α, thereby leading to a decrease in critical VEGF production (39; 76; 77). One potential explanation for the lackluster performance of rapamycin in other trials is a recently identified feedback mechanism that

activates the PI3K-Ras and PI3K-Akt pathways in response to mTORC1 inhibition (78-80). This problem may be circumvented by combinatorial therapy that targets both mTOR and the PI3K-Akt pathway. Another promising avenue for mTOR-targeted therapy is the recent development of ATP-competitive mTOR kinase inhibitors that block the activities of both mTORC1 and mTORC2. Promising pre-clinical results using these molecules have led to the initiation of new, ongoing clinical trials (81).

mTOR signaling is a highly complex and dynamic process that integrates numerous environmental inputs and orchestrates multi-faceted cellular responses to maintain homeostasis throughout the life of a cell. Considering mTOR's vital role in cell health and disease, it is clear that we have not yet harnessed its full potential as a pharmacological target in the treatment of complex diseases. The work of this dissertation attempts to address this issue through 1) the development of an assay for the discovery of mTORC2-specific small molecule probes and 2) the discovery of a novel mTORC1-regulated function of PRAS40, linking mTORC1 to the regulation of nucleolar stress-induced p53 activation.

1.4 Stress Signaling - p53 and the Nucleolar Stress Response Pathway

When cells experience stress conditions, a number of proteins are activated to inhibit cell proliferation or induce apoptosis; chief among these is the tumor suppressor p53, a transcriptional co-activator whose transcriptional program induces cell cycle arrest, senescence, or apoptosis (82-84). Because of its pivotal role in determining cell fate, p53 is highly regulated. This regulation can occur at the transcriptional, translational, or post-translational levels; however, the predominant mechanism

controlling p53 activity involves alterations of p53 ubiquitination and protein stability through the E3 ubiquitin ligase HDM2 (mouse ortholog Mdm2). p53 is generally a highly ubiquitinated protein that is rapidly degraded by the proteasome. Under cellular stress conditions, HDM2 is inhibited, thereby stabilizing p53 and allowing induction of p53 transcriptional target genes (82-85). p53 is responsive to a wide array of cellular stressors, including genotoxic insults, oxidative stress, oncogene expression, and disruption of ribosome biogenesis – a condition also known as nucleolar stress (86). Recently it has been shown that ribosomal protein L11 (RPL11) plays a key role in coordinating the p53 response to nucleolar stress. Specifically, when the process of ribosome production is disturbed, RPL11 translocates from the nucleoli to the nucleoplasm where it binds and inhibits HDM2, resulting in increased protein stability of p53 (**Figure 1-4**) (87-90). Ribosomal proteins L5 and L23 have also been found to play similar roles (91-93). Although the importance of the RPL11-HDM2-p53 nucleolar stress response pathway is well-established, little is known about its regulation. Specifically, the molecular mechanisms keeping the pathway inactive under pro-growth or pro-proliferative conditions remain largely unknown (94). The findings reported in this dissertation suggest a novel model by which the RPL11-HDM2-p53 pathway is regulated by the Akt-mTORC1 signaling axis through PRAS40.

1.5 PRAS40 – Molecular and Cellular Functions at the Crossroads of Akt and mTORC1 Signaling

Since its discovery, PRAS40 has been linked to cell survival and cancer progression; however, the mechanistic details of this relationship remain elusive.

PRAS40 was originally identified as *CLAR1*, an mRNA transcript moderately upregulated in advanced stage prostate cancer (95). The protein product of this gene was later identified as a prominent growth factor-stimulated Akt substrate and 14-3-3 binding partner (58). Additionally, a protein dubbed p39 (likely the same protein as PRAS40) was independently identified as a major growth factor- and nutrient-dependent 14-3-3 binding partner (59). Non-phosphorylated PRAS40 was subsequently found to bind mTORC1 through Raptor and to negatively regulate the kinase activity of mTORC1 by competing for substrate binding (51-57). Owing to its established role as a negative regulator of mTORC1, PRAS40 may reasonably be expected to have an overall suppressive effect on cell growth and/or proliferation. Indeed, other inhibitors of mTORC1 activity, such as TSC2 and LKB1, are *bona fide* tumor suppressors (96-99). However, in nearly all studies of PRAS40 cellular function, PRAS40 has been shown to promote cell survival, tumorigenesis, or tumor progression. *In vivo* overexpression of phospho-PRAS40 has been shown to increase neuronal survival in rodent models of transient focal cerebral ischemia and spinal cord injury (100-102). Additionally, PRAS40 knock-down (KD) was found to decrease the tumorigenicity of melanoma cells in a murine xenograft tumor model to the same extent as KD of the known melanoma-promoting protein and upstream PRAS40 regulator Akt3 (103). In another study, PRAS40 mRNA was identified as a primary target of the Ewing sarcoma protein (EWS) for translational repression in healthy cells. In Ewing sarcoma this repression is disrupted, leading to PRAS40 upregulation. Importantly, PRAS40 KD is able to reverse the increased proliferation observed upon EWS disruption, identifying PRAS40 as a key mediator of cell proliferation in Ewing sarcoma (104). Furthermore, unpublished data

from our lab show that PRAS40 is upregulated in tumors from lung cancer patients and that this upregulation is positively correlated with poor patient survival. Taken together, these findings suggest that phosphorylated, mTORC1-dissociated PRAS40 may have its own pro-survival function, independent of mTORC1 inhibition. To explore this possibility I have studied the subcellular localization and interactome of PRAS40. Here I present evidence for a model in which phosphorylation of PRAS40 by Akt and mTORC1 promotes the formation of a nuclear-specific, mTORC1-independent PRAS40- and RPL11-containing complex that limits the ability of RPL11 to induce p53 stabilization and thereby suppresses induction of cellular senescence.

Figure 1-1. Growth factors promote cell survival through the PI3K-Akt pathway and its downstream targets. Growth factor-stimulated PI3K generates PIP_3, creating a plasma membrane docking site for Akt. Once localized to the plasma membrane, Akt is phosphorylated and activated by PDK-1. Active Akt can phosphorlate many different substrates to inhibit apoptosis and promote cell survival. Three examples, Caspase 9, Bcl-X_L, and the FOXO family of transcription factors are depicted here.

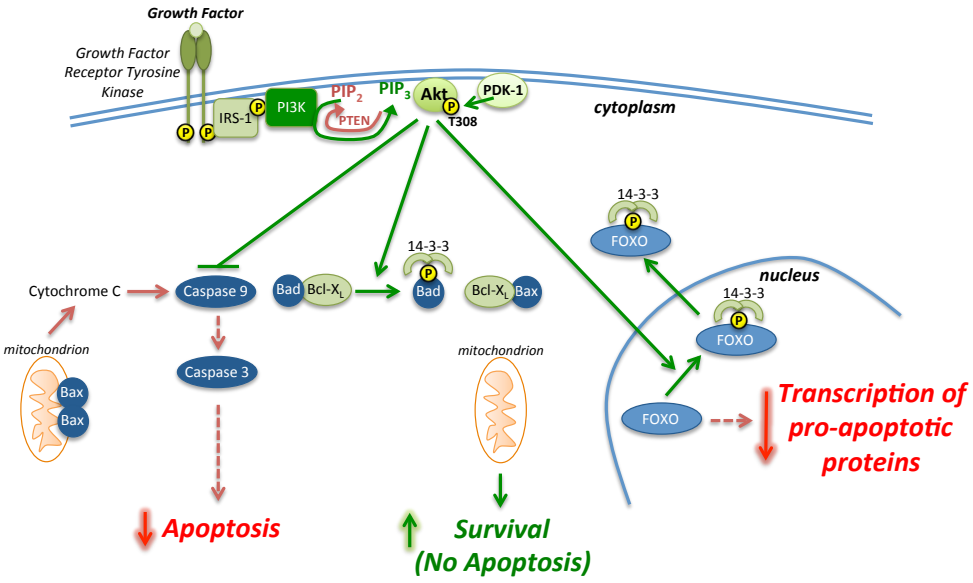
Growth Factor
Growth Factor Receptor Tyrosine Kinase
IRS-1
PI3K
PIP2
PTEN
PIP3
Akt
T308
PDK-1
cytoplasm
14-3-3
FOXO
nucleus
Cytochrome C
Caspase 9
Bad
Bcl-XL
Bax
mitochondrion
Caspase 3
Transcription of pro-apoptotic proteins
Apoptosis
Survival
(No Apoptosis)

Figure 1-2. Regulation and Function of mTOR. mTOR is a large Ser/Thr protein kinase that serves as the catalytic subunit of two distrinct multi-protein kinase complexes – mTORC1 and mTORC2. mTORC1 senses and responds to changes in cellular energy levels, extracellular growth factors, and amino acids. As depicted in this diagram, separate signaling mechanisms relay each of these signals to mTORC1. Once activated, mTORC1 phosphorylated p70 and 4EBP to promote cap-dependent translation, thereby enabling cell growth. mTORC1 can also promote sterol biosynthesis and inhibit autophagy through phosphorylation of SREBP-1 and ULK1, respectively. Far less is known about the upstream regulation or downstream functions of mTORC2. This is due in large part to the lack of a specific pharmacological inhibitors for mTORC2. It is known, however, that mTORC2 phosphorylates the secondary activation site, S473, in the hydrophobic domain of Akt to promote full Akt activation.

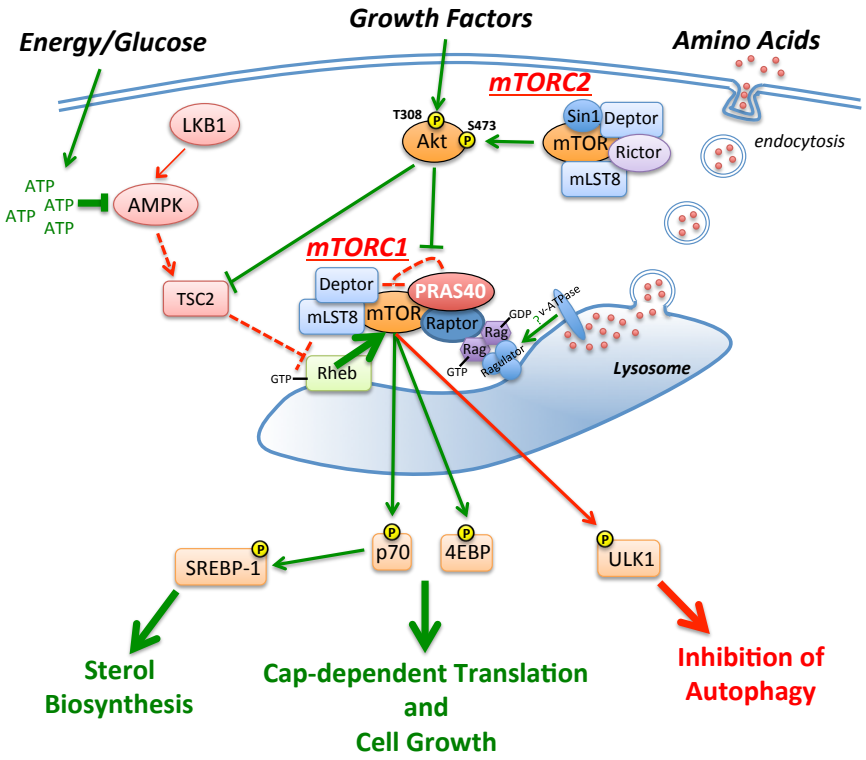
Energy/Glucose
Growth Factors
Amino Acids
mTORC2
LKB1
T308
S473
Akt
Sin1
Deptor
mTOR
Rictor
mLST8
endocytosis
ATP
ATP
ATP
ATP
AMPK
mTORC1
TSC2
Deptor
PRAS40
mLST8
mTOR
Raptor
Rag
Rag
Ragulator
GDP
?
v-ATPase
GTP
Rheb
GTP
Lysosome
p70
4EBP
ULK1
SREBP-1
Sterol
Biosynthesis
Cap-dependent Translation
and
Cell Growth
Inhibition of
Autophagy

Figure 1-3. PRAS40 is a target of growth factor and nutrient signaling whose function is incompletely understood. When in its non-phosphorylated state, PRAS40 binds mTORC1 through direct interaction with Raptor and is thought to inhibit mTORC1 function by competing for substrates. PRAS40 is a major target of the kinases Akt and mTORC1. Phosphorylation of PRAS40 induces 14-3-3 binding and dissociation of PRAS40 from mTORC1. The fate and function of mTORC1-dissociated PRAS40 is currently unknown.

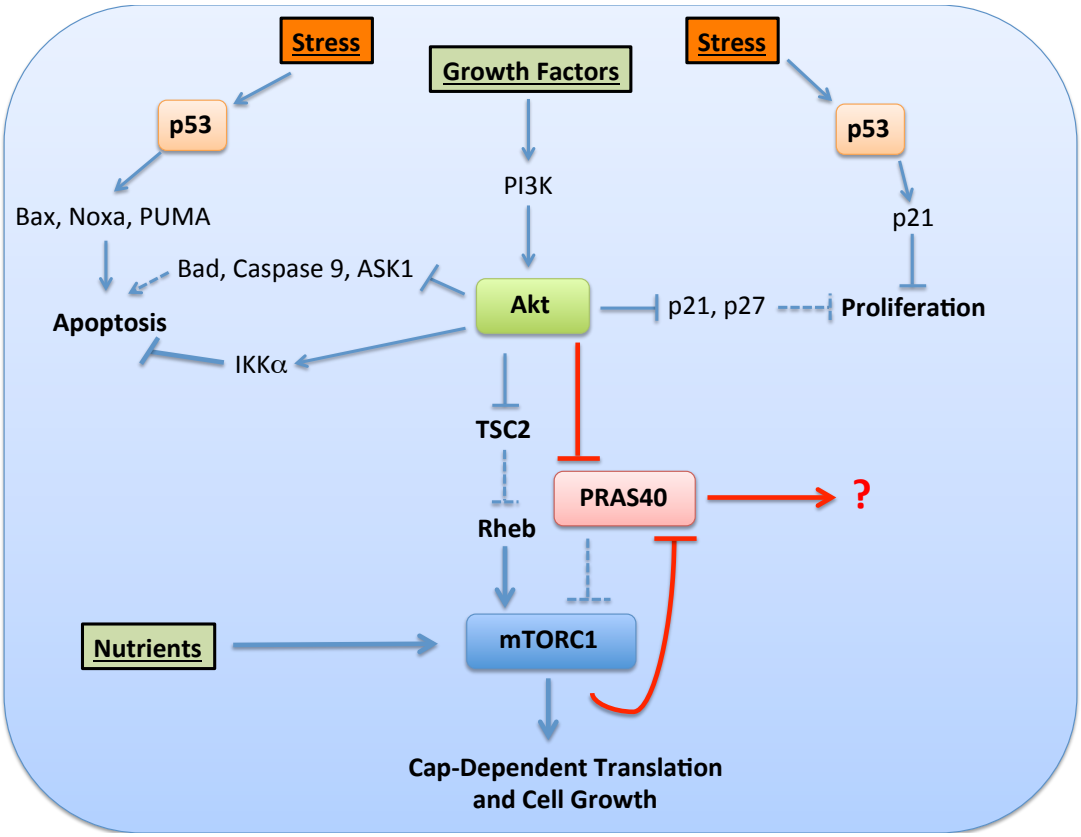
Stress
Growth Factors
Stress
p53
p53
PI3K
Bax, Noxa, PUMA
p21
Bad, Caspase 9, ASK1
Akt
p21, p27
Proliferation
Apoptosis
IKKα
TSC2
PRAS40
?
Rheb
Nutrients
mTORC1
Cap-Dependent Translation
and Cell Growth

Figure 1-4. The RPL11-HDM2-p53 Nucleolar Stress Response Pathway. Various stimuli can lead to imbalance in ribosome components – a condition referred to as nucleolar stress. In response to nucleolar stress, RPL11 translocates from the nucleolus to the nucleoplasm, where it directly binds and inhibits the p53-directed E3 ubiquitin ligase HDM2, thereby leading to increased protein stability of p53. It has been shown that this pathway serves a tumor suppressive function in a mouse model of c-myc-driven tumorigenesis (90). The mechanisms by which this pathway is regulated, particularly in response to changing microenvironmental conditions, are largely unknown.

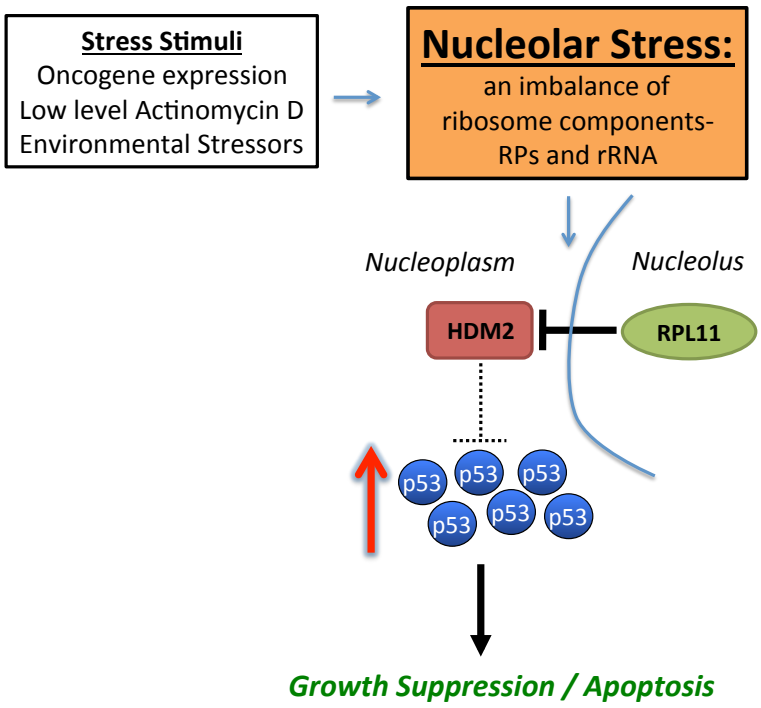
Stress Stimuli
Oncogene expression
Low level Actinomycin D
Environmental Stressors
Nucleolar Stress:
an imbalance of
ribosome components-
RPs and rRNA
Nucleoplasm
Nucleolus
HDM2
RPL11
p53
p53
p53
p53
p53
p53
Growth Suppression / Apoptosis

CHAPTER 2

Development of a Novel Technology for the Detection of Ternary Protein Complex Dynamics in Living Cells

2.1 Introduction

Virtually all cellular signaling pathways depend upon the ability of biomolecules to interact with one another; however, convenient methods for the study of these complexes, especially larger-order complexes, in their native environment are conspicuously lacking. As our enumeration of signaling pathway components becomes more and more exhaustive, it will become increasingly important to be able to study the nuances of signaling pathway function, such as temporal and hierarchical binding dynamics, in living cells in real-time. Two techniques currently available for the study of protein-protein interactions in living calls are the protein-fragment complementation assay (PCA) and resonance energy transfer (RET) approaches such as FRET (fluorescence-based) and BRET (bioluminescence-based) (105; 106). PCA is based on the principle of splitting a reporter molecule, such as Venus or Renilla luciferase into two non-functional fragments and genetically fusing these fragments to two interacting partners. When the two fused binding partners interact with one another, the reporter fragments are brought into sufficient proximity to reconstitute the full-length reporter and produce either a fluorescent or bioluminescent signal. Importantly, reconstitution of split-Renilla luciferase has been shown to be reversible and therefore capable of detecting protein interaction dynamics in living cells (107). However, this technique is limited to the study of binary complexes. FRET is a physical phenomenon that occurs when two fluorophores with overlapping emission and excitation spectra, respectively, are in very close proximity to one another. In such a scenario, emission energy from the donor fluorophore can be non-radiatively transferred to the acceptor fluorophore, causing it to emit light. Importantly, this only occurs when the fluorophores are less than ~10 nm

apart, which is serendipitously the range over which many biomolecular interactions occur (108). Therefore, interacting partners can be genetically fused to a donor/acceptor fluorophore pair to permit detection of their interaction. If the interaction partners are physically associated with one another, excitation of the donor fluorophore generates emission from the acceptor fluorophore, indicating a positive protein-protein interaction (106). If the donor is replaced by Renilla luciferase, the energy transfer phenomenon is referred to as BRET (bioluminescence resonance energy transfer). Both FRET and BRET are useful in studying protein-protein interactions, but are again limited to the study of binary complexes. Therefore, I propose to combine split-Renilla PCA and BRET for the study of ternary protein complex dynamics in living cells. Notably, since I began working on this project, others have begun to demonstrate its utility in the published literature (109; 110). Here I apply a combined PCA-BRET technique to the study of the established growth factor-regulated, phosphorylation-dependent interaction between PRAS40 and 14-3-3 dimers as a proof-of-principle.

2.2 Materials and Methods

Plasmids

Venus cDNA was a kind gift from Dr. Atsushi Miyawaki (RIKEN, Japan). A flexible linker sequence – $(GGGGS)_2$ – was added to the C-terminal end of Venus via PCR amplification. The Venus-$(GGGGS)_2$ PCR product was sub-cloned into the HindIII site of pSCM167, a pcDNA 3.1-based plasmid generated previously in our lab for use as a Gateway® Cloning Destination Vector. pSCM167 contains a Flag epitope tag upstream of attR sites which flank the ccdB death gene. Insertion of Venus-$(GGGGS)_2$ into the

HindIII site of pSCM167 places Venus-$(GGGGS)_2$ upstream of the Flag epitope tag to generate a Venus-Flag Gateway® Cloning Destination vector named pJJH24. PRAS40 cDNA was PCR amplified and introduced into pDONR201 (Invitrogen) via a BP reaction to generate a PRAS40 Entry Clone. The PRAS40 Entry Clone and pJJH24 were used in an LR reaction to generate a plasmid encoding Venus-Flag-PRAS40.

Amino- and carboxy-terminal Renilla luciferase fragments were designed as previously described (107) and PCR amplified from the humanized Renilla Luciferase gene (pGL4.74 - Promega). A flexible linker sequence – $(GGGGS)_2$ – was added to the C-terminal end of each fragment during PCR amplification. The N-terminal Renilla luciferase fragment (consisting of codons 1-110) was sub-cloned into the HindIII site of pSCM167 as described above to generate an N-RenLuc-Flag Gateway® Destination vector called pJJH6. The C-terminal Renilla luciferase fragment (consisting of codons 111-310) was sub-cloned into the SacII site of pDEST26 (Invitrogen) to generate a C-RenLuc-His_6 Gateway Destination vector called pJJH4. A 14-3-3ε Entry Clone (generated previously in our lab) was used in LR reactions with pJJH6 or pJJH4 to produce plasmids encoding N-RenLuc-Flag-14-3-3ε and C-RenLuc-His_6-14-3-3ε, respectively.

All plasmid sequences were confirmed by sequencing.

Cell Culture

HeLa cells were maintained in DMEM (Cellgro) supplemented with 10% FBS and 1x Penicillin/Streptomycin Solution (Cellgro) at 37°C and 5% CO_2 in humidified conditions.

Transfections

For PCA-BRET assays, 1x10^4 HeLa cells were seeded per well in cell culture-treated white-walled 96-well plates (Falcon). Cells were transfected 24 hours later with 160 ng of total DNA per well – 40 ng each of split Renilla luciferase-tagged constructs and 80 ng Venus-PRAS40. Eight replicate wells were used for each sample. For control samples lacking any one of these plasmids, empty pcDNA vector was added to keep the DNA amount constant in all samples. Transfections were performed with FuGene® HD transfection reagent (Roche) according to the manufacturer's instructions using a 3:1 ratio of transfection reagent (μL) to DNA (μg). Fusion proteins were allowed to express for 24 hours. Two sets of samples were then washed three times with serum-free DMEM and incubated in serum-free DMEM for 24 hours. One of these was changed back to DMEM containing 10% FBS for one hour for "serum rescue."

BRET Assay

ViviRen™ Live Cell Renilla luciferase substrate (Promega) was diluted to 60 μM in PBS containing 0.5% gelatin. Diluted ViviRen™ was then added directly to media in cell culture wells in a 1:1 ratio, three columns at a time to give a final substrate concentration of 30 μM. Wells were read three plate columns at a time at 470 nm and 527 nm on a Spectramax® L luminometer (Molecular Devices) with a 1 sec integration, exactly 2.5 min after substrate addition. This was repeated until luminescence readings for all columns were recorded.

Analysis of BRET Results

Raw BRET ratios were calculated as the ratio of emission at 527 nm to emission at 470 nm. Average bleedthrough was defined as the average raw BRET ratio from cells expressing only N-RenLuc-14-3-3 and C-RenLuc-14-3-3 (and lacking Venus-PRAS40). Average bleedthrough was then subtracted from all raw BRET ratios to give corrected BRET ratios.

2.3 Results

2.3.1 A combined PCA-BRET technique detects environmentally-cued dissociation of PRAS40 from intact 14-3-3 dimers in living cells.

Plasmids encoding Venus-tagged PRAS40, 14-3-3ε fused to the N-terminal fragment of Renilla luciferase, and 14-3-3ε fused to the C-terminal fragment of Renilla luciferase were transiently co-transfected in HeLa cells. Upon addition of ViviRen™ Renilla luciferase substrate (Promega) to live cells maintained in media containing serum, both a positive BRET signal (**Figure 2-1A**) and a Renilla luciferase signal (**Figure 2-1B**) are detected, allowing monitoring of the ternary 14-3-3 dimer-PRAS40 complex and the 14-3-3 dimer alone regardless of PRAS40 association, respectively. 24-hour serum withdrawal causes a nearly 90% drop in BRET, indicating dissociation of the PRAS40-14-3-3 dimer ternary complex. Notably, a one-hour serum reintroduction restores the BRET signal to its maximum level, indicating reassembly of the PRAS40-14-3-3 dimer ternary complex and demonstrating the ability of the combined PCA-BRET approach to detect reversible ternary protein complex dynamics in live cells in response to extracellular signals. However, from the BRET signal alone it is impossible to know

whether the entire ternary complex dissociates during serum withdrawal or if PRAS40 alone dissociates, leaving the 14-3-3 dimer intact. Importantly, using the combined PCA-BRET technique, this issue can be addressed by simultaneously monitoring the Renilla luciferase signal (**Figure 2-1**). Upon serum withdrawal the Renilla luciferase signal, representing 14-3-3 dimer association, only decreases by approximately 50% (**Figure 2-1B**), indicating that the 14-3-3 dimer remains largely intact during serum withdrawal. Considering this together with the fact that the BRET signal is ratiometric, these results indicate that the combined PCA-BRET technique is capable of detecting binding dynamics of a single member of a ternary complex in response to extracellular signals in living cells.

2.4 Conclusions and Discussion

This proof-of-principle experiment demonstrates that the combined PCA-BRET technique is capable of monitoring ternary protein complex dynamics in living cells. This technique will be particularly useful for the detailed study of complexes with hierarchical binding dynamics in which one component dissociates while the others remain intact, such as trimeric G-proteins and multi-subunit kinases such as the Inhibitor of κB Kinase (IKK) complex. Another, more specific, application is anticipated in the field of 14-3-3 protein biology. 14-3-3 proteins are believed to exist as obligate dimers *in vivo*. There are seven human isoforms of 14-3-3, and they can associate in nearly any manner of homo- or heterodimers. Therefore, a salient question in the field is whether 14-3-3 client proteins have a binding preference for a specific 14-3-3 homo- or heterodimer. This could be addressed relatively easily with combined PCA-BRET by

separately transfecting all 28 possible combinations of split-Renilla-tagged 14-3-3 isoforms with the same Venus-tagged client protein and measuring the BRET and Renilla signals produced by each combination. Such an experiment may reveal a novel mechanism by which 14-3-3 proteins can simultaneously regulate so many diverse cellular processes.

One obvious limitation of this assay is that it relies entirely on exogenously expressed proteins. Therefore, care should be taken to keep overexpression to a minimum and conditions should be optimized so that the minimum amount of tagged protein necessary to observe a robust signal is expressed. It will also be necessary to ensure, if possible, that the over-expressed proteins retain the functionality of native proteins. When testing novel interactions, lack of a signal should not necessarily be interpreted as a lack of interaction because both the PCA and BRET techniques are proximity-based and highly dependent on tag orientation. If the complex being studied is known to interact from other methods, it may be necessary to try different tag arrangements to obtain optimal signal. When testing the effects of a drug or hormone on an interaction, it will be important to use conditions that are known to induce and disrupt the interaction as controls to help ensure that the effect or lack of effect seen with the test compound is real, i.e. to help rule out false positive and false negative effects of the test compound. The use of interaction-disrupting point mutations, if available, will also be a powerful control to help rule out false positive interactions.

Thus, taking these caveats into consideration it appears that the combined PCA-BRET technique will help sharpen the agility and focus with which investigators can probe protein complex dynamics in living cells.

Figure 2-1. A combined Protein-Fragment Complementation – Bioluminescence Resonance Energy Transfer technique detects ternary protein complex dynamics in living cells. HeLa cells were transfected with the indicated plasmids and allowed to express the fusion proteins for 24h ("N- or C-RenLuc": amino- or carboxy-terminal fragment of Renilla luciferase). As indicated, the cells were then grown in serum-free media for 24h. Serum was re-introduced to one set of samples for 1h. ViviRen™ Live Cell Renilla luciferase substrate (Promega) was added directly to the media and readings were taken at 470nm (Renilla luciferase) and 527 (Venus) using a Spectramax® L luminometer (Molecular Devices). (Note: Equal expression of Ven-PRAS40 was confirmed via epifluorescence microscopy. [Data not shown]) **A)** BRET ratios (527nm to 470nm) were calculated and corrected by subtracting the average bleedthrough ratio obtained from cells transfected with N-RenLuc- and C-RenLuc-tagged 14-3-3 only. BRET signal is indicative of the existence of a ternary complex consisting of two 14-3-3 molecules and one PRAS40 molecule. **B)** Renilla luciferase signal from the same experiments as in **A**. This signal monitors the interaction of two 14-3-3 molecules only, regardless of the presence of Ven-PRAS40 in the complex. Eight wells per sample group were measured in each experiment. Data are reported as the average of two independent experiments +/-SEM. (*$p < 0.5$, **$p < 0.01$, ***$p < 0.001$ compared to control, *i.e.* triply-transfected cells maintained in serum, using the Bonferroni Multiple Comparisons Test)

A

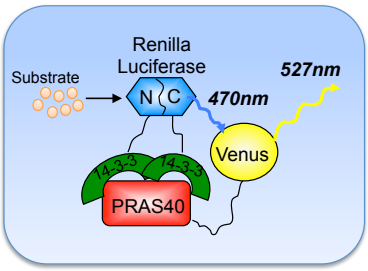

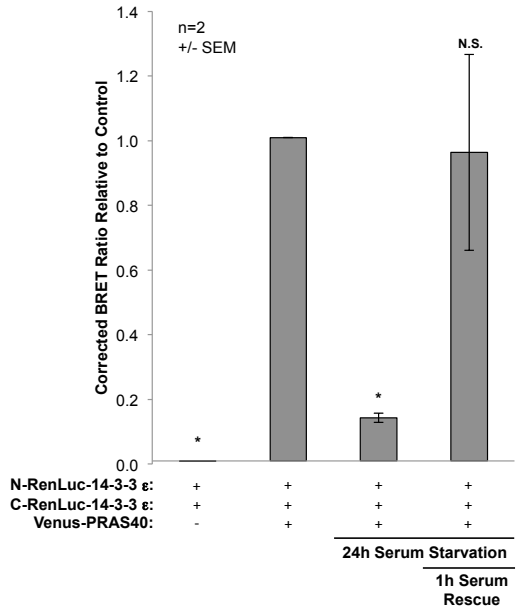

B

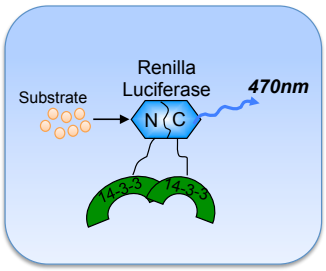

***Note:** This diagram is used only to clarify the signal source for the graph in B. These data come from the same experiment as A and as such, were measured in the presence of Venus-PRAS40.

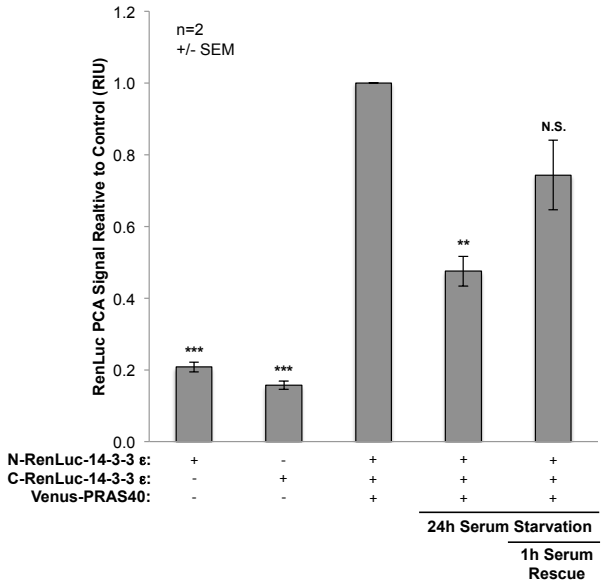

CHAPTER 3

Development of a Time-Resolved Fluorescence Resonance Energy Transfer Assay for the High-throughput Discovery of Small Molecule mTORC2 Inhibitors

A portion of the introduction of this chapter was published previously as:

Du Y and Havel JJ (2011). "Förster Resonance Energy Transfer Technologies in High-Throughput Screening." In Chemical Genomics (Fu, H. Ed; Cambridge University Press).

3.1 Introduction

mTOR is a critical regulator of cell growth and proliferation and serves as the catalytic subunit for two distinct multi-protein complexes named mTORC1 and mTORC2. mTORC1 is responsive to nutrients, growth factors, energy status, and oxygen levels. Much is known about mTORC1-mediated control of protein synthesis, cell growth, ribosome biogenesis, metabolism, and autophagy (39-41). While mTORC2 is known to function as a primary kinase of the S473 activation site in the hydrophobic domain of Akt, relative to mTORC1, very little is known of mTORC2's function. The primary reason for this discrepancy is the existence of a potent and specific mTORC1 inhibitor, rapamycin, and the lack of a complementary pharmacological mTORC2-specific inhibitor (39-41; 72). In this chapter, I describe the early development of a TR-FRET-based assay for the potential discovery of a small molecule mTOR-Rictor binding inhibitor through high-throughput screening.

Förster Resonance Energy Transfer (FRET) is the non-radiative transfer of energy between two fluorophores, termed the donor and the acceptor, with overlapping emission/excitation spectra. When a donor fluorophore absorbs light of a certain wavelength it is promoted to an excited electronic state. Upon vibrational relaxation, this energy is typically released as heat and light of a longer wavelength; however, if the donor is in sufficient proximity to an acceptor with specific spectral properties, energy can be transferred directly to the acceptor through long range dipole-dipole interactions, resulting in photon release from the acceptor (108; 111; 112). The maximum distance over which FRET events can occur is approximately 10 nm. Serendipitously, this also happens to be the distance over which many biomolecular interactions occur, making

FRET an appealing approach for the study of intra- or intermolecular interactions in biology (108; 111; 112). In a typical biomolecular FRET assay, a protein "A" is genetically fused to a donor fluorescent protein such as Cyan Fluorescent Protein (CFP), and "Protein B" is fused to an acceptor such as Yellow Fluorescent Protein (YFP). If A and B interact, CFP and YFP will be brought into sufficient proximity for FRET to occur. Therefore, a positive FRET signal is indicative of a protein-protein interaction between A and B.

There are three primary methods for the detection of FRET events – donor photobleaching, acceptor photobleaching, and measurement of sensitized emission. In the first method, the rate of donor photobleaching is measured in the presence and absence of the acceptor. If a FRET event is occurring, the half-life of the donor's excited state will be decreased due to energy transfer. Because fluorophores are only susceptible to photobleaching when in their excited state, a decreased rate of donor photobleaching in the presence of the acceptor is indicative of FRET. The second approach, acceptor photobleaching, requires only one sample containing both the donor and acceptor. In this method, donor emission intensity is measured before and after acceptor photobleaching. Because the non-radiative energy transfer of FRET quenches the emission of the donor, photobleaching the acceptor will disrupt the energy transfer and cause an increase in donor emission in the case of a positive FRET event. In the final method, detection of sensitized emission, acceptor emission is detected upon donor excitation. Although it seems straightforward, this method is subject to two major confounding factors – spectral bleedthrough and media autofluorescence. Due to the overlapping spectral properties of many FRET fluorophore pairs, the FRET channel (i.e. donor excitation, acceptor

detection) is often contaminated by spectral bleedthrough from A.) a wide donor emission spectrum and B.) direct excitation of the acceptor by the donor's excitation wavelength. This spectral bleedthrough must be corrected by preparing donor-only and acceptor-only samples in addition to the FRET pair sample. Bleedthrough coefficients can be determined from the single fluorophore controls and used to correct bleedthrough in the FRET pair sample. The second confounding factor, media autofluorescence, is more difficult to avoid using traditional FRET fluorophore pairs (108; 111; 112).

While the first two FRET detection approaches are desirable because they lack spectral bleedthrough problems, they require advanced microscopy techniques and therefore are not amenable to high-throughput screening applications. The "measurement of sensitized emission" method can be easily performed by a high-throughput fluorometer; however, the use of this approach raises significant concerns about signal contamination from spectral bleedthrough and environmental autofluorescence. One effective solution to this problem is the use of rare earth metals, or lanthanides, as the FRET donor in a modification of traditional FRET known as time-resolved FRET (TR-FRET) (113-115). In TR-FRET the lanthanide ions Terbium^{2+} and Europium^{3+} are typically used as FRET donors because of their exceptionally long emission half-life (300-1500 μs). This long-lived donor emission allows for a temporal delay between donor excitation and detection of acceptor emission. Because autofluorescence of biological media decays rapidly, this temporal delay virtually eliminates signal contamination due to media autofluorescence. Spectral bleedthrough from direct excitation of the acceptor is also avoided because the emission half-life of the acceptor is much shorter than that of the donor. As such, any acceptor emission due to direct excitation by the incident light will decay during the

temporal delay, leaving only acceptor emission due to FRET at the time of detection (**Figure 3-1**). Furthermore, the use of an acceptor with a red-shifted emission such as allophycocyanin or Alexa® 680 obviates concerns about donor emission bleedthrough into the acceptor emission detection channel (113; 114). Thus, TR-FRET assays are ideally suited for HTS applications due to their homogenous design and high signal to noise ratios. In this chapter, the principle of TR-FRET is applied to the development of a cell lysate-based assay for monitoring mTOR-Rictor binding.

3.2 Materials and Methods

Plasmids

The Flag-mTOR plasmid was kindly provided by Dr. Jing Huang, UCLA (Addgene Plasmid 22998). The myc-Rictor plasmid was kindly provided by Dr. David Sabatini, MIT (Addgene Plasmid 11367). The mTOR and Rictor coding sequences were PCR amplified and inserted into pDONR201 (Invitrogen) through BP Reactions to generate mTOR and Rictor Entry Clones. The mTOR Entry Clone and pDEST27 (Invitrogen) were used in an LR Reaction to produce a plasmid encoding GST-mTOR. The Rictor Entry Clone and pJJH24 (see section **2.2** for a description) were used in an LR Reaction to produce a plasmid encoding Ven-Flag-Rictor. mTOR truncations were generated by inserting a 3' stop codon during PCR amplification from the Flag-mTOR template. mTOR truncations-STOP PCR products were inserted into pDONR201 via BP reactions to generate mTOR truncation Entry Clones. These Entry Clones were used in LR reactions with pDEST27 (Invitrogen) to generate plasmids encoding GST-mTOR truncations. A stop codon was entered into pDEST27 (Invitrogen) immediately

downstream of the final GST-coding codon via site-directed mutagenesis to generate a plasmid that expresses only GST.

Cell Culture

HEK293T cells were maintained in DMEM (Cellgro) supplemented with 10% FBS and 1x Penicillin/Streptomycin Solution (Cellgro) at 37°C and 5% CO_2 in humidified conditions.

TR-FRET Assays

1x10^6 HEK293T cells were seeded per well in 6-well cell culture-treated plates (Corning) and were allowed to grow until they reached ~80% confluency. Cells were then transfected with 2 μg DNA per well using a 3:1 ratio of FuGene® HD transfection reagent (Roche) (μL) to DNA(μg). For competition with GST-mTOR 1-640 experiment, "low" 1-640 was 333 ng plus 333 ng pcDNA to keep total DNA even, and "high" was 667 ng GST-mTOR 1-640 plasmid. 24 hours later, cells were rinsed once with ice cold PBS [137 mM NaCl, 2.7 mM KCl, 10 mM Na_2HP0_4, 1.8 mM KH_2PO_4, pH 7.4] and scraped into 80 μL cold 0.3% CHAPS Buffer [40 mM HEPES pH 7.5, 120 mM NaCl, 1 mM EDTA, 0.3% CHAPS, 5 mM sodium pyrophosphate, 5 mM sodium fluoride, 2 mM sodium orthovanadate, 1 mM PMSF, 10 μg/mL aprotinin, and 10 μg/mL leupeptin], adapted from (116). Lysates were allowed to sit on ice for 10 min and were then clarified by centrifugation at 16,100xg for 10 min at 4°C. The TR-FRET assays were performed in opaque, black-walled 384-well plates (Corning). Lysates were transferred in triplicate to the 384-well plate. A series of 2-fold dilutions in TR-FRET Buffer [20 mM Tris-HCl

pH 7.0, 50 mM NaCl, 0.01% NP40] was prepared across the plate columns. One column was left with only TR-FRET buffer (no lysate) to determine background signal. A 1:500 dilution of Terbium-tagged anti-GST or Terbium-tagged anti-Flag antibody (cisbio Bioassays) was prepared in TR-FRET Buffer. Diluted antibody was added to the sample wells in the 384-well plate 1:1 (v:v) to give a final antibody dilution of 1:1000. The plate was spun down at 800 rpm for 5 min at ambient temperature. The plate was then covered (to prevent quenching of fluorescence) and incubated at ambient temperature or at 37°C for various times. FRET and Venus intensity signals were measured with an Envision® Multilabel plate reader (PerkinElmer). For FRET signal, Terbium was excited at 340 nm. After a 50 μs time delay, terbium emission was read at 486 nm and Venus emission was read at 520 nm. For Venus intensity (expression), Venus was excited at 485nm and Venus emission was read at 535 nm. TR-FRET signals were calculated as the ratio of 520 nm emission to 486 nm emission. The ratios were multiplied by an arbitrary factor of 10,000 for ease of presentation.

GST Pull-Down

HEK293T cells were seeded, transfected, and lysed as above, except 200 μL of 0.3% CHAPS Buffer was used for each well. 130 μL of each lysate was added to 40 μL of a 50% solution of glutathione-conjugated Sepharose beads (GE Healthcare) in 0.3% CHAPS Buffer. The remainder of each lysate was saved as input control. GST Pull-downs (PDs) were rotated slowly at 4°C for 6 hours. Beads were then washed three times with 0.3% CHAPS Buffer. GST-mTOR and associated proteins were eluted by addition of 15 μL 3xSDS loading buffer containing freshly added 2.5% β-

mercaptoethanol to the beads and boiling for four minutes. Inputs and eluates were analyzed by SDS-PAGE and Western Blotting.

SDS-PAGE and Western Blotting.

Samples were resolved using SDS-PAGE 4-15% TGX 15-well gels (Bio-Rad). Resolved proteins were transferred to nitrocellulose at 100V for 45 minutes. Membranes were blocked in TBST [50 mM Tris, 137 mM NaCl, 0.05% Tween, pH 7.6] containing 5% dry milk for 30 minutes at ambient temperature. Membranes were left in primary antibody dilutions and gently shaken over night at 4°C. The following day, membranes were washed three times for ten minutes each in TBST and incubated in secondary antibody dilution for 50 minutes at ambient temperature with gentle shaking. Membranes were washed three times for ten minutes each in TBST. Chemiluminescent signal was developed by adding West Pico or West Dura enhanced chemiluminescence detection reagent (Pierce) for five minutes. Membranes were then exposed to autoradiography film for various times.

Antibodies and Dilutions

Rabbit anti-GST – Santa Cruz, sc-459, 1:2000 in 5% milk /TBST; rabbit anti-Raptor – Cell Signaling, 2280, 1:1000 in 5% milk/TBST; Horseradish Peroxidase-conjugated goat anti-rabbit secondary antibody – Santa Cruz, sc-2005, 1:5000 in TBST

3.3 Results

3.3.1 Optimization of mTOR-Rictor TR-FRET signal

I first wanted to determine if a TR-FRET signal could be measured between GST-mTOR and Venus-Rictor. Lysates from cells expressing either GST and Venus-Rictor or GST-mTOR and Venus-Rictor were serially diluted because TR-FRET can be very sensitive to protein concentration. No signal was detected immediately following addition of Terbium(Tb)-anti-GST antibody; however a TR-FRET signal about 2-fold over background was observed after incubation of the plate at ambient temperature for two hours (**Figure 3-2A**). Venus-Rictor (**Figure 3-2B**) and GST/GST-mTOR (**Figure 3-2C**) expression was fairly even between the two samples.

3.3.2 Identification of the Rictor-binding domain of mTOR

Although a TR-FRET signal significantly greater than background is observed for the GST-mTOR-Venus-Rictor pair, a 2-fold signal-to-noise ratio is typically not large enough for a successful screening assay. Both mTOR and Rictor are very large proteins, so it is possible that the protein size combined with tag orientation places the donor and acceptor fluorophores too far apart physically to generate a robust FRET signal. Therefore I sought to identify a minimal region of mTOR that binds Rictor so that the size of the proteins involved in the assay could be decreased. A minimal binding region peptide may also be useful as a positive control for mTOR-Rictor binding inhibition. A GST Pull-Down of various mTOR truncations indicates that a region within the mTOR HEAT Repeat domain between residues 99 and 180 is required for mTOR-Rictor binding (**Figure 3-3**). This finding was confirmed by TR-FRET using cell lysates expressing the same GST-mTOR truncations and Venus-Rictor (**Figure 3-4A**). While Venus-Rictor expression is not entirely even (**Figure 3-4B**), it is actually higher in samples that do not

show Venus-Rictor co-precipitation compared to those that do. Therefore, it is unlikely that the binding pattern seen by both GST Pull-Down and TR-FRET is an artifact of uneven protein expression.

3.3.3 TR-FRET is capable of detecting mTOR fragment-mediated disruption of the mTOR-Rictor interaction.

Interestingly, a much-improved signal-to-noise ratio is observed when Flag-mTOR is used in the TR-FRET assay instead of GST-mTOR (**Figure 3-5A**). This may reflect the apparent importance of the mTOR N-terminus in mediating interaction with Rictor. Flag-PRAS40 was used as a negative control because PRAS40 is known to associate only with Raptor, and not with Rictor (53). Importantly, when co-expressed at higher levels, GST-mTOR 1-640 is able to partially inhibit the TR-FRET signal generated by Flag-mTOR and Venus-Rictor (**Figure 3-5B**). This indicates that the mTOR-Rictor TR-FRET assay may be capable of detecting mTOR-Rictor interaction inhibitors in high-throughput screening.

3.4 Discussion

Some insight into mTORC2's function and significance in disease has been gleaned from studies in which mTORC2 specific components such as Raptor or Sin1 are stably knocked down or knocked out. Indeed, one study has shown that Rictor is dispensible for the health of regular prostate epithelia, but required for the formation of PTEN loss-driven tumors, indicating that targeting mTORC2 in cancer might provide an acceptable therapeutic window (117). However, in absence of the ability to acutely and

specifically inhibit mTORC2 function, the possibility of compensatory mechanisms plagues the interpretation of Rictor or Sin1 stable knock-down or knock-out experiments. A similar, but not identical, problem arises with the use of ATP-competitive kinase inhibitors that target both mTORC1 and mTORC2. Comparison of the effects of these drugs with those of rapamycin, may reveal mTORC2-specific functions; however, compensatory, feedback mechanisms are triggered when mTORC1 is inhibited (78-80). Therefore, inhibiting the activity of mTORC1 may indirectly affect the function of mTORC2. Therefore, an mTORC2-specific inhibitor, i.e. an mTOR-Rictor binding inhibitor, would be an invaluable tool in reliably elucidating the function of mTORC2. As indicated by the prostate cancer study mentioned previously, an mTORC2-specific inhibitor may have therapeutic potential as well. Because mTORC2 phosphorylates the S473 and not the T308 site of Akt, there is the possibility for therapeutic synergy between a theoretical mTORC2 inhibitor and traditional inhibitors of the PI3K-Akt pathway (39; 72).

The use of TR-FRET technology to monitor protein-protein interactions in a high-throughput screening setting has a number of advantages. Because of the strict proximity requirements of FRET, a FRET signal essentially detects only direct protein-protein interactions. As described above, by allowing signal contaminants to decay during a time delay between donor excitation and acceptor detection, TR-FRET provides a high signal to noise ratio, allowing for more sensitive detection of protein-protein interactions compared to traditional FRET pairs. The assay is also performed in an entirely homogenous, “mix-and-read” format, obviating the need for potentially disruptive wash steps. This saves a considerable amount of time and reagents when the assay is scaled up

for a high-throughput format. In the setup I am using, one drawback is that both proteins measured are overexpressed. Therefore, care must be taken to ensure that the over-expressed proteins behave similarly to endogenous proteins. If this becomes a significant concern, it is possible to perform the TR-FRET assay using endogenous proteins by covalently labeling antibodies directed to epitopes in the endogenous proteins with the necessary fluorophores. However, this approach can be difficult, as the antibodies used must have high specificity for the proteins of interest and must be able to bind the proteins in the native conformations. When testing novel interactions, lack of a signal should not necessarily be interpreted as a lack of interaction because both the FRET technique is proximity-based and highly dependent on tag orientation. If the complex being studied is known to interact from other methods, it may be necessary to try different tag arrangements to obtain optimal signal. When testing the effects of a drug or hormone on an interaction, it will be important to use conditions that are known to induce and disrupt the interaction as controls to help ensure that the effect or lack of effect seen with the test compound is real, i.e. to help rule out false positive and false negative effects of the test compound. The use of interaction-disrupting point mutations, if available, will also be a powerful control to help rule out false positive interactions. Keeping these caveats in mind, the further development and application of the assay described in this chapter may lead to the discovery of small molecules with great benefit to both science and medicine.

Figure 3-1. Time-Resolved Fluorescence Resonance Energy Transfer (TR-FRET) provides greater signal to noise ratios compared to traditional FRET. A) Lanthanide fluorophores such as europium and terbium have exceptionally long emission half-lives, in the range of hundreds of μsec. **B)** The long emission half-life of the lanthanide donor allows the true FRET signal to persist long after the other signal contaminants, such as direct excitation of the acceptor by incident light and autofluorescence of media or test compounds, have decayed. **C)** The lack of FRET signal contaminants at the time of detection allows for greatly increased signal to noise ratios, thereby improving the sensitivity of FRET-based assays.

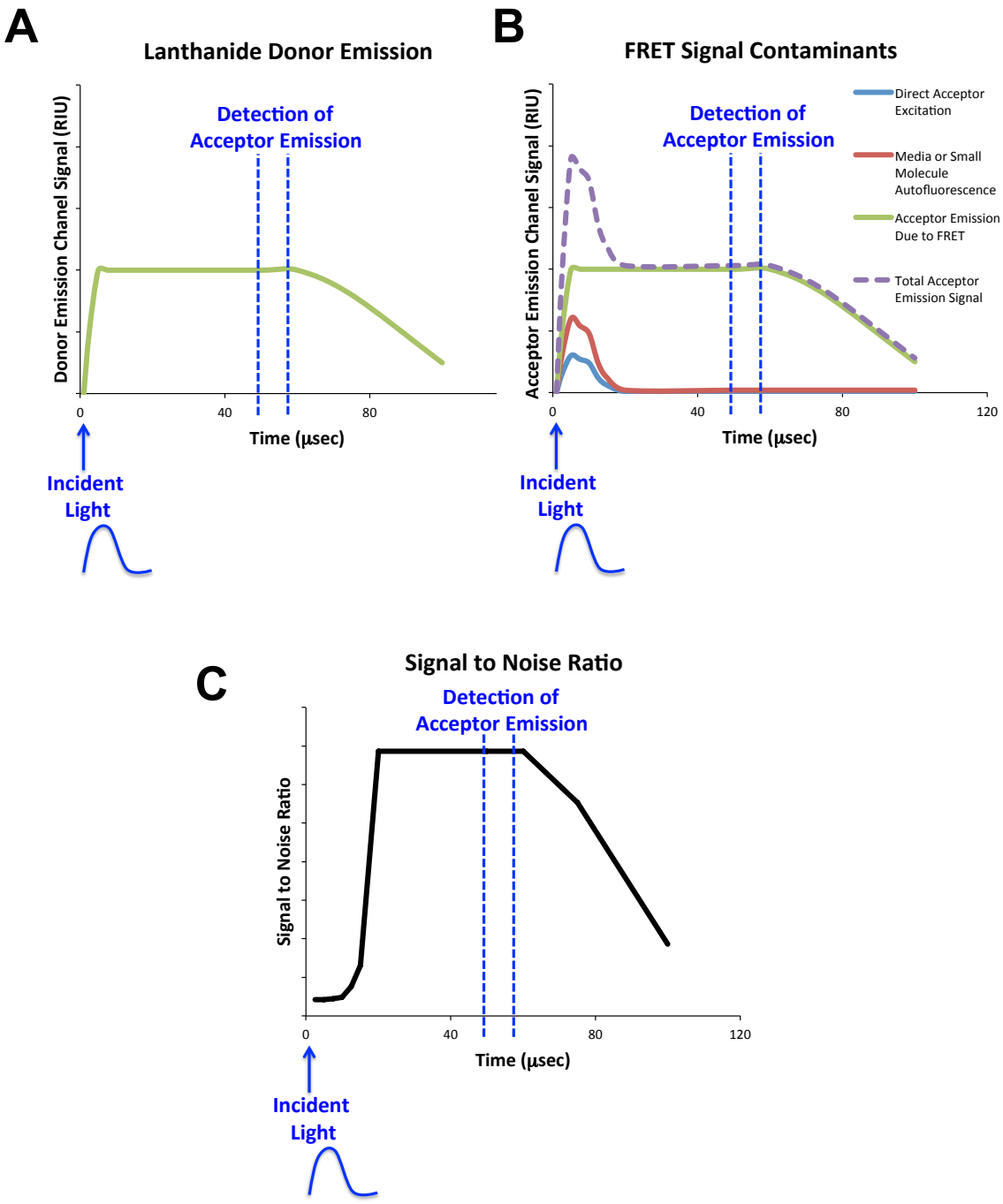
A
Lanthanide Donor Emission
Donor Emission Chanel Signal (RIU)
Detection of
Acceptor Emission
0
40
80
Time (µsec)
Incident
Light
B
FRET Signal Contaminants
Acceptor Emission Chanel Signal (RIU)
Detection of
Acceptor Emission
Direct Acceptor
Excitation
Media or Small
Molecule
Autofluorescence
Acceptor Emission
Due to FRET
Total Acceptor
Emission Signal
0
40
80
120
Time (µsec)
Incident
Light
C
Signal to Noise Ratio
Detection of
Acceptor Emission
Signal to Noise Ratio
0
40
80
120
Time (µsec)
Incident
Light

Figure 3-2. Optimization of TR-FRET signal using GST-mTOR and Venus-Rictor. Whole-cell lysates of HEK293T cells co-expressing GST and Venus-Rictor or GST-mTOR and Venus-Rictor were prepared in a series of 2-fold serial dilutions in a 384-well plate and incubated with Terbium-conjugated anti-GST antibody for the times indicated. Using an Envision® Multilabel plate reader (PerkinElmer), Terbium was excited at 340 nm. After a 50 μs time delay, terbium emission was read at 486 nm and Venus emission was read at 520 nm. Data were measured in triplicate. Error bars represent standard deviation. **A)** TR-FRET signal was recorded as the ratio of 520 nm to 486 nm emission. (For convenience, the ratios were multiplied by an arbitrary factor of 10,000.) **B)** Venus fluorescence was also measured as an indicator of relative Ven-Rictor expression levels. Venus was excited at 485 nm and Venus emission was read at 535 nm. Data were measured in triplicate. Error bars represent standard deviation. **C)** Western Blot to determine relative GST and GST-mTOR expression levels

A

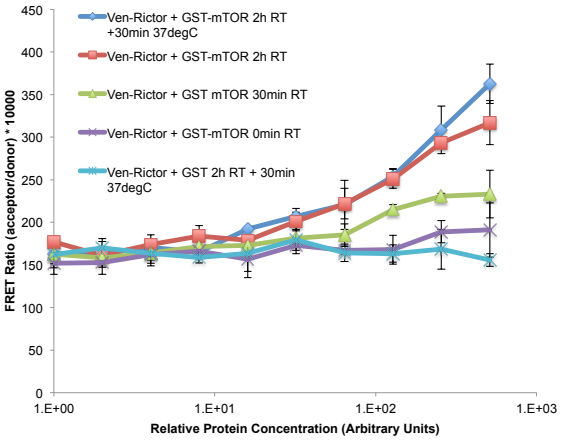
Ven-Rictor + GST-mTOR 2h RT +30min 37degC
Ven-Rictor + GST-mTOR 2h RT
Ven-Rictor + GST mTOR 30min RT
Ven-Rictor + GST-mTOR 0min RT
Ven-Rictor + GST 2h RT + 30min 37degC
FRET Ratio (acceptor/donor) * 10000
450
400
350
300
250
200
150
100
50
0
1.E+00
1.E+01
1.E+02
1.E+03
Relative Protein Concentration (Arbitrary Units)

B

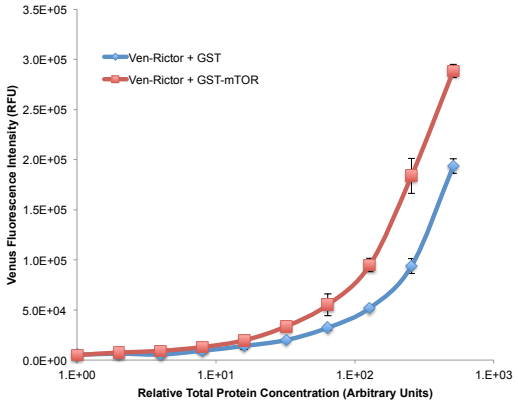
Ven-Rictor + GST
Ven-Rictor + GST-mTOR
Venus Fluorescence Intensity (RFU)
3.5E+05
3.0E+05
2.5E+05
2.0E+05
1.5E+05
1.0E+05
5.0E+04
0.0E+00
1.E+00
1.E+01
1.E+02
1.E+03
Relative Total Protein Concentration (Arbitrary Units)

C

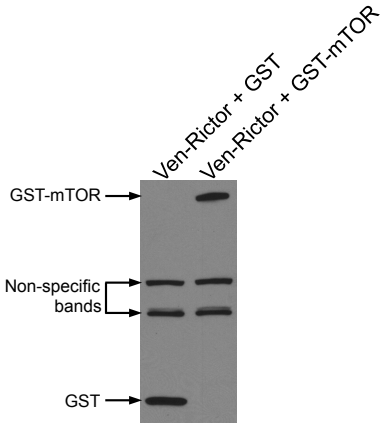
Ven-Rictor + GST
Ven-Rictor + GST-mTOR
GST-mTOR
Non-specific bands
GST

Figure 3-3. mTOR HEAT repeat domain residues 99-180 are necessary for Rictor binding as determined by GST-Pull-Down. A) Diagram of mTOR protein domains and GST-tagged truncation constructs generated **B)** HEK293T cells were transfected with plasmids encoding myc-Rictor and the indicated GST-tagged mTOR truncations. GST-tagged proteins were precipitated from whole-cell lysates using glutathione-conjugated beads. The inputs and eluates were processed via SDS-PAGE. myc-Rictor and GST-tagged mTOR truncations were detected via Western Blotting.

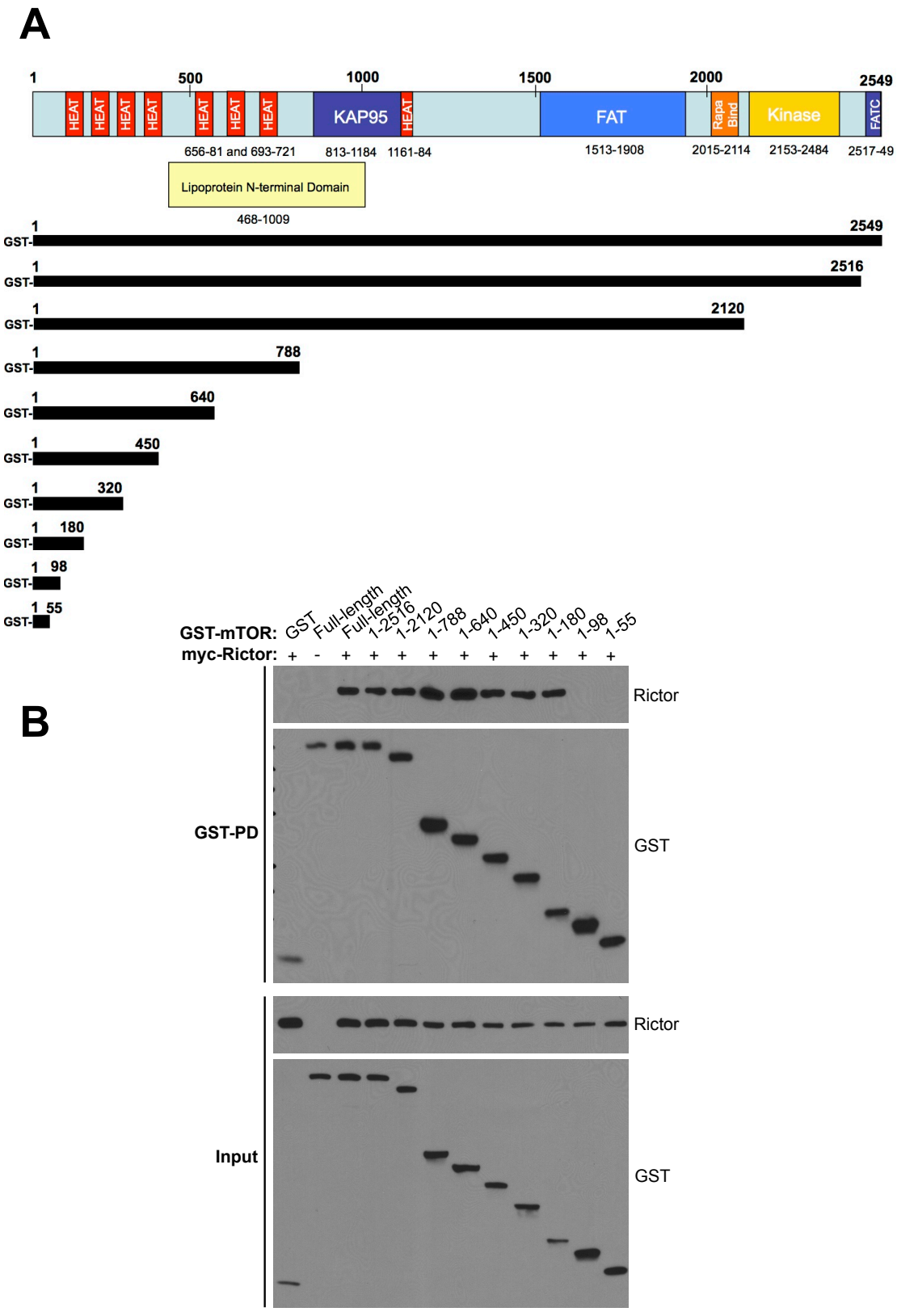
A
1
500
1000
1500
2000
2549
HEAT
KAP95
FAT
Rapa Bind
Kinase
FATC
656-81 and 693-721
813-1184
1161-84
1513-1908
2015-2114
2153-2484
2517-49
Lipoprotein N-terminal Domain
468-1009
GST-
2549
2516
2120
788
640
450
320
180
98
55
B
GST-mTOR:
myc-Rictor:
GST
Full-length
Full-length
1-2516
1-2120
1-788
1-640
1-450
1-320
1-180
1-98
1-55
Rictor
GST-PD
GST
Rictor
Input
GST

Figure 3-4. mTOR HEAT repeat domain residues 99-180 are necessary for Rictor binding as determined by TR-FRET. Whole-cell lysates of HEK293T cells co-expressing GST and Venus-Rictor or GST-mTOR truncations and Venus-Rictor, as indicated, were prepared in a series of 2-fold serial dilutions in a 384-well plate and incubated with Terbium-conjugated anti-GST antibody for 16h at ambient temperature. Using an Envision® Multilabel plate reader (PerkinElmer), Terbium was excited at 340 nm. After a 50 μs time delay, terbium emission was read at 486 nm and Venus emission was read at 520 nm. Data were measured in triplicate. Error bars represent standard deviation. **A)** TR-FRET signal was recorded as the ratio of 520 nm to 486 nm emission (For convenience, the ratios were multiplied by an arbitrary factor of 10,000). **B)** Venus fluorescence was also measured as an indicator of relative Ven-Rictor expression levels. Venus was excited at 485 nm and Venus emission was read at 535 nm. Data were measured in triplicate. Error bars represent standard deviation. **C)** Western Blot to determine relative GST and GST-mTOR truncation expression levels

A

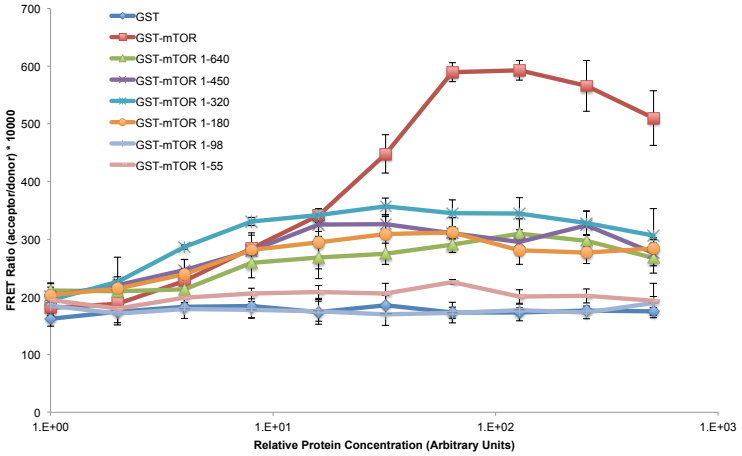
GST
GST-mTOR
GST-mTOR 1-640
GST-mTOR 1-450
GST-mTOR 1-320
GST-mTOR 1-180
GST-mTOR 1-98
GST-mTOR 1-55
FRET Ratio (acceptor/donor) * 10000
700
600
500
400
300
200
100
0
1.E+00
1.E+01
1.E+02
1.E+03
Relative Protein Concentration (Arbitrary Units)

B

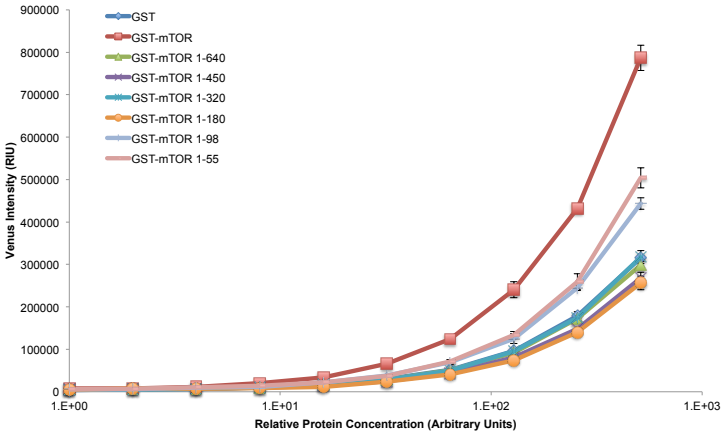
GST
GST-mTOR
GST-mTOR 1-640
GST-mTOR 1-450
GST-mTOR 1-320
GST-mTOR 1-180
GST-mTOR 1-98
GST-mTOR 1-55
Venus Intensity (RIU)
900000
800000
700000
600000
500000
400000
300000
200000
100000
0
1.E+00
1.E+01
1.E+02
1.E+03
Relative Protein Concentration (Arbitrary Units)

C

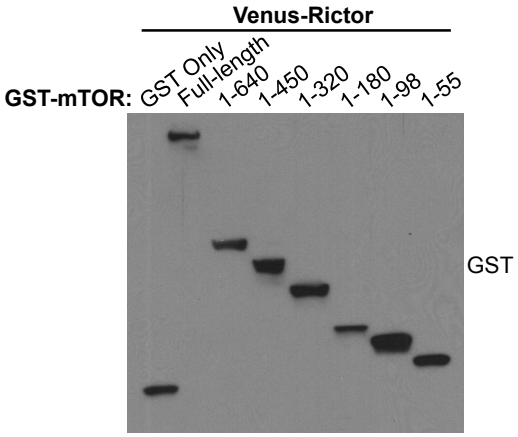
Venus-Rictor
GST-mTOR:
GST Only
Full-length
1-640
1-450
1-320
1-180
1-98
1-55
GST

Figure 3.5. TR-FRET detects disruption of the mTOR-Rictor interaction by a truncated form of mTOR. Whole-cell lysates of HEK293T cells expressing the indicated constructs were prepared in a series of 2-fold serial dilutions in a 384-well plate and incubated with Terbium-conjugated anti-Flag antibody for 4 hours at ambient temperature. Using an Envision® Multilabel plate reader (PerkinElmer), Terbium was excited at 340 nm. After a 50 μs time delay, terbium emission was read at 486nm. Following another 50 μs time delay, Venus emission was read at 520 nm. Data were measured in triplicate. Error bars represent standard deviation. **A)** The use of Flag-mTOR produces a larger assay window (~6-fold over background) than GST-mTOR (~3-fold over background) (See **Figure 3-3A**). Flag-PRAS40 was used as a negative control because PRAS40 is known to associate only with Raptor, and not with Rictor. **B)** Disruption of the Flag-mTOR-Ven-Rictor interaction by GST-mTOR 1-640 is detected by TR-FRET.

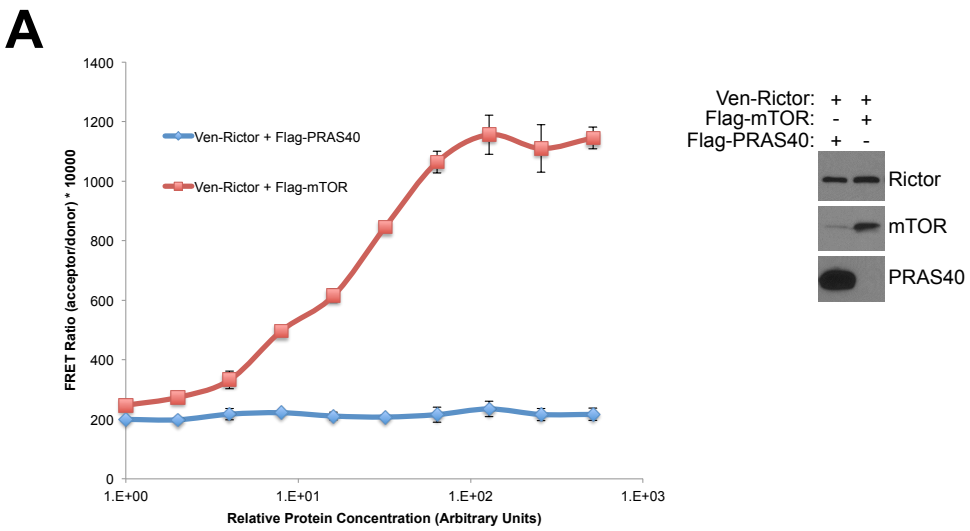
A
1400
1200
1000
800
600
400
200
0
FRET Ratio (acceptor/donor) * 10000
Ven-Rictor + Flag-PRAS40
Ven-Rictor + Flag-mTOR
1.E+00
1.E+01
1.E+02
1.E+03
Relative Protein Concentration (Arbitrary Units)
Ven-Rictor: + +
Flag-mTOR: - +
Flag-PRAS40: + -
Rictor
mTOR
PRAS40

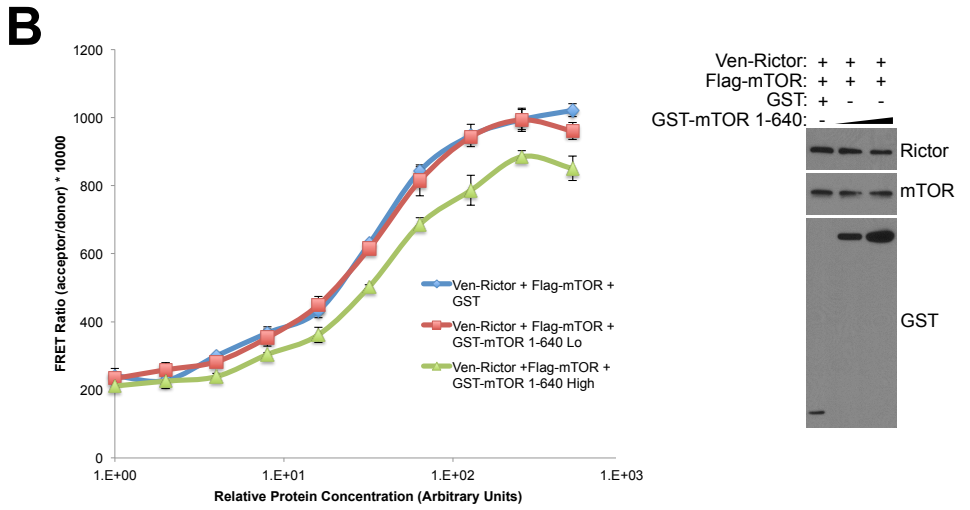
B
1200
1000
800
600
400
200
0
FRET Ratio (acceptor/donor) * 10000
Ven-Rictor + Flag-mTOR + GST
Ven-Rictor + Flag-mTOR + GST-mTOR 1-640 Lo
Ven-Rictor +Flag-mTOR + GST-mTOR 1-640 High
1.E+00
1.E+01
1.E+02
1.E+03
Relative Protein Concentration (Arbitrary Units)
Ven-Rictor: + + +
Flag-mTOR: + + +
GST: + - -
GST-mTOR 1-640: -
Rictor
mTOR
GST

CHAPTER 4

Nuclear PRAS40 links the Akt-mTORC1 signaling axis to the RPL11-HDM2-p53 nucleolar stress response pathway to suppress cellular senescence

4.1 Introduction

The Proline-Rich Akt Substrate of 40kDa (PRAS40) has recently been identified as a member and inhibitor of the mechanistic Target of Rapamycin Complex 1 (mTORC1), a kinase whose activity is known to promote protein synthesis and cell growth. Biochemical methods have rigorously demonstrated that PRAS40 can inhibit mTORC1 activity (51-57). These findings suggest a tumor suppressive function for PRAS40, as two other negative inhibitors of mTORC1, LKB1 and TSC2, are *bona fide* tumor suppressors (96-99). However, nearly all studies of PRAS40 function at the cellular and organismal level suggest a pro-survival and pro-tumorigenic function for PRAS40. *In vivo* overexpression of PRAS40 promotes neuronal survival in rodent models of spinal cord injury and stroke (100-102). PRAS40 levels have been found to be upregulated and correlated with disease severity in melanoma. Importantly, PRAS40 knock-down (KD) in a murine xenograft model of melanoma decreases tumorigenesis to the same extent as KD of Akt3, the primary Akt isoform activated in melanoma (103). Furthermore, PRAS40 is also upregulated in Ewing sarcoma cells and PRAS40 KD inhibits the pro-proliferative effect of EWS protein disruption (104). Additionally, unpublished findings from our lab show that total PRAS40 levels are upregulated in lung cancer patient tumor samples relative to patient-matched non-cancerous tissue. This study also finds that PRAS40 levels are positively correlated with poor patient survival. Because PRAS40 displays pro-tumorigenic activity through an unknown mechanism and the function of mTORC1-dissociated PRAS40 is completely unknown, I hypothesized that phosphorylated, mTORC1-dissociated PRAS40 has its own pro-survival function, independent of its ability to inhibit mTORC1. To explore this possibility I have studied

the subcellular localization and interactome of PRAS40. My findings identify nuclear PRAS40 as a link between the Akt-mTOR signaling axis and the RPL11-HDM2-p53 nucleolar stress response pathway and provide a potential explanation for PRAS40's pro-tumorigenic function.

4.2 Materials and Methods

Plasmids

pDONR201, pDEST27, BP Clonase II, and LR CLonase II are all products of the Gateway® Cloning System, Invitrogen. Human PRAS40 cDNA was obtained by PCR from a tumor cDNA library. A SNP causing substitution of Pro for Ala at residue 47 was identified by sequencing. This SNP was corrected by site-directed mutagenesis using the QuikChange Lightning Kit (Stratagene). The corrected PRAS40 cDNA was PCR amplified and inserted into pDONR201 through a BP Reaction to generate a PRAS40 Entry Clone. The PRAS40 Entry Clone was then used in LR Reactions with either pSCM167 (described above in section **2.2**), pJJH24 (described above in section **2.2),** or pDEST27 to generate plasmids encoding Flag-PRAS40, Venus-Flag-PRAS40, and GST-PRAS40, respectively, for mammalian expression. PRAS40 truncations were generated via introduction of a stop codon during PCR amplification of the desired region of PRAS40 sequence. The PCR products were then introduced into pDONR201 through BP reactions to generate PRAS40 truncation Entry Clones. LR reactions were performed using these Entry Clones together with either pJJH24 or pDEST27 to generate plasmids encoding Venus-Flag-PRAS40 truncations or GST-PRAS40 truncations, respectively, for mammalian expression. PRAS40 deletions were generated via deletional site-directed

mutagenesis using the QuikChange Lightning Kit (Stratagene) and the PRAS40 Entry Clone as a template to generate PRAS40 deletion Entry Clones. These Entry Clones were then used together with pJJH24 in LR reactions to generate plasmids encoding Venus-Flag-PRAS40 deletions (Δ28-31 and Δ218-227) for mammalian expression. PRAS40 point mutations were generated via site-directed mutagenesis using the QuikChange Lightning Kit (Stratagene) and the PRAS40 Entry Clone as a template to generate PRAS40 point mutant Entry Clones. These Entry Clones were then used together with pSCM167 in LR reactions to generate plasmids encoding Flag-PRAS40 point mutants (F129A, S183A, S212A, S221A, and T246A) for mammalian expression. To generate C-terminally tagged PRAS40-HA-Flag, PRAS40 was PCR amplified from the PRAS40 Entry Clone using primers that removed the stop codon and added the HA-Flag tag followed by a stop codon. This PCR product was then ligated into pcDNA3.1 using traditional restriction site digestion and DNA ligase-mediated sub-cloning. N-terminally tagged Flag-HA-PRAS40 was generated in a similar manner.

Human RPL11 cDNA was kindly provided by Dr. Yue Xiong, University of North Carolina at Chapel Hill (Addgene Plasmid 20936). RPL11 cDNA was PCR amplified and sub-cloned into pDONR201 using a BP reaction to generate an RPL11 Entry Clone. This Entry Clone was then used with pJJH22 (like pJJH24 in section **2.2**, but with pDEST26 as the backbone, thus introducing a His_6 tag instead of Flag) in an LR reaction to generate a plasmid encoding Venus-His_6-RPL11 for mammalian expression. All plasmids generated were confirmed by sequencing.

Non-silencing, PRAS40-targeted, and RPL11-targeted shRNA plasmids were purchased from Open Biosystems. PRAS40 shRNA 2 corresponds to clone

V3LHS_340055; PRAS40 shRNA 3 corresponds to clone V2LHS_138819. PRAS40 shRNA clone V3LHS_408646 was used in the cycloheximide/MG132 experiment. RPL11 shRNA 1 corresponds to clone V2LHS_131577; RPL11 shRNA 2 corresponds to clone V3LHS_383206.

p53 shRNA was kindly provided by Dr. William Hahn, Harvard Medical School (Addgene Plasmid 10672). p53 luciferase reporters – PG13Py-Luc ("wt") and MG15Py-Luc ("Mut") – were kindly provided by Dr. Bert Vogelstein, Howard Hughes Medical Institute and Johns Hopkins Medical Institute (Addgene Plasmids 16442 and 16443, respectively).

Cell Culture

HeLa cervical adenocarcinoma cells (ATCC CCL-2) were maintained in DMEM (Cellgro) supplemented with 10% FBS and 1x Penicillin/Streptomycin Solution (Cellgro) at 37°C and 5% CO_2 in humidified conditions. U2OS osteosarcoma cells (ATCC HTB-96) were maintained in McCoy's 5A media (Cellgro) supplemented with 10% FBS and 1x Penicillin/Streptomycin Solution (Cellgro) at 37°C and 5% CO_2 in humidified conditions. For serum starvation, cells were rinsed two times with serum-free media and grown in serum-free media for 24 hrs. For Leu/Met starvation and rescue, cells were rinsed twice in DMEM lacking Leu and Met (Pierce 30030) but containing 10% dialyzed FBS (Sigma F0392) and grown in this media for 6.5 hrs. The media was changed to complete growth media containing either no additive, 0.01% DMSO, or 20nM Rapamycin for 2 hrs.

SDS-PAGE and Western Blotting

These methods were performed as described in section **3.2**, although 1.5 mm, 15-well, hand-cast 12% polyacrylamide gels were used here in some cases. The primary antibodies used are as follows:

Rabbit anti-PRAS40, IBL

Rabbit anti-PARP, Cell Signaling, 9542

Mouse anti-GAPDH, Chemicon/Millipore

Rabbit anti-Calnexin, Cell Signaling, 2433

Rabbit anti-RPL11, Abcam, ab79352

Rabbit anti-Raptor, Millipore, 09-217

Rabbit anti-14-3-3 epsilon, Santa Cruz, sc-1020

Rabbit anti-pan-14-3-3, Santa Cruz, sc -629

Mouse anti-HSP90, Santa Cruz, sc-13119

Mouse anti-Flag, Sigma M2

Rabbit anti-mTOR, Cell Signaling, 2972

Rabbit anti-GST, Santa Cruz, sc-459

Rabbit anti-phospho-PRAS40 T246, Invitrogen

Rabbit anti-phospho-PRAS40 S183, IBL

Mouse anti-HA, Santa Cruz, sc-7392

Rabbit anti-phospho-p70, Cell Signaling, 9205

Rabbit anti-p70, Cell Signaling, 2708

Mouse anti-p53, Cell Signaling, 2524

Mouse anti-p21, Cell Signaling, 2946

Rabbit anti-Bax, Cell Signaling 5023

Mouse anti-β-actin, Sigma, A2228

Transfections

FuGene HD (Roche) was used in a ratio of 3 (μL FuGene HD) to 1 (μg DNA) for HeLa cells according to the manufacturer's instructions. XtremeGene XP (Roche) was used in a ratio of 2 (μL XtremeGene HP) to 1 (μg DNA) for U2OS cells according to the manufacturer's instructions. Cells were transfected when they had grown to ~80% confluency.

Sucrose Cushion Sub-cellular Fractionation

This procedure was performed essentially as previously described with slight modification (118). 7x10^5 HeLa cells were seeded in a 10cm dish and allowed to grow for 40 hours. Cells were rinsed with ice cold PBS [137 mM NaCl, 2.7 mM KCl, 10 mM Na_2HP0_4, 1.8 mM KH_2PO_4, pH 7.4] and scraped into 5 mL PBS. 1 mL of the cell suspension was set aside for whole-cell lysate. Cell suspensions were spun down at 500 x g for five minutes at 4°C. Pellets for whole-cell lysates were resuspended in 100 μL RIPA Buffer [1% Triton X, 0.5% sodium deoxycholate, 0.1% SDS, 500 mM NaCl, 50 mM Tris pH 7.5, 2 mM EDTA, 5 mM sodium pyrophosphate, 2 mM sodium orthovanadate, 1 mM PMSF, 10 μg/mL aprotinin, and 10 μg/mL leupeptin], incubated at 4°C for one hour and spun down at 16,100 x g. The supernatant was saved as whole-cell lysate. The pellet from the remainder of the cell suspension was subjected to sub-cellular fractionation. This cell pellet was resuspended in 1 mL Sucrose Buffer I [320 mM

sucrose, 3 mM CaCl2, 2 mM magnesium acetate, 0.1 mM EDTA, 10 mM Tris-Cl pH 8.0, 0.45% CHAPS, 1 mM dithiothreitol, 5 mM sodium pyrophosphate, 2 mM sodium orthovanadate, 1 mM PMSF, 10 μg/mL aprotinin, and 10 μg/mL leupeptin] and transferred to an ice cold Dounce Homogenizer. The cell suspension was subjected to 25 strokes of the "B" pestle. 5 μL was examined for Tryphan Blue staining using light microscopy to ensure that the plasma membranes were efficiently lysed and that the nuclei were still intact. This suspension was then transferred to a 1.7 mL microcentrifuge tube and spun down at 3,000 x g for five minutes at 4 °C. The supernatant was saved as the post-nuclear (cytoplasmic) fraction. The nuclear pellet was resuspended in 2.5 mL of Sucrose Buffer I. 2.5 mL of Sucrose Buffer II [2M sucrose, 5 mM magnesium acetate, 0.1 mM EDTA, 10 mM Tris-Cl pH 8.0, 1 mM dithiothreitol, 5 mM sodium pyrophosphate, 2 mM sodium orthovanadate, 1 mM PMSF, 10 μg/mL aprotinin, and 10 μg/mL leupeptin] was added to this suspension. 4.4. mL Sucrose Buffer II was added to a polyallomer ultracentrifuge tube (Beckman). The nuclear suspension was poured carefully on top of the Sucrose Buffer II "cushion." The cell suspension was then spun down in an SW41Ti Swinging Bucket Rotor (Beckman) in an ultracentrifuge at 13,200 rpm (30,000 x g) for 45 min at 4°C. The supernatant was discarded and the nuclear pellet was suspended in 100 μL RIPA Buffer. Protein concentrations of whole-cell lysate, post-nuclear fraction, and nuclear fraction were determined by the BCA Assay (Pierce). 11 μg of each fraction was resolved by SDS-PAGE and analyzed by Western Blotting.

Large-scale Sub-cellular Fractionation and Flag-Immunoprecipitation for Mass Spectrometry Analysis

45 15-cm dishes were seeded with 2.4 x 10^6 HeLa cells per dish. 48 hours later, fifteen dishes were transfected with 16 μg Flag-HA-PRAS40 per dish, another fifteen were transfected with 16 μg PRAS40-HA-Flag per dish, and the remaining fifteen were left untransfected. 36 hours later, the cells were rinsed once with 10 mL ice cold PBS per dish and scraped and resuspended in 4 mL ice cold PBS containing Phosphatase Inhibitors Cocktails 2 and 3 and Protease Inhibitors Cocktail (Sigma) in a 1:500 dilution. Suspensions from each transfection group were pooled and spun down at 500 x g for five minutes at 4°C. The pellets were resuspended in 15 mL Sucrose Buffer I, transferred to an ice cold Dounce Homogenizer, and subjected to ten strokes of the "B" pestle. The suspension was checked for Trypan Blue staining by light microscopy to ensure the plasma membranes were efficiently lysed and that the nuclei remained intact. The resulting nuclear suspensions were spun down at 750 x g for five minutes at 4°C. The supernatants were collected and saved as cytoplasmic fractions. 7 mL CHAPS Buffer [40 mM HEPES pH 7.5, 120 mM NaCl, 1 mM EDTA, 0.3% CHAPS, 1:500 each of Sigma Phosphatase Inhibitor Cocktails 2 and 3 and Protease Inhibitor Cocktail] was added to the cytoplasmic fractions. Nuclear pellets were suspended in 5 mL Nuclear Lysis Buffer [20 mM HEPES pH 7.9, 300 mM NaCl, 2.5% glycerol, 1 mM EDTA, 0.5 mM dithiothreitol, 1:500 each of Sigma Phosphatase Inhibitor Cocktails 2 and 3 and Protease Inhibitor Cocktail] and subjected to three freeze/thaw cycles: -86°C to ambient temperature to lyse the nuclei. 17 mL CHAPS Buffer was then added to dilute the nuclear fractions and equilibrate the salt and detergent concentrations between the cytoplasmic and nuclear fractions. The cytoplasmic and nuclear fractions were clarified by ultracentrifugation in polyallomer tubes in a SW41Ti swinging bucket rotor at 24,200 rpm (100,000 x g) at 4°C

for 30 minutes. 200 μL of each fraction was saved as input. 500 μL 50% anti-Flag-agarose (Sigma) slurry was added to each clarified fraction. IPs proceeded for 2.5 hours at 4°C with gentle rotation. Beads were spun down at 3,000 x g for two minutes at 4°C and washed three times in SigmaPrep spin tubes with CHAPS Buffer (spun down at 3,000 x g for 30 seconds at 4°C between washes). Flag-PRAS40 and associated proteins were eluted using 3x Flag peptide according to the manufacturer's instructions (Sigma). Eluates were divided into four aliquots and subjected to acetone precipitation in polypropylene microcentrifuge tubes. A 4x volume of -20°C acetone was added to each tube. The tubes were vortexed and incubated at -20°C for one hour, then spun down at 13,000 x g for 10 min at 4 °C. The acetone was carefully decanted and the pellets were allowed to dry at ambient temperature for 45 minutes. Dried pellets were resuspended in 10 μL 1xSDS loading buffer. Eluates aliquoted from the same sample were pooled (to give 40 μL of eluate per sample) and boiled for four minutes.

Eluate Analysis by Liquid Chromatography – Tandem Mass Spectrometry (LC-MS/MS)

The analysis was essentially carried out using a previously optimized proteomics platform (119). 20 μL (50%) of each eluate was resolved on an SDS gel followed by in-gel tryptic digestion. Peptide samples were analyzed by nanoscale LC-MS/MS on an LTQ mass spectrometer (Thermo Finnigan). Peptides were dissolved in buffer A [0.4% acetic acid, 0.005% heptafluorobutyric acid, and 5% acetonitrile], loaded onto a 75 μm (inside diameter) × 10 cm C18 column (5 μm magic C18AQ; pore size, 200 Å; Michrom Bioresources, Auburn, CA), and then eluted during a gradient from 10 to 30% buffer B [0.4% acetic acid, 0.005% heptafluorobutyric acid, and 95% acetonitrile, at a flow rate

of ~250 nL/min]. Eluted peptides were analyzed by a standard TOP10 MS/MS method. The acquired MS/MS spectra were searched against a human protein database for identification. The matched peptides/proteins were further filtered by mass accuracy and matching scores to reduce protein false discovery rate to less than 1%. (Note: Mass spectrometry analysis was performed by Dr. Dongmei Cheng in the laboratory of Dr. Junmin Peng.)

Other Sub-cellular Fractionation and Immunoprecipitation Studies

Other Flag-IP studies followed the same procedure as for the large-scale approach, except that between one and three 15-cm culture dishes of HeLa cells were used per sample and buffer volumes were scaled down accordingly. For endogenous PRAS40 immunoprecipitation, five 15-cm culture dishes of HeLa cells were used. Nuclear and cytoplasmic fractions were divided into three aliquots of equal volume. 10 μL rabbit monoclonal anti-PRAS40 antibody (Cell Signaling, 2691) was added to one aliquot, 10 μL of the same antibody pre-incubated for one hour with 3 μL of immunogenic PRAS40 peptide (Cell Signaling, 1 μg/μL) was added to another aliquot, and 3.75 μL (equivalent IgG mass) non-specific rabbit IgG (Santa Cruz) was added to the third aliquot. These samples were rotated slowly at 4°C for three hours. 50 μL of a 50% slurry of Protein A-conjugated beads was added, and the samples were rotated for another hour. Beads were washed three times in Sigma Prep spin columns with CHAPS Buffer and eluted by boiling in 30 μL 3xSDS loading buffer for four minutes. Inputs and IPs were resolved via SDS-PAGE and analyzed by Western Blotting.

Sub-cellular Fractionation and Gel Filtration Chromatography

7 x 10^6 HeLa cells were seeded in five 15-cm dishes and were left untransfected. Sub-cellular fractionation was performed as above for the large-scale Flag-IP. Nuclear extract was concentrated using a 15 mL Concentration Filter Tube, 10,000 MWCO (Amicon) according to the manufacturer's instructions. During the concentration process the buffer was exchanged to CHAPS Buffer. The concentrated nuclear extract was filtered through a 0.2 μm filter using a syringe. 700 μL concentrated nuclear extract was loaded in a 0.5 mL injection loop for injection onto a 25 mL Superose 6 column using the Äkta Purifier FPLC system (GE Healthcare). The loop was emptied with 0.75 mL running buffer [10 mM HEPES pH 7.45, 137 mM NaCl, 2.5% glycerol, filtered and degassed] and the samples were resolved on the Superose 6 column at a rate of 0.3 mL/minute. 0.5 mL fractions were collected and 30 μL aliquots of the odd-numbered fractions were resolved by SDS-PAGE and analyzed via Western Blotting.

Indirect Immunofluorescence and Confocal Microscopy

3 x 10^5 U2OS or HeLa cells were grown on poly-D-lysine-coated 18 mm glass coverslips in 12-well cell culture plates (Corning) and transfected with 500 ng Ven-Flag-PRAS40, Ven-Flag-PRAS40^{F129A}, Ven-His$_6$-RPL11, Flag-HA-PRAS40, or a combination of the latter two and allowed to express the fusion proteins for 24 hrs (Ven-PRAS40 plasmids) or 48 hrs (Ven-RPL11 plasmids). The Ven-PRAS40 samples were treated with Leptomycin B (LMB) or EtOH (vehicle) as indicated. Cells were protected from light throughout all procedures to avoid photobleaching the Venus-tagged fusion proteins. Cells were fixed by incubation in 4% paraformaldehyde in PBS for 15 min.

Cells were rinsed three times with PBS. At this point, cells expressing only Venus-fusion proteins were stained with 1μg/mL Hoechst 33342 and mounted onto glass slides using Anti-Fade Gold (Invitrogen) according to the manufacturer's instructions. Cells expressing Flag-HA-PRAS40 were solubilized and blocked by incubation in PBS containing 0.2% TritonX-100 and 3% BSA for 30 minutes at ambient temperature. These cells were rinsed once in PBS and were incubated in primary antibody (1:500 mouse anti-Flag, Sigma M2, in 3% BSA/PBS) for four hours at ambient temperature (protected from light). The coverslips were washed three times with PBS and incubated with secondary antibody (1:500 anti-mouse-Texas Red, Invitrogen, in 3% BSA/PBS) containing 1 μg/mL Hoechst 33342 for 30 minutes at ambient temperature (protected from light). The coverslips were washed three times with PBS and mounted onto glass slides using Anti-Fade Gold (Invitrogen) according to the manufacturer's instructions. Once the slides had cured for 24 hours, images were acquired using a Zeiss LSM 510 inverted confocal microscope.

Epifluorescence Microscopy

Images were captured using an Image Express^{Micro} high-throughput microscope (Molecular Devices).

GST Pull-Down

This procedure was performed as in section **3.2**, except that HeLa cells were used instead of HEK293T cells.

shRNA-mediated Knock-downs and Whole-cell Lysate Preparation

U2OS cells were transfected with the indicated shRNA plasmids. shRNAs were allowed to express for 48 hours. Transfected cells were then selected by incubation in growth media containing 2 μg/mL puromycin. Selection was carried out for four days. The selection media was renewed once during selection. Whole-cell lysates of selected U2OS cells were prepared by rinsing the cells twice with ice-cold PBS, then scraping the cells into M-Per Cell Extraction Buffer (Pierce) supplemented with 150 mM NaCl and 1:500 each of Phosphatase Inhibitor Cocktails 2 and 3 and Protease Inhibitor Cocktail (Sigma).

Luciferase Reporter Assay

U2OS cells were grown in 12-well cell culture dishes and co-transfected with 500 ng of the indicated shRNA plasmids and 250 ng of the indicated reporter construct. Total DNA was kept constant at 1.25 μg per well by the addition of non-silencing shRNA plasmid where necessary. Transfected cells were selected as described above. Cells were lysed in Glo Lysis Buffer (Promega) supplemented with 1:500 Protease Inhibitor Cocktail (Sigma) at ambient temperature according to the manufacturer's instructions. Protein concentration was measured by the BCA assay (Pierce) and concentrations were normalized by addition of Glo Lysis Buffer as necessary. Normalized lysates were transferred in triplicate to wells of an opaque, white-walled 96-well plate (Falcon). Bright-Glo™ Reagent (Promega) was added in a 1:1 (v:v) ratio and luminescence was measured immediately using an Envision® Multilabel plate reader (PerkinElmer) with a 0.1 sec integration time.

X-Gal Staining for Senescence-Associated β-Galactosidase Activity

U2OS cells were grown in 6-well cell culture dishes transfected with 1 μg of each shRNA plasmid as indicated. Total DNA was kept constant at 2 μg per well by the addition of non-silencing shRNA plasmid where necessary. Transfected cells were selected as described above. X-gal staining for senescence-associated β-galactosidase activity was performed using the Senescence β-galactosidase Staining Kit from Cell Signaling (9860) according to the manufacturer's instructions. A pH meter was used to ensure that the staining solution was at a pH between 5.9 and 6.0 and staining was allowed to proceed for 24 hours in a "dry" 37°C incubator without CO_2 control or humidified conditions. Cells were then rinsed twice with PBS and covered with 70% glycerol for long-term storage. Images were captured using a Zeiss Axiovert inverted microscope. Cells were scored and counted by two blinded, impartial investigators. Nine sites per well were counted in each experiment.

4.3 Results

4.3.1 PRAS40 dynamically shuttles between the cytoplasm and the nucleus.

Although mTORC1 is thought to function primarily in the cytoplasm, various reports have indicated that PRAS40 and other mTORC1 components can be found in the nucleus (100; 101; 120-127). To rigorously test the subcellular localization of PRAS40, I purified nuclei from HeLa cells by centrifuging through a sucrose cushion. The nuclear fraction obtained via this method is void of cytosolic and endoplasmic reticulum (ER) contamination as evidenced by lack of the marker proteins GAPDH and calnexin,

respectively. As expected, PRAS40 is found in great abundance in the post-nuclear fraction. Importantly, I also detected a distinct population of PRAS40 present in the nuclear fraction, albeit in lower abundance (**Figure 4-1**). Because PRAS40 is theoretically small enough to freely diffuse between the cytoplasm and the nucleus (27kDa, despite running near 40kDa on SDS polyacrylamide gels) (128), I hypothesized that an active nuclear shuttling process is responsible for the concentration differential of PRAS40 between the cytoplasm and nucleus. To test this, I treated cells expressing Venus-PRAS40 with the nuclear export inhibitor Leptomycin B (LMB). As determined by confocal microscopy, PRAS40 accumulates in the nuclei of U2OS (**Figure 4-2**) and HeLa (**Figure 4-3**) cells treated with LMB, but not with vehicle control, suggesting that PRAS40 subcellular localization is controlled at least in part by active, dynamic nucleocytoplasmic shuttling. In all LMB experiments a portion of Ven-PRAS40 remains in the cytoplasm regardless of treatment time, suggesting that only a sub-population of PRAS40 is involved in nucleocytoplasmic shuttling. Importantly, no difference is observed between wild-type Venus-PRAS40 and Raptor-binding null Venus-PRAS40^{F129A} (52; 55; 56) in response to LMB treatment, suggesting that PRAS40 nucleocytoplasmic shuttling does not require interaction with mTORC1 (**Figure 4-4**).

4.3.2 PRAS40 residues 218-227 serve as a Nuclear Export Signal (NES) Sequence.

I next sought to identify Nuclear Localization or Nuclear Export Signal (NLS or NES) sequences responsible for PRAS40's dynamic nucleocytoplasmic shuttling. Deletion of the C-terminus of PRAS40 abolishes its subcellular concentration differential, producing a construct (Ven-PRAS40 1-110) that localizes in a diffuse pattern

throughout the cytoplasm and nucleus and is unresponsive to LMB treatment. Conversely, deletion of the N-terminus of PRAS40 (Ven-PRAS40 110-256) has no effect on its subcellular localization or response to LMB, suggesting that sequence motifs critical to subcellular localization lie in the C-terminus of PRAS40 (**Figure 4-5A**). Although PRAS40 residues ^{251}KLKRKY^{256} represent a potential NLS in the C-terminus, deletion of these residues induces no observable change in subcellular localization or response to LMB (data not shown). Sequence analysis identifies at least two putative NES sequences in PRAS40 – ^{28}LVLL^{31} in the N-terminus and, as noted by others (129; 130), ^{218}IAASMRALVL^{227} in the C-terminus. Deletion of residues 218-227, but not 28-31, results in diffuse cytoplasmic and nuclear localization of PRAS40, suggesting that residues 218-227 serve as a functional NES sequence in PRAS40 (**Figure 4-5B**).

4.3.3 PRAS40 is a member of a nuclear-specific RPL11-containing complex.

It is completely unknown what, if any, function PRAS40 may serve in the nucleus. The existence of proline-rich domains in its N-terminus and 14-3-3-binding phospho-sites in its C-terminus suggests that PRAS40 may participate in or serve as a scaffold for various protein-protein interactions. Therefore, I decided to probe the PRAS40 interactome of the cytoplasm and nucleus. To achieve this, I immunoprecipitated (IPed) N-terminally or C-terminally tagged Flag-PRAS40 from post-nuclear and nuclear fractions of HeLa cells. The eluates were subjected to tryptic digestion and analyzed by liquid chromatography-tandem mass spectrometry (**Figure 4-6A**). Eluates from post-nuclear and nuclear fractions of untransfected HeLa cells were used as negative controls. As expected, the known PRAS40 binding partner 14-3-3 was

identified in eluates from both the cytoplasm and nucleus, thus supporting the validity of this approach. **Table 4-1** lists all the potential PRAS40-associated proteins identified and their spectral counts averaged between N- and C-terminally tagged PRAS40 IPs in the nuclear and cytoplasmic fractions. To identify binding partners enriched in the nucleus we normalized spectral counts of putative binding partners ("prey") in each subcellular fraction to those of PRAS40 ("bait") from the same fraction. Any putative binding partner with a normalized nuclear to cytoplasmic ratio greater than 1 (or with zero cytosolic spectral counts) was identified as a potential nuclear-enriched PRAS40 binding partner (**Fig. 4-6B**). Of the identified proteins by this analysis, we chose to focus on ribosomal protein L11 (RPL11) because its average spectral count value is similar to that of some 14-3-3 isoforms, which are know PRAS40-binding proteins. Notably, despite their high cellular concentrations, no ribosomal proteins other than L11 were identified in our eluates. As predicted from the IP-MS results, endogenous RPL11 robustly co-precipitates with N-terminally- and C-terminally-tagged Flag-PRAS40 from nuclear, but not cytoplasmic extract (**Fig. 4-7A**). It is important to note that PRAS40 and RPL11 are both present in each subcellular fraction, thus supporting the notion that the PRAS40-RPL11 association is nuclear-specific. Furthermore, endogenous RPL11 co-precipitates with endogenous PRAS40 IPed from the nuclear, but not cytoplasmic fraction of untransfected HeLa cells (**Fig. 4-7B**). Neither non-specific IgG nor PRAS40-specific antibody pre-blocked with a PRAS40 peptide is capable of precipitating RPL11, supporting the specificity of the endogenous PRAS40-RPL11 association (**Fig. 4-7B**). In further support of a nuclear-specific association, Flag-PRAS40 co-localizes with Venus-RPL11 in the nucleoli of U2OS cells via confocal microscopy (**Fig. 4-8**).

4.3.4 The nuclear PRAS40- and RPL11-containing complex is distinct from mTORC1.

To determine whether the nuclear PRAS40-RPL11 co-precipitation represents a variant of the established mTOR Complex 1 or a novel complex independent of mTORC1, nuclear extract was isolated from HeLa cells and processed via gel filtration chromatography using a Superose 6 column in an FPLC setup. At least two separate peaks of PRAS40 were observed, representing different high molecular-weight complexes (**Figure 4-9**). The larger of these complexes is approximately 2600 kDa and co-migrates with the mTORC1 components mTOR and Raptor, but not RPL11. The smaller PRAS40 complex is approximately 450-700 kDa and co-migrates with RPL11, but not mTOR or Raptor. A second Raptor peak was observed around 100-200 kDa, most likely representing monomeric Raptor (predicted molecular weight = 150 kDa). These results suggest that the nuclear-specific PRAS40- and RPL11-containing complex is distinct from mTORC1 and may contain other, as-of-yet unidentified components.

4.3.5 The nuclear-specific PRAS40- and RPL11-containing complex requires PRAS40 residues S221 and T246 and is phosphorylation-dependent.

I next sought to identify the sequences or residues of PRAS40 critical for nuclear association with RPL11. In order to narrow down the binding region, constructs encoding GST-tagged PRAS40 truncations were generated and used in a GST pull-down (PD) assay to assess co-precipitation of endogenous RPL11. Notably, one binding determinant may be present within PRAS40 residues 98-109, as indicated by the sharp

increase in relative RPL11 co-precipitation between the 110-256 and 98-256 PRAS40 constructs (**Figure 4-10, Compare quantification of lanes 5 and 6)**. This short region contains a long string of negatively charged amino acids – ^{101}EDNEEDEDE^{109} – suggesting that electrostatic forces may contribute to the PRAS40-RPL11 association. This isn't altogether surprising, given that PRAS40 is an acidic protein, with a theoretical pI of 4.65, while RPL11 is basic, with a theoretical pI of 10.00. Additionally, deletion of C-terminal, but not N-terminal regions of PRAS40 abrogates RPL11 co-precipitation, indicating that sequences or residues critical for RPL11 binding are also likely found within the C-terminus, *i.e.* residues 171-256, of PRAS40 (**Figure 4-10**). Importantly, phosphorylation of residues within this C-terminal domain is known to control the interaction of PRAS40 with its established binding partners, Raptor and 14-3-3. Specifically, non-phosphorylated PRAS40 binds and inhibits mTORC1 through direct interaction with Raptor, while phosphorylation of PRAS40 at residues S221 and T246 promotes 14-3-3 binding and dissociation of the PRAS40-14-3-3 complex from mTORC1 (51-56; 58; 59). Therefore, I hypothesized that phosphorylation might also control the novel, nuclear-specific PRAS40- and RPL11-containing complex. To test this, Flag-PRAS40 plasmids harboring single, non-phosphorylatable Ser or Thr to Ala point mutations of all the major previously identified PRAS40 phosphorylation sites were generated. These sites include the mTORC1-targeted residues S183, S212, and S221, as well as the Akt-targeted residue T246 (52; 55-57). An F129A mutation in PRAS40's Tor Signaling (TOS) motif was also generated. This mutation is known to drastically attenuate the interaction of PRAS40 with Raptor/mTORC1 (52; 55; 56). The effect of each of these mutations on PRAS40-RPL11 and PRAS40-Raptor co-precipitation was

assessed by immunoblot analysis of Flag-PRAS40 immunocomplexes isolated from HeLa nuclear extracts. Mutation of PRAS40 F129, S183, and S212 has minimal effect on RPL11 association. However, mutation of the mTORC1-targeted residue S221 or the Akt-targeted residue T246 abolishes RPL11 binding, suggesting that these residues are critical for PRAS40-RPL11 association (**Figure 4-11**). Although PRAS40 residues S221 and T246 are clearly important, this finding does not directly implicate phosphorylation in the regulation of the PRAS40-and RPL11-containing complex. To address this issue, IP's of wt or T246A Flag-PRAS40 from HeLa nuclear extracts were performed using buffers either containing or lacking phosphatase inhibitors. The wild-type PRAS40-RPL11 co-precipitation, while robust in the presence of phosphatase inhibitors, is abolished in the absence of phosphatase inhibitors (**Figure 4-12, Lane 2 and 5**). As anticipated from the results shown in **Figure 4-11**, Flag-PRAS40^{T246A} fails to co-precipitate RPL11 regardless of the presence of phosphatase inhibitors (**Figure 4-12, Lanes 3 and 6**). Importantly, use of a phospho-specific antibody confirms that the absence of phosphatase inhibitors does in fact abolish phosphorylation of PRAS40 at T246 (**Figure 4-12, compare Input Lanes 2 and 5**). Taken together, these results indicate that the nuclear PRAS40- and RPL11-containing complex not only requires PRAS40 residues S221 and T246, but is phosphorylation-dependent as well.

4.3.6 The nuclear-specific PRAS40- and RPL11-containing complex is controlled by amino acids and serum factors through the kinase activities of mTORC1 and Akt. Because PRAS40 residues S221 and T246 are known targets of mTORC1 (57) and Akt (58), respectively, I hypothesized that these kinases and their upstream

microenvironmental activators can regulate the nuclear PRAS40- and RPL11-containing complex. PI3K-Akt signaling is potently activated by growth factors found in serum. As demonstrated by Flag-PRAS40 coIP from HeLa nuclear extracts, serum withdrawal reduces PRAS40-RPL11 co-precipitation to background levels. This effect of serum withdrawal is negated by expression of constitutively active Akt (HA-AktΔPH) during serum withdrawal, whereas expression of dominant negative Akt (HA-Akt^{K179M}) abolishes PRAS40-RPL11 co-precipitation in the presence of serum (**Figure 4-13**). mTORC1 kinase activity requires both growth factors and an ample supply of extracellular nutrients such as amino acids and glucose. To specifically manipulate mTORC1 activity without significantly affecting Akt, HeLa cells were incubated in media lacking Leu and Met but replete with serum. Nuclear PRAS40-RPL11 co-precipitation is enhanced by stimulation with Leu- and Met-rich media (**Figure 4-14, Lanes 1 and 2**). This effect is robustly inhibited by treatment with the potent and specific mTORC1 inhibitor rapamycin, but not vehicle (DMSO) control (**Figure 4-14**). It is important to note that upon rapamycin treatment (**Figure 4-14, Lane 4**) mTORC1 activity is suppressed as evidenced by disruption of p70^{S6K} and PRAS40^{S183} phosphorylation, while Akt remains active as demonstrated by continuous phosphorylation of PRAS40^{T246}. This finding suggests that inhibition of mTORC1 activity alone is sufficient to disrupt the nuclear PRAS40- and RPL11-containing complex. Together with the point mutation studies (**Figures 4-11 and 4-12**), these findings indicate that the nuclear PRAS40- and RPL11-containing complex requires the amino acid- and serum-stimulated kinase activities of both mTORC1 and Akt.

4.3.7 PRAS40 negatively regulates p53 protein stability and activity in an RPL11-dependent manner.

It is unknown what, if any, effect PRAS40 might have on nuclear RPL11 function. In addition to its role in protein synthesis as a component of the ribosome, RPL11 is also a key signaling molecule in communicating aberrant ribosome biogenesis to the cellular stress response machinery. Specifically, when ribosome assembly is disrupted (a condition referred to as nucleolar stress) RPL11 translocates from the nucleoli to the nucleoplasm where it binds and inhibits the E3 ubiquitin ligase HDM2. This triggers protein stabilization of HDM2's primary target, the tumor suppressor p53, leading to cell cycle arrest, senescence, or apoptosis mediated by p53's transcriptional targets (87-90; 94; 131; 132). Because PRAS40 displays pro-survival (100-102) and pro-tumorigenic (103; 104) activity through an unknown mechanism, I hypothesized that PRAS40 can negatively regulate p53 through RPL11. To explore this possibility, U2OS osteosarcoma cells were depleted of PRAS40 using plasmids expressing shRNAs targeted to various regions of the PRAS40 transcript. U2OS cells express wildtype p53 and possess a functional RPL11-HDM2-p53 pathway, but do not express $p14^{ARF}$ (87-89), another known inhibitor of HDM2. Transient transfection was used to avoid issues of compensation and artifacts of clonal selection potentially associated with stable knock down (KD). Interestingly, KD of PRAS40 induces an increase in p53 protein levels compared to control cells transfected with non-silencing (NS) shRNA (**Figure 4-15**). This p53 upregulation is accompanied by an increase in protein levels of the p53 transcriptional targets p21 and Bax. Importantly, these effects are proportional to the efficiency of PRAS40 KD by two different shRNAs, suggesting that the observed effects

are directly related to PRAS40 KD (**Figure 4-15**). Because p53 is a critical mediator of cell fate, it is subject to multiple layers of regulation, including transcriptional, translational, and post-translational control mechanisms. The RPL11-HDM2 pathway acts specifically at the post-translational level by inhibiting the E3 ubiquitin-ligase activity of HDM2, thereby increasing p53 protein stability. Considering this, I sought to test whether PRAS40 might also control p53 through regulation of protein stability. To explore this possibility I treated cells expressing either NS or PRAS40-targeted shRNAs with the translation inhibitor cycloheximide for various times. PRAS40 KD increases p53 protein half-life approximately 6-fold compared to the NS control (**Figure 4-16**). This effect, and p53 degradation in general, is abolished by co-treatment with the proteasome inhibitor MG132, suggesting that PRAS40 negatively regulates p53 protein levels in a proteasome-dependent manner (**Figure 4-16**). Importantly, I find that the effect of PRAS40 KD on p53 protein level is abolished by co-KD of RPL11 using two different shRNAs (**Figure 4-17)**. To test whether the observed PRAS40 KD-induced p53 upregulation corresponds to an increase in p53 transcriptional activity, a p53 reporter plasmid in which the consensus p53-binding promoter sequence drives luciferase transcription was used. PRAS40 KD significantly increases p53 transcriptional activity compared to the NS control. Importantly, this effect is abolished by co-KD of either p53 or RPL11 **(Figure 4-18)**. Taken together, these findings suggest that PRAS40 negatively regulates p53 protein stability and activity in an RPL11-dependent manner.

4.3.8 PRAS40 KD induces p53 upregulation through a mechanism similar to low concentration Actinomycin D.

The disruption of ribosome biogenesis, also known as nucleolar stress (86), can be induced by various cellular insults including oncogene expression (90), serum starvation (89), and various immunosuppressant and chemotherapeutic drugs including mycophenolic acid (133), 5-fluorouracil (134; 135), and Actinomycin D (ActD) (87-92; 136-138). ActD is a polypeptide antibiotic that binds GC-rich regions of DNA. At very low concentrations, i.e. <10nM, ActD binds primarily to rDNA and specifically inhibits RNA Polymerase 1 (136; 137). This results in disruption of ribosome biogenesis without inducing DNA damage and triggers p53 upregulation specifically through the RPL11-HDM2 nucleolar stress response pathway (87-92; 136-138). Therefore, I used a low concentration dose curve of ActD in conjunction with PRAS40 KD to test whether PRAS40 plays a role in regulating RPL11-HDM2-p53 nucleolar stress response pathway. While PRAS40 KD and ActD have an additive effect at low ActD concentration, there is no combinatorial effect at high ActD concentrations, suggesting that PRAS40 KD and ActD activate p53 through a similar mechanism **(Figure 4-19)**. Taken together with my previous results, this finding suggests that PRAS40 is an Akt- and mTORC1-controlled regulator of the p53 response to nucleolar stress.

4.3.9 PRAS40 suppresses induction of cellular senescence in a p53-dependent manner.

Finally, I sought to test whether PRAS40 KD-associated p53 upregulation has any effect on cell survival or growth. In efforts to suppress tumorigenesis, p53 transcriptional activity is known to induce cell death, temporary cell cycle arrest, or a permanent loss of replicative potential known as cellular senescence. While I was not able to detect any

significant induction of cell death in the U2OS cells studied [data not shown], I did find that PRAS40-depleted cells possess significantly increased levels of senescence-associated β-galactosidase (SA-β-gal) activity compared to NS control cells, as indicated by conversion of the β-gal substrate X-gal to the insoluble blue dye 5,5'-dibromo-4,4'-dichloro-indigo at pH 6.0. Importantly, this effect is abrogated by co-KD of p53 **(Figure 4-20)**. Taken together, these results suggest that PRAS40 acts to keep p53 levels and activity low in an RPL11-dependent manner, thus helping to suppress the p53-mediated induction of premature cellular senescence.

Figure 4-1. PRAS40 is present in the nuclear and post-nuclear fractions of HeLa cells. HeLa cells were fractionated via swelling in hypotonic buffer, Dounce homogenization, and centrifugation through a sucrose gradient. Total cell lysate and post-nuclear (cytoplasmic) and nuclear extracts were resolved via SDS-PAGE. Endogenous PRAS40 and fractionation markers were detected via Western Blotting. The results presented are representative of greater than three independent experiments.

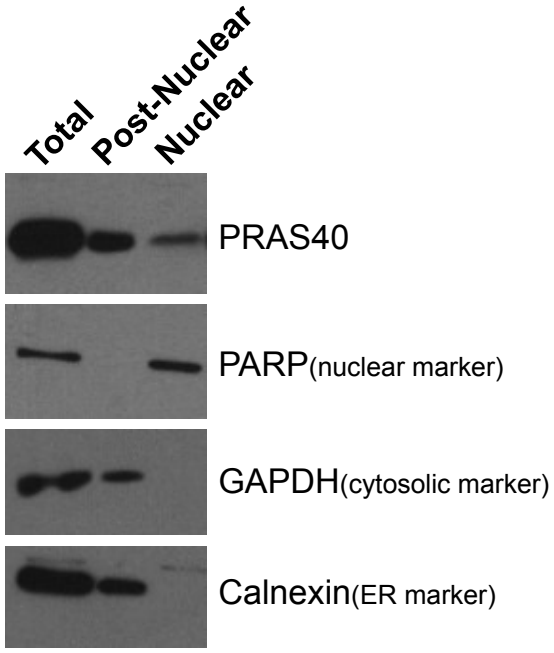
Total
Post-Nuclear
Nuclear
PRAS40
PARP(nuclear marker)
GAPDH(cytosolic marker)
Calnexin(ER marker)

Figure 4-2. PRAS40 undergoes dynamic nucleocytoplasmic shuttling in U2OS cells. U2OS cells growing on poly-D-lysine-coated glass coverslips were transfected with cDNA encoding Venus-PRAS40 and treated with 100 nM Leptomycin B (LMB), a potent inhibitor of Crm1/Exportin-1-dependent nuclear export, or vehicle control (EtOH) for six hours. The cells were then fixed and mounted on glass slides. Images were obtained using a Zeiss LSM 510 META inverted confocal microscope. Scale bars represent 10 μM. **A)** Single slice image; **B)** Z-stack

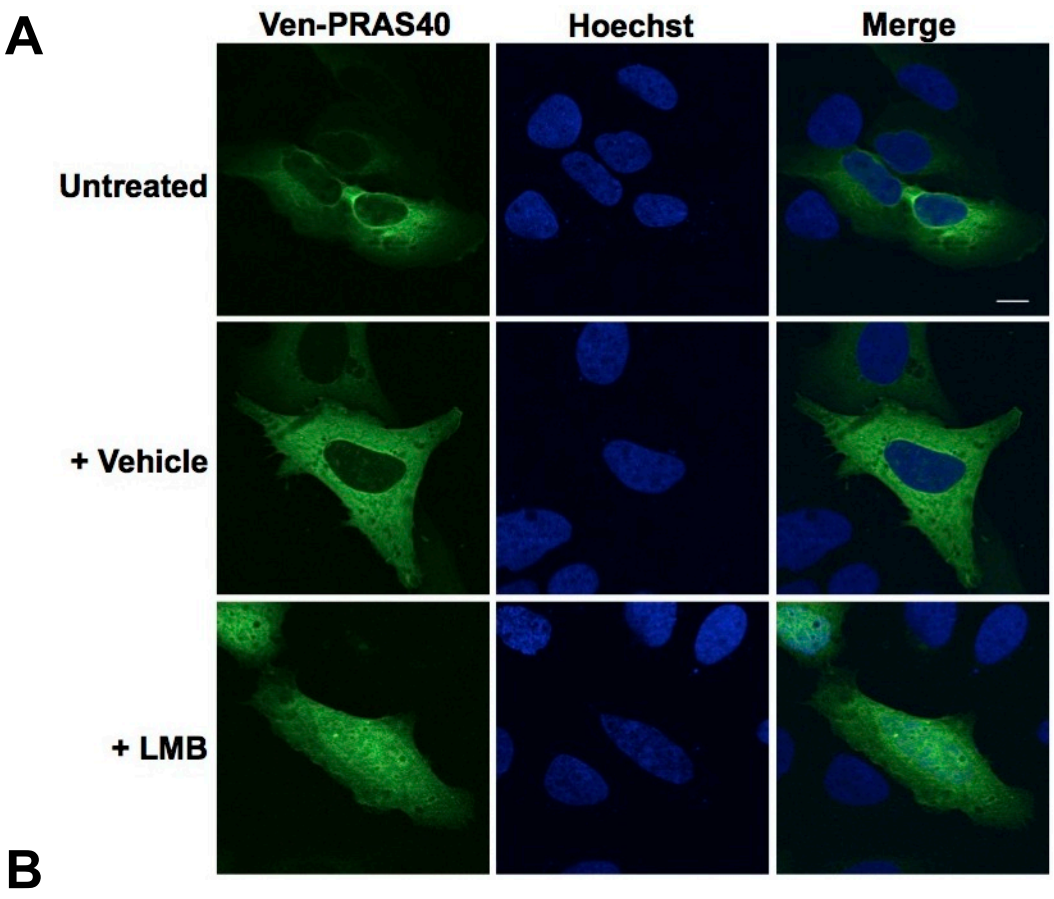
A
Ven-PRAS40
Hoechst
Merge
Untreated
+ Vehicle
+ LMB
B
Z-Stack
Vehicle
Ven-PRAS40
Hoechst
LMB
Ven-PRAS40
Hoechst

Figure 4-3. PRAS40 undergoes dynamic nucleocytoplasmic shuttling in HeLa cells. HeLa cells growing on poly-D-lysine-coated glass coverslips were transfected with cDNA encoding Venus-PRAS40 and treated with 100 nM Leptomycin B (LMB), a potent inhibitor of Crm1/Exportin-1-dependent nuclear export, or vehicle control (EtOH) for six hours. The cells were then fixed and mounted on glass slides. Images were obtained using a Zeiss LSM 510 META inverted confocal microscope. Scale bars represent 10 μM. Results are representative of three independent experiments.

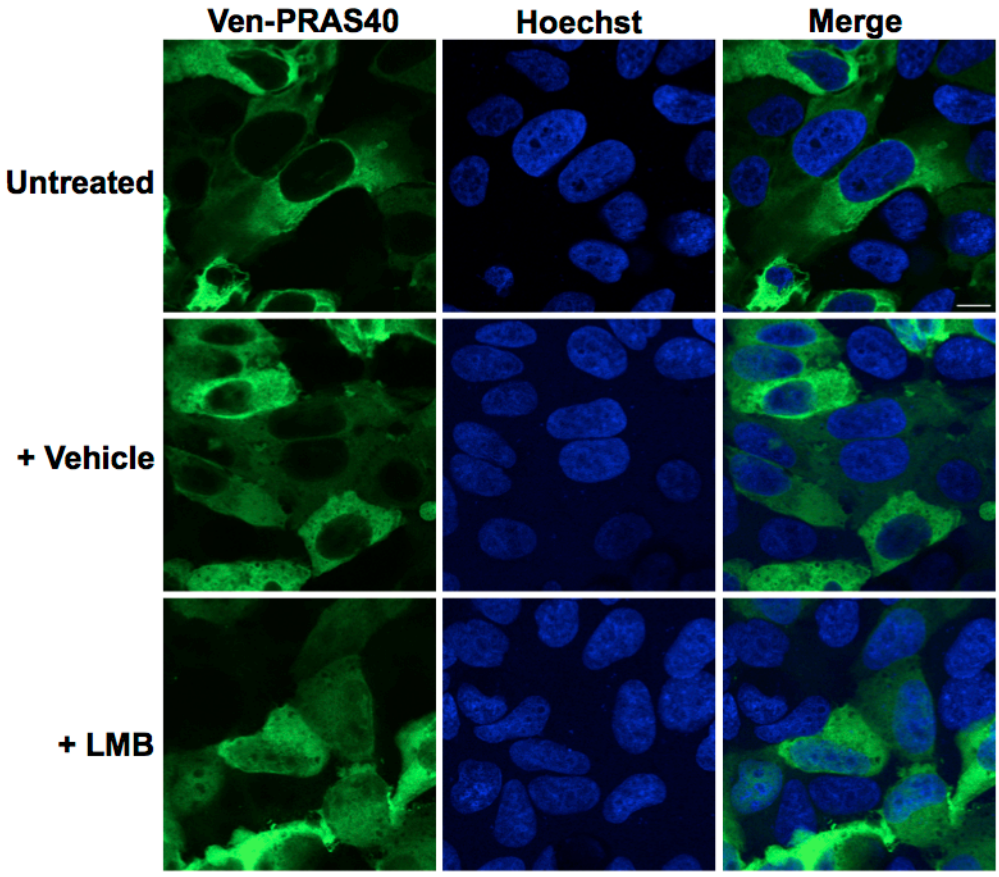
Ven-PRAS40
Hoechst
Merge
Untreated
+ Vehicle
+ LMB

Figure 4-4. PRAS40 nucleocytoplasmic shuttling does not require interaction with mTORC1. U2OS cells growing on poly-D-lysine-coated glass coverslips were transfected with cDNA encoding Raptor/mTORC1 binding-null Venus-PRAS40^{F129A} and treated with 100 nM Leptomycin B (LMB), a potent inhibitor of Crm1/Exportin-1-dependent nuclear export, or vehicle control (EtOH) for six hours. The cells were then fixed and mounted on glass slides. Images were obtained using a Zeiss LSM 510 META inverted confocal microscope. Scale bars represent 10 μM. Results are representative of three independent experiments.

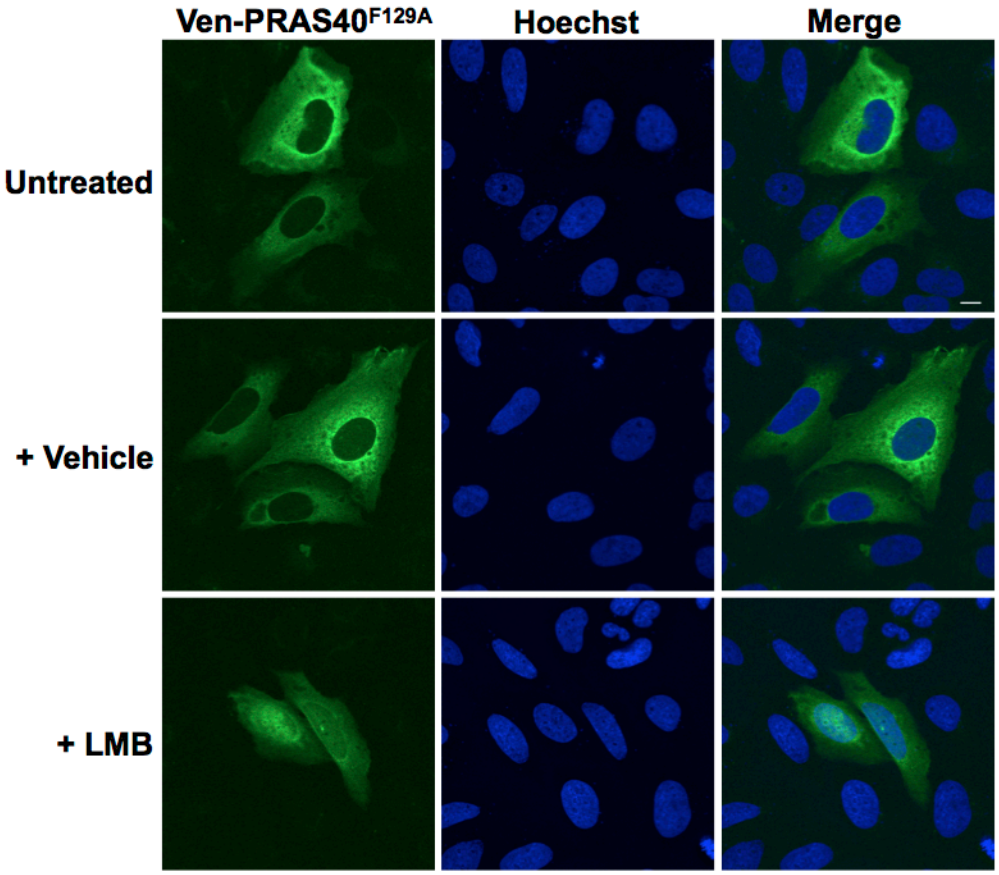
Ven-PRAS40F129A
Hoechst
Merge
Untreated
+ Vehicle
+ LMB

Figure 4-5. PRAS40 residues 218-227 serve as a functional NES sequence. A) HeLa cells were transfected with cDNAs encoding Venus-tagged full length, 1-110, or 110-256 PRAS40. Cells were either left untreated or were treated with the nuclear export inhibitor Leptomycin B (LMB) (20 nM) for 1 hour.

B) Two putative leucine-rich nuclear export signal (NES) sequences were identified by analysis of the PRAS40 primary amino acid sequence – ^{28}LVLL^{31} in the N-terminus and ^{218}IAASMRALVL^{227} in the C-terminus. HeLa cells were transfected with cDNAs encoding Venus-tagged PRAS40 harboring a deletion of either 28-31 (Δ28-31) or 218-227 (Δ218-227). Cells were not treated with Leptomycin B prior to imaging. All images were acquired using an Image Express$^{Micro®}$ epifluorescence microcope (Molecular Devices).

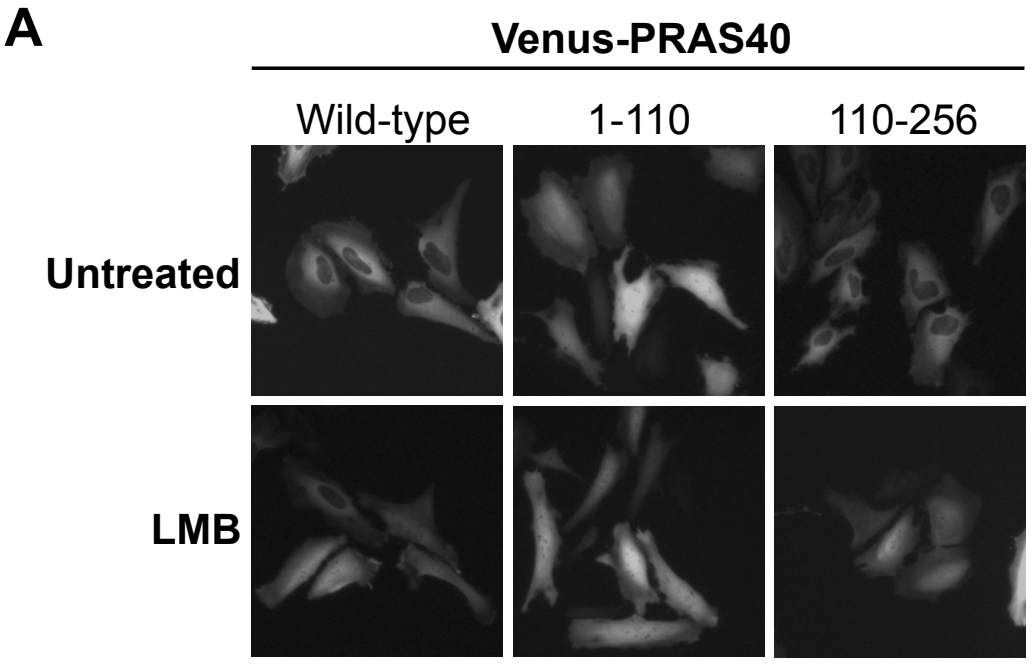
A
Venus-PRAS40
Wild-type
1-110
110-256
Untreated
LMB

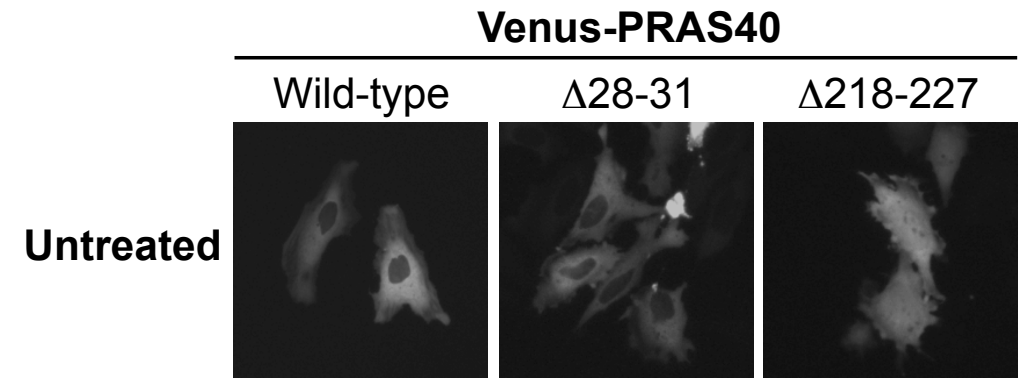
B
Venus-PRAS40
Wild-type
Δ28-31
Δ218-227
Untreated

Table 4-1. Putative PRAS40-interacting proteins identified by IP-MS.

Protein	Average Nuclear SCs	Average Cytoplasmic SCs
HSP70	153.0	297.0
PRAS40	87.0	109.5
14-3-3 ε	21.5	88.0
14-3-3 γ	6.0	18.0
RPL11	4.5	2.0
14-3-3 ζ	3.5	8.5
14-3-3 η	3.0	6.5
Hypothetical Protein	2.5	2.5
14-3-3 β	1.5	8.0
14-3-3 τ	1.5	4.5
14-3-3 σ	1.5	4.0
Albumin Preproprotein	1.0	1.0
Chaperonin	2.0	0.0
TOPO I	1.5	0.0
SNRPD1	1.0	0.0
GRPEL1	0.0	4.0
GAPDH	0.0	3.0
PFK	0.0	1.5
ZF425	0.0	1.5
HspBP1	0.0	1.0
VWF	0.0	1.0

Figure 4-6. Flag-immunoprecipitation and mass spectrometry analysis identifies putative nuclear PRAS40-interacting proteins. A) Schematic for IP-MS approach used to identify putative novel PRAS40 binding proteins. **B)** Analysis of IP-MS results. Spectral counts of putative binding partners ("prey") in each subcellular fraction were normalized to those of PRAS40 ("bait") from the same fraction. Any putative binding partner with a normalized nuclear to cytoplasmic ratio less than 1 was considered a potential cytoplasmic-specific PRAS40 binding partner, while a ratio greater than 1 (or with zero cytoplasmic spectral counts) was identified as a potential nuclear-specific PRAS40 binding partner.

A

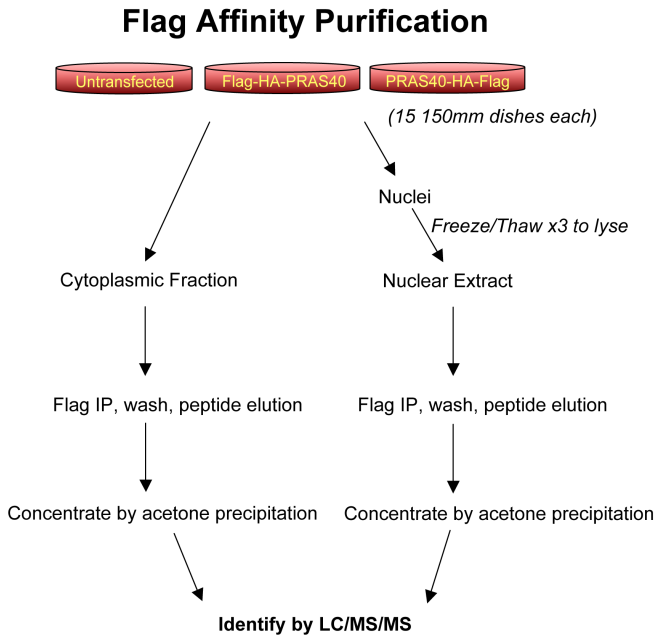
Flag Affinity Purification
Untransfected
Flag-HA-PRAS40
PRAS40-HA-Flag
(15 150mm dishes each)
Nuclei
Freeze/Thaw x3 to lyse
Cytoplasmic Fraction
Nuclear Extract
Flag IP, wash, peptide elution
Flag IP, wash, peptide elution
Concentrate by acetone precipitation
Concentrate by acetone precipitation
Identify by LC/MS/MS

B

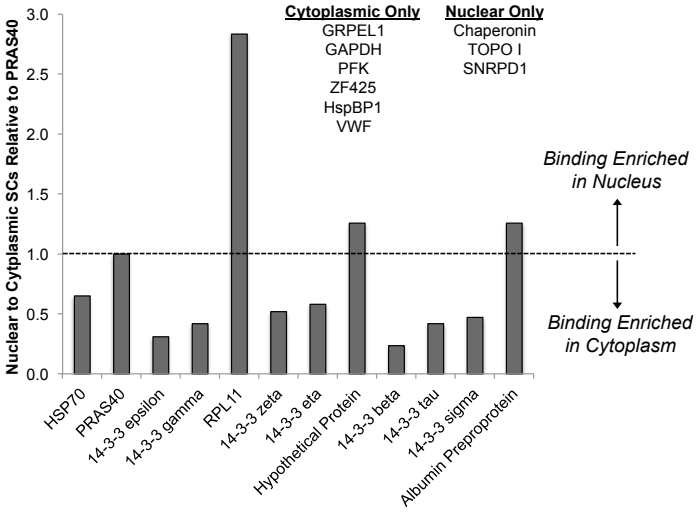
Nuclear to Cytplasmic SCs Relative to PRAS40
3.0
2.5
2.0
1.5
1.0
0.5
0.0
Cytoplasmic Only
GRPEL1
GAPDH
PFK
ZF425
HspBP1
VWF
Nuclear Only
Chaperonin
TOPO I
SNRPD1
Binding Enriched in Nucleus
Binding Enriched in Cytoplasm
HSP70
PRAS40
14-3-3 epsilon
14-3-3 gamma
RPL11
14-3-3 zeta
14-3-3 eta
Hypothetical Protein
14-3-3 beta
14-3-3 tau
14-3-3 sigma
Albumin Preproprotein

Figure 4-7. PRAS40 is a member of a nuclear-specific RPL11-containing complex. **A)** HeLa cells were either untransfected, transfected with N-terminally tagged Flag-PRAS40, or transfected with C-terminally tagged PRAS40-Flag. Cells were fractionated via swelling in hypotonic buffer, Dounce homogenization, and centrifugation. Isolated nuclei were subjected to three freeze/thaw cycles to obtain nuclear extract. Cytoplasmic (Cyt) and nuclear (Nuc) fractions were then subjected to immunoprecipitation with anti-Flag- agarose. Immunoprecipitates were eluted using a competitive Flag peptide. Eluates and inputs were processed by SDS-PAGE and analyzed by Western Blotting. **B)** Untransfected HeLa cells were fractionated as in **A**. PRAS40 was immunoprecipitated from nuclear and cytoplasmic extract using a PRAS40-specific monocolonal antibody. Non-specific, species-matched IgG or PRAS40 antibody pre-blocked with the immunogenic PRAS40 peptide were used as negative controls. Eluates and inputs were processed by SDS-PAGE and analyzed by Western Blotting. Results are representative of three independent experiments.

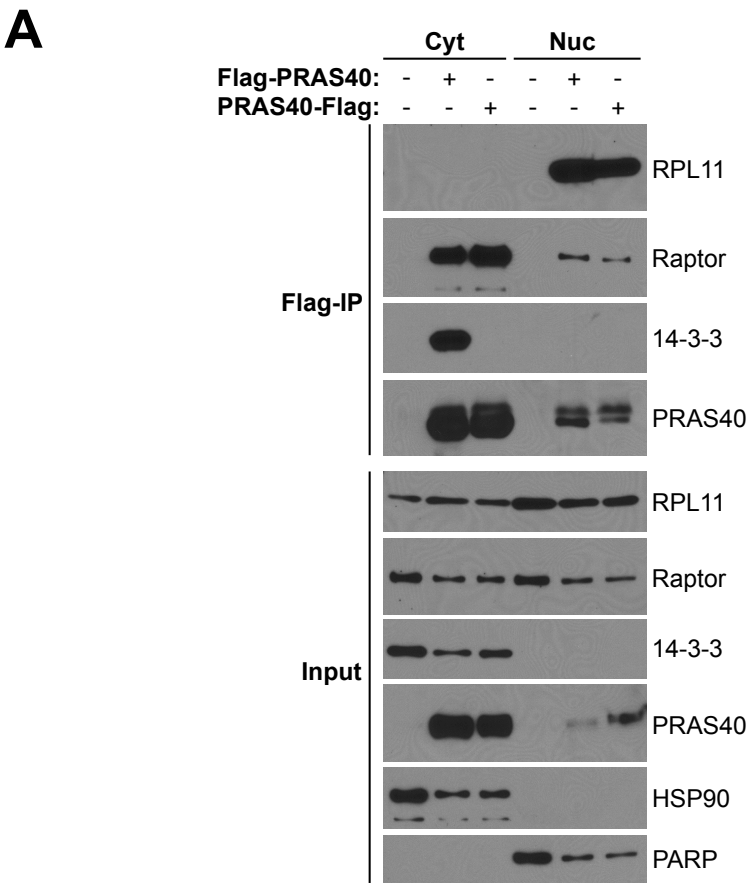
A
Cyt
Nuc
Flag-PRAS40: - + - - + -
PRAS40-Flag: - - + - - +
Flag-IP
RPL11
Raptor
14-3-3
PRAS40
Input
RPL11
Raptor
14-3-3
PRAS40
HSP90
PARP

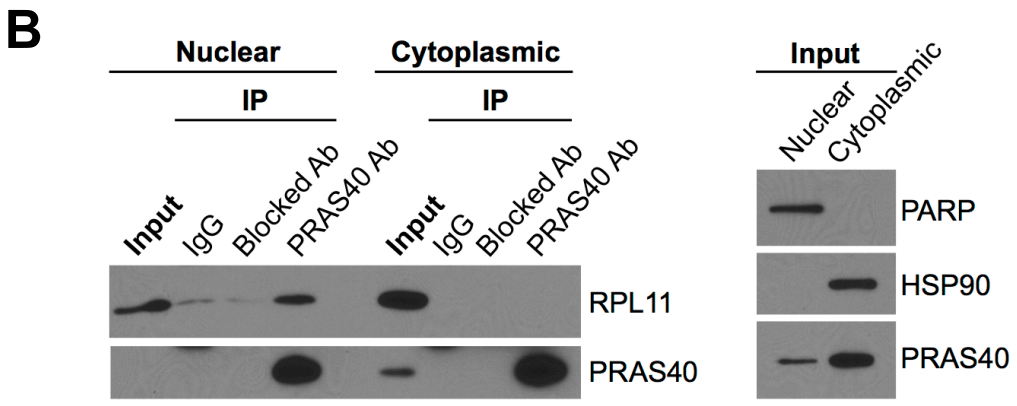
B
Nuclear
Cytoplasmic
IP
IP
Input
IgG
Blocked Ab
PRAS40 Ab
Input
IgG
Blocked Ab
PRAS40 Ab
RPL11
PRAS40
Input
Nuclear
Cytoplasmic
PARP
HSP90
PRAS40

Figure 4-8. Flag-PRAS40 and Ven-RPL11 co-localize within nucleoli. U2OS cells growing on poly-D-lysine-coated cover slips were transfected with plasmids expressing Flag-PRAS40 and Ven-RPL11, fixed, and mounted on glass slides. Images were obtained using a Zeiss LSM 510 META inverted confocal microscope. Scale bars represent 10 μM. **A** and **B** are representative images from different sites on the same coverslip.

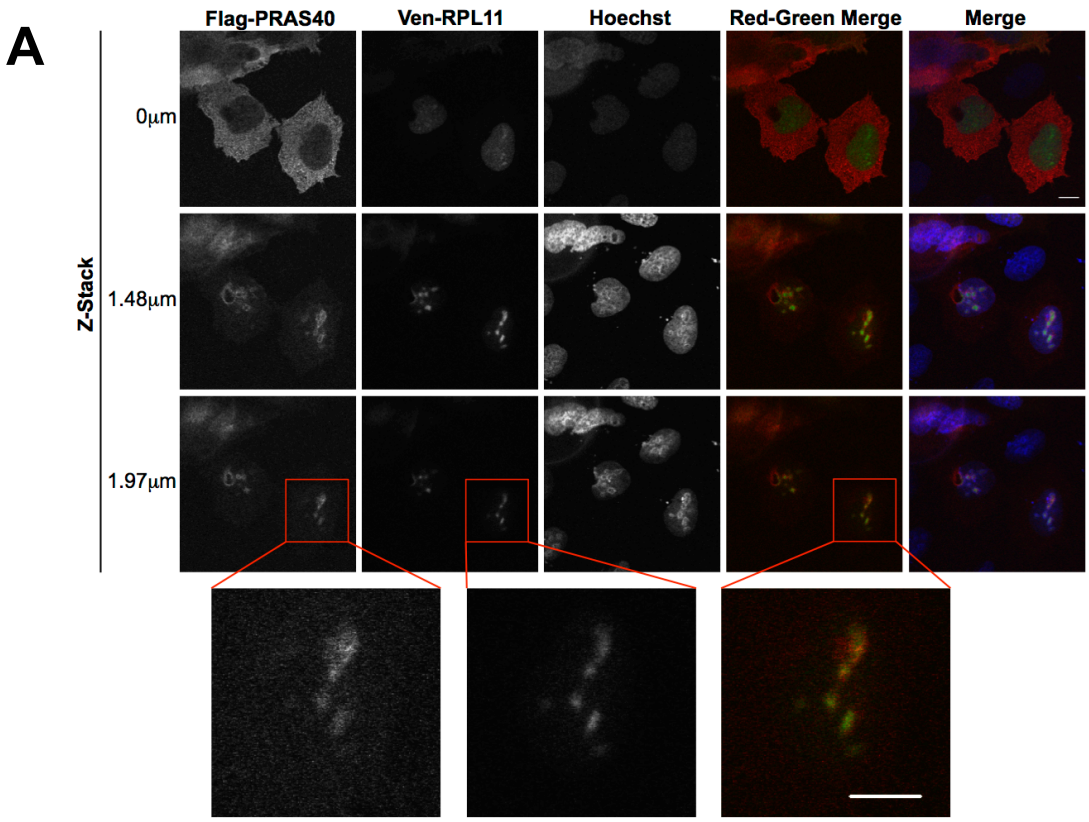
A
Flag-PRAS40
Ven-RPL11
Hoechst
Red-Green Merge
Merge
Z-Stack
0μm
1.48μm
1.97μm

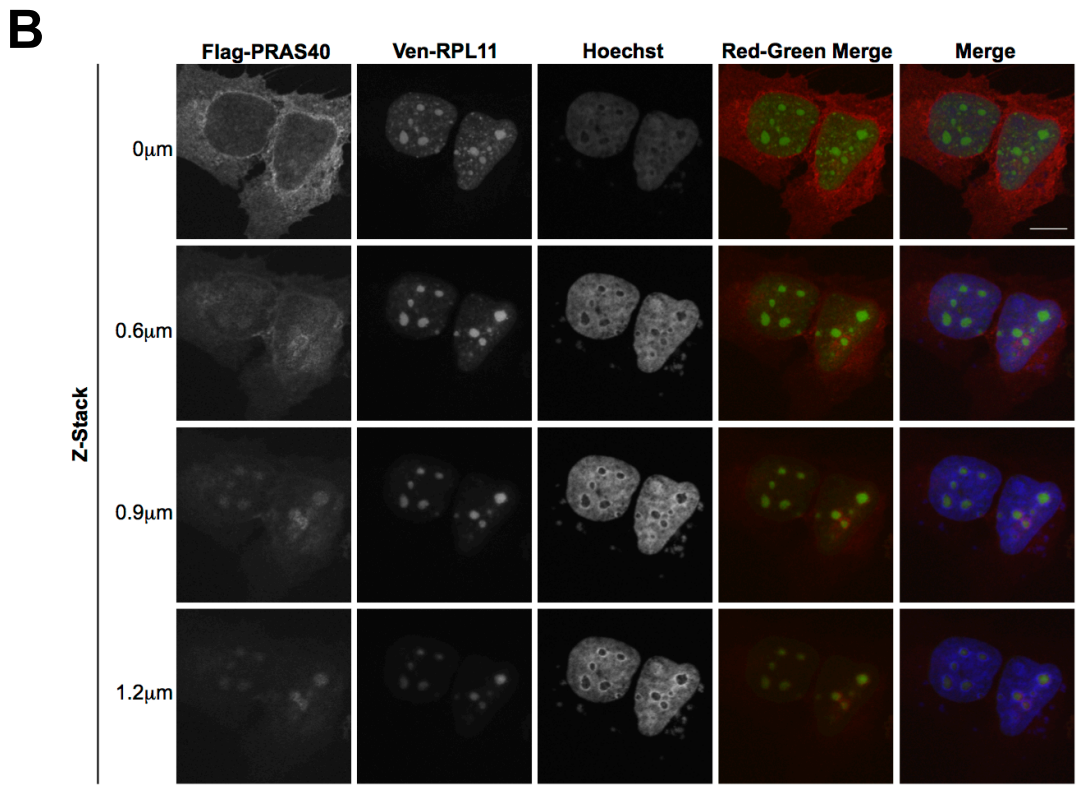
B
Flag-PRAS40
Ven-RPL11
Hoechst
Red-Green Merge
Merge
Z-Stack
0μm
0.6μm
0.9μm
1.2μm

Figure 4-9. The nuclear PRAS40- and RPL11-containing complex is distinct from mTORC1. HeLa nuclear extract was resolved by gel filtration chromatography using a Superose 6 size exclusion column. 0.5 mL fractions were collected. Odd-numbered fractions were processed by SDS-PAGE and analyzed by Western Blotting. The left-most box (purple) represents the void volume of the column. The middle box (blue) highlights fractions in which PRAS40, Raptor, and mTOR, but not RPL11, co-migrate on the column. These fractions likely contain fully formed mTORC1. Finally, the right-most box (red) highlights fractions in which PRAS40 co-migrates with RPL11 but not Raptor, implying that these fractions contain a ~300-700 kDa complex containing PRAS40, RPL11, and potentially other as-of-yet unidentified proteins.

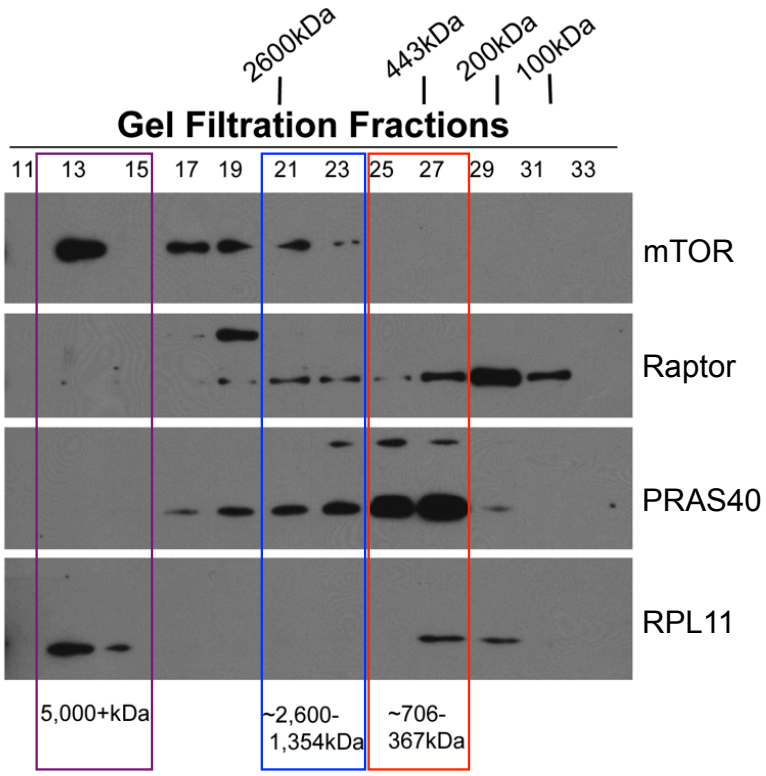
2600kDa
443kDa
200kDa
100kDa
Gel Filtration Fractions
11 13 15 17 19 21 23 25 27 29 31 33
mTOR
Raptor
PRAS40
RPL11
5,000+kDa
~2,600-
1,354kDa
~706-
367kDa

Figure 4-10. Critical determinants for formation of the nuclear PRAS40- and RPL11-containing complex are found within residues 98-109 and the C-terminal region of PRAS40. HeLa cells were transfected with plasmids encoding Flag-RPL11 and the indicated GST-tagged PRAS40 truncations. GST-tagged proteins were precipitated from whole-cell lysates using glutathione-conjugated beads. The inputs and eluates were processed via SDS-PAGE. Flag-PRAS40 and GST-tagged PRAS40 truncations were detected via Western Blotting. Results were quantified by densitometry using ImageJ software.

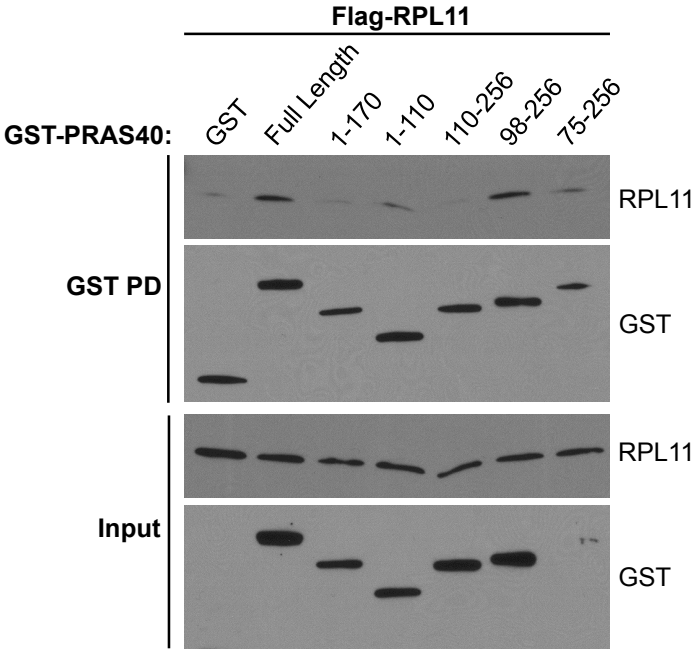
Flag-RPL11
GST-PRAS40:
GST
Full Length
1-170
1-110
110-256
98-256
75-256
GST PD
RPL11
GST
Input
RPL11
GST

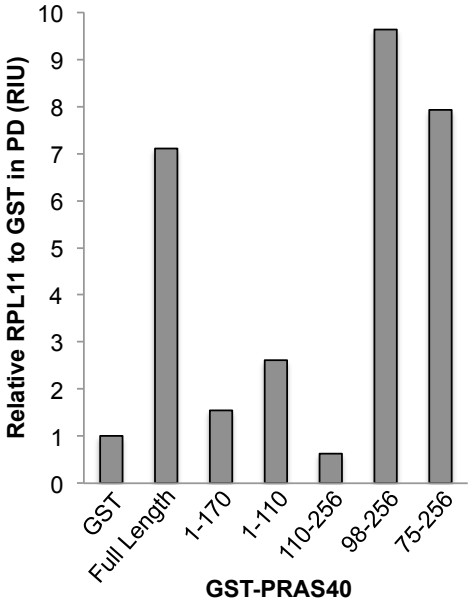
Relative RPL11 to GST in PD (RIU)
0
1
2
3
4
5
6
7
8
9
10
GST
Full Length
1-170
1-110
110-256
98-256
75-256
GST-PRAS40

Figure 4-11. Formation of the nuclear PRAS40- and RPL11-containing complex is dependent upon PRAS40 residues S221 and T246. HeLa cells were transfected with plasmids encoding wild-type or mutated Flag-PRAS40 as indicated. Cells were fractionated via swelling in hypotonic buffer, Dounce homogenization, and centrifugation. Isolated nuclei were lysed by three freeze/thaw cycles to obtain nuclear extracts, which were then subjected to immunoprecipitation with anti-Flag-agarose beads. Immunoprecipitates were eluted using a competitive Flag peptide. Eluates and inputs were processed by SDS-PAGE and analyzed by Western Blotting. Results presented are representative of three independent experiments.

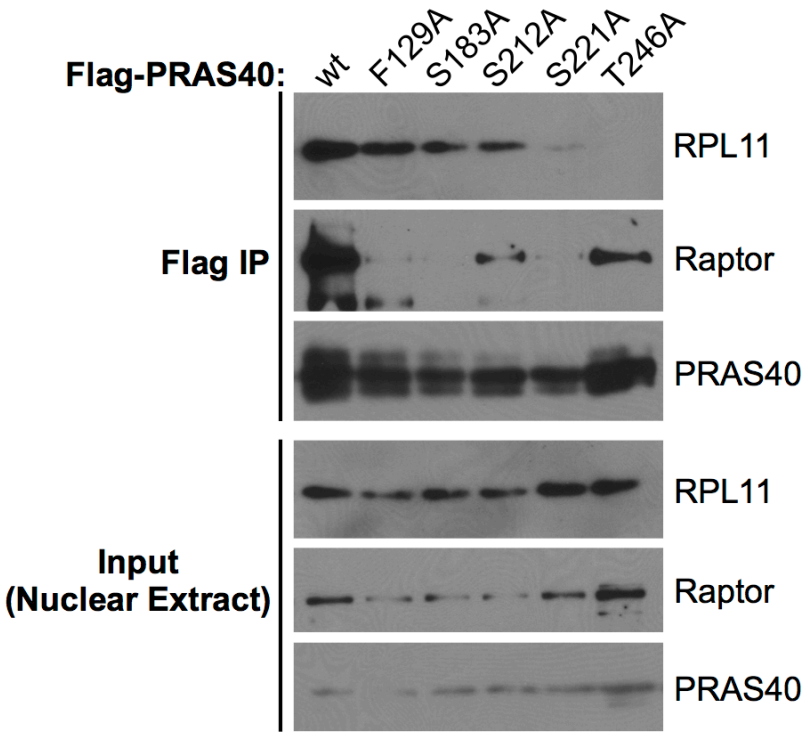
Flag-PRAS40:
wt
F129A
S183A
S212A
S221A
T246A
Flag IP
RPL11
Raptor
PRAS40
Input
(Nuclear Extract)
RPL11
Raptor
PRAS40

Figure 4-12. Formation of the nuclear PRAS40- and RPL11-containing complex is dependent upon phosphorylation. HeLa cells were either untransfected, transfected with Flag-PRAS40, or transfected with Flag-PRAS40^{T246A} as indicated. One set of samples was prepared using buffers containing phosphatase inhibitors, while the other set was prepared simultaneously using buffers lacking phosphatase inhibitors. Cells were fractionated via swelling in hypotonic buffer, Dounce homogenization, and centrifugation. Isolated nuclei were lysed by three freeze/thaw cycles to obtain nuclear extracts, which were then subjected to immunoprecipitation with anti-Flag-agarose beads. Immunoprecipitates were eluted using a competitive Flag peptide. Eluates and inputs were processed by SDS-PAGE and analyzed by Western Blotting.

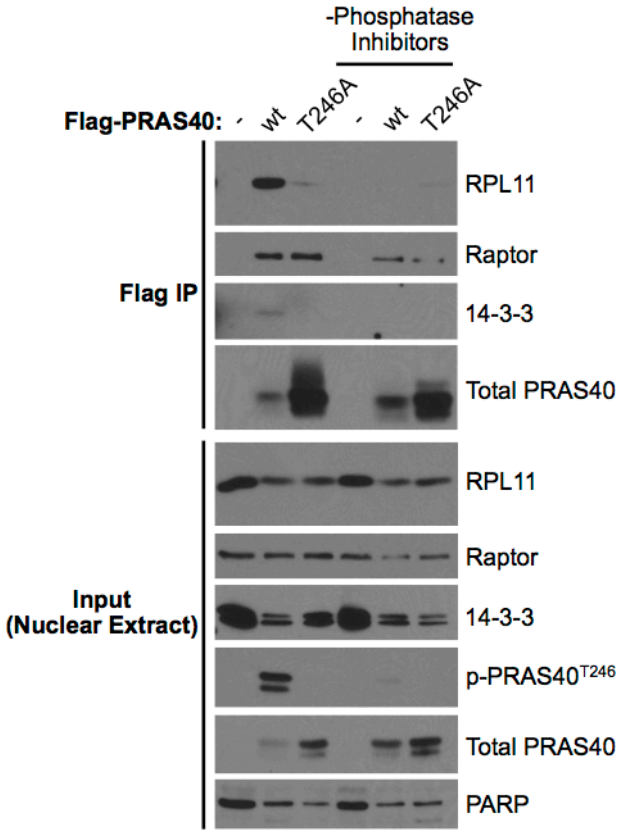
-Phosphatase Inhibitors
Flag-PRAS40: - wt T246A - wt T246A
Flag IP
RPL11
Raptor
14-3-3
Total PRAS40
Input (Nuclear Extract)
RPL11
Raptor
14-3-3
p-PRAS40T246
Total PRAS40
PARP

Figure 4-13. The nuclear PRAS40- and RPL11-containing complex requires the serum-activated kinase activity of Akt. HeLa cells were either untransfected or transfected with plasmids encoding the indicated PRAS40 and Akt constructs. 40 hours after transfection, the indicated samples (-FBS) were serum-starved for 24 hours. Cells were fractionated via swelling in hypotonic buffer, Dounce homogenization, and centrifugation. Isolated nuclei were lysed by three freeze/thaw cycles to obtain nuclear extracts, which were then subjected to immunoprecipitation with anti-Flag-agarose beads. Eluates and inputs were processed by SDS-PAGE and analyzed by Western Blotting. Results presented are representative of three independent experiments.

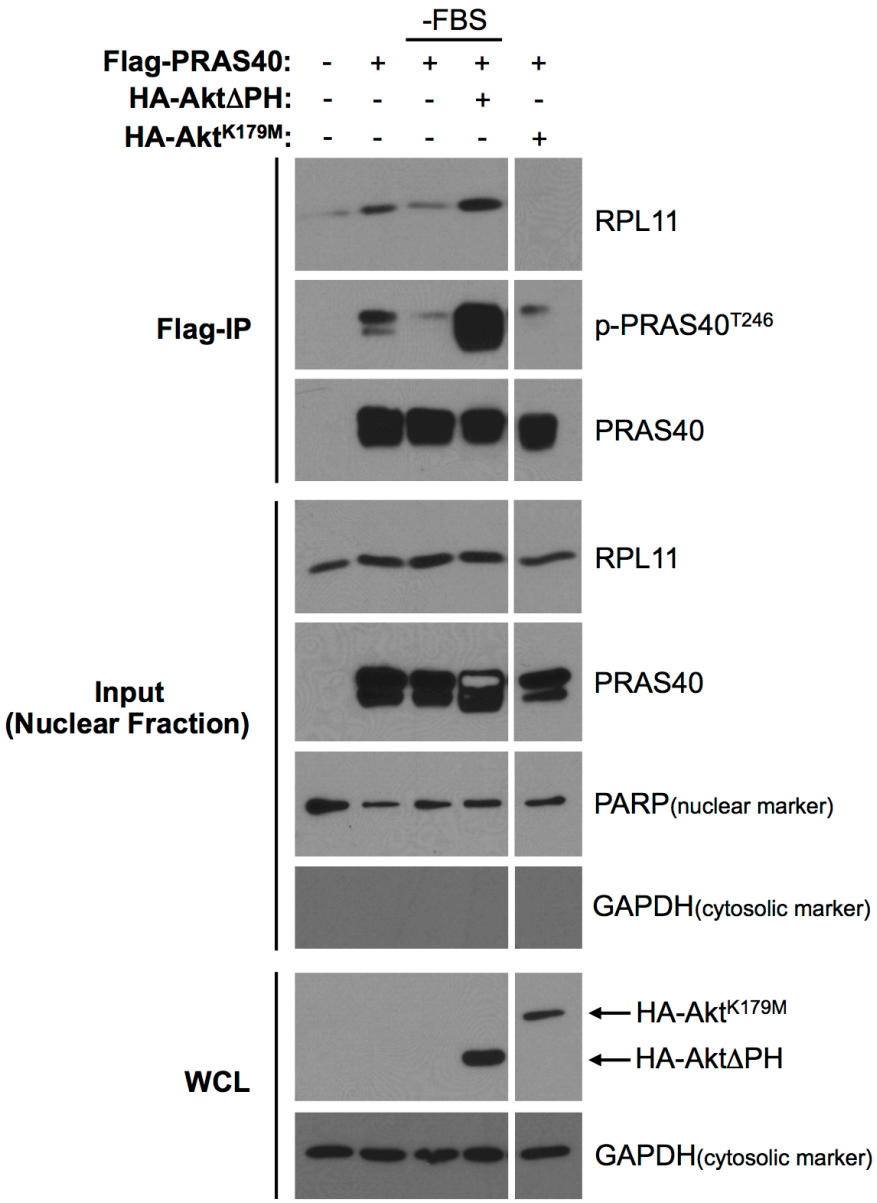
-FBS
Flag-PRAS40: - + + + +
HA-AktΔPH: - - - + -
HA-Akt^{K179M}: - - - - +
Flag-IP
RPL11
p-PRAS40^{T246}
PRAS40
Input
(Nuclear Fraction)
RPL11
PRAS40
PARP(nuclear marker)
GAPDH(cytosolic marker)
WCL
HA-Akt^{K179M}
HA-AktΔPH
GAPDH(cytosolic marker)

Figure 4-14. The nuclear PRAS40- and RPL11-containing complex requires the amino acid-activated kinase activity of mTORC1. HeLa cells were transfected with a plasmid encoding Flag-PRAS40. 40 hours after transfection, the cells were starved of Leu and Met for 24 hours. Cells were either left in amino acid limiting media or returned to Leu- and Met-rich media for 6h in the presence of either no additive, vehicle (DMSO), or 20 nM rapamycin (Rapa.) as indicated. Cells were fractionated via swelling in hypotonic buffer, Dounce homogenization, and centrifugation. Isolated nuclei were lysed by three freeze/thaw cycles to obtain nuclear extracts, which were then subjected to immunoprecipitation with anti-Flag-agarose beads. Immunoprecipitates were eluted using a competitive Flag peptide. Eluates and inputs were processed by SDS-PAGE and analyzed by Western Blotting. Results presented are representative of three independent experiments.

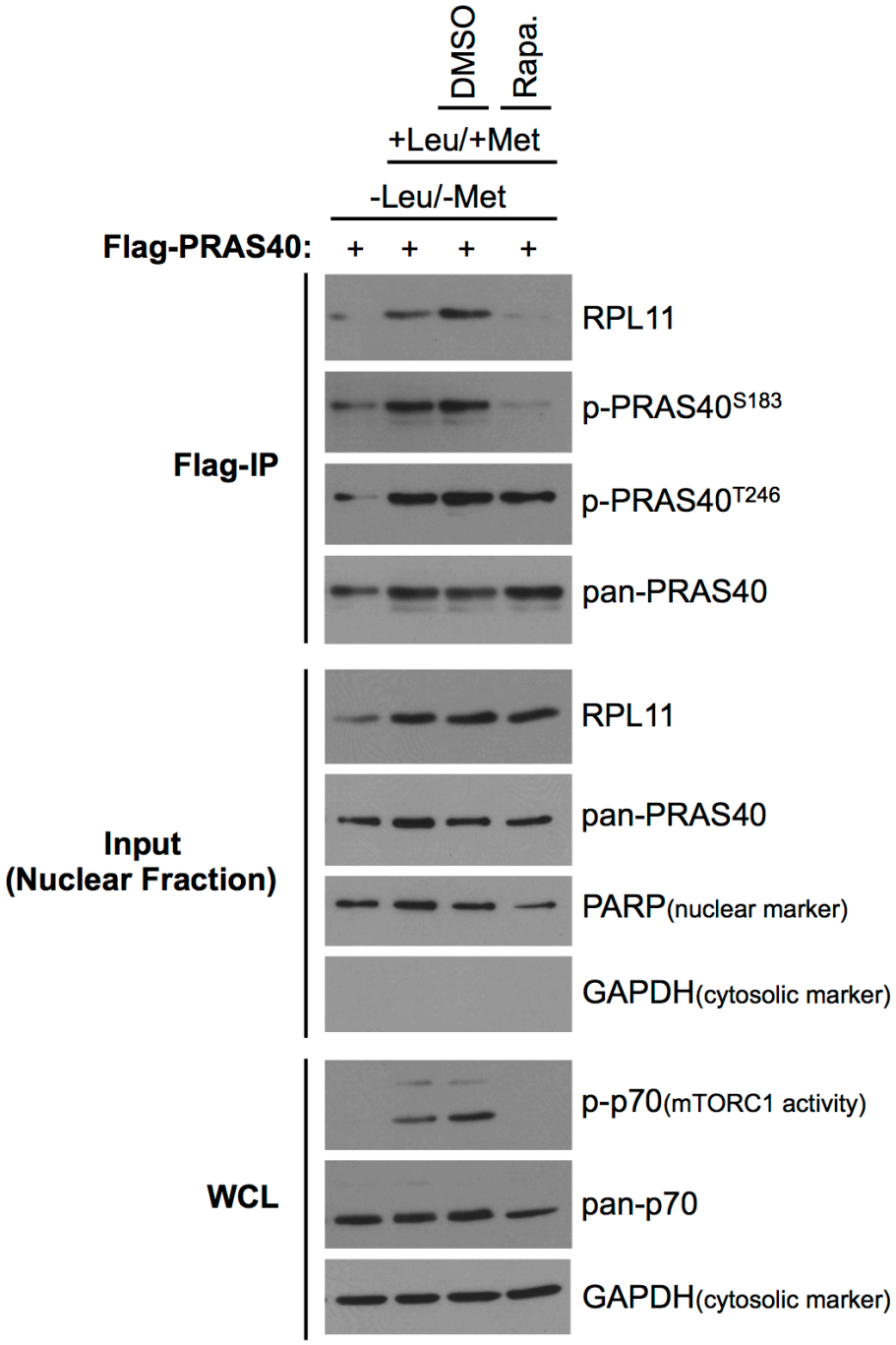
DMSO
Rapa.
+Leu/+Met
-Leu/-Met
Flag-PRAS40: + + + +
Flag-IP
RPL11
p-PRAS40S183
p-PRAS40T246
pan-PRAS40
Input
(Nuclear Fraction)
RPL11
pan-PRAS40
PARP(nuclear marker)
GAPDH(cytosolic marker)
WCL
p-p70(mTORC1 activity)
pan-p70
GAPDH(cytosolic marker)

Figure 4-15. PRAS40 KD induces upregulation of p53 and its transcriptional targets p21 and Bax. U2OS cells were transfected with plasmids encoding shRNAs as indicated. The two different PRAS40 shRNAs used target different regions of the PRAS40 transcript. Transfected cells were selected by puromycin treatment. Whole-cell lysates were prepared, processed by SDS-PAGE, and analyzed by Western Blotting. Results are representative of greater than five independent experiments.

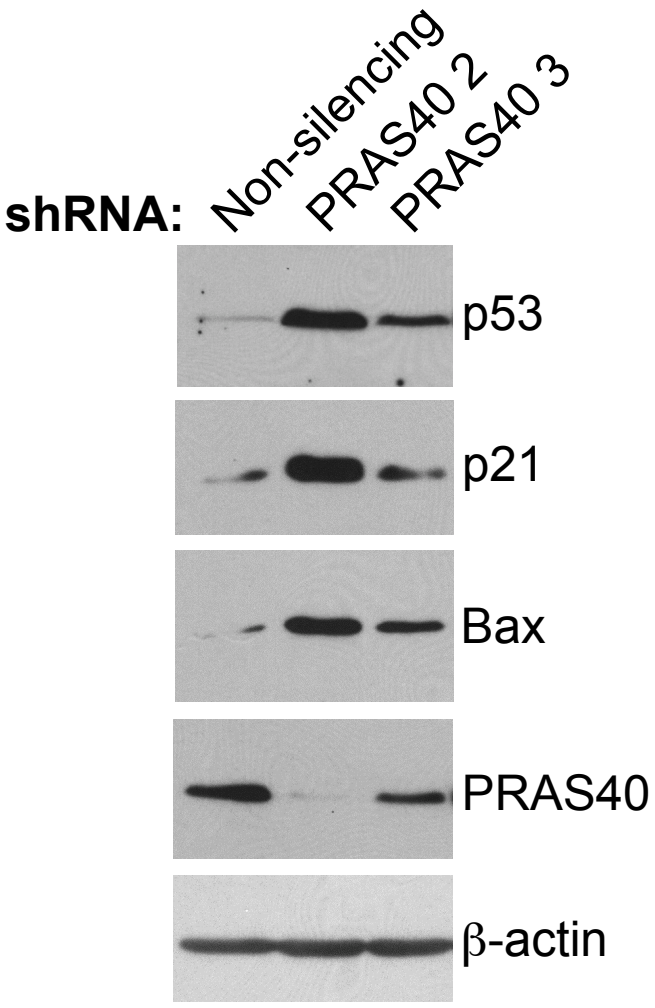
shRNA:
Non-silencing
PRAS40 2
PRAS40 3
p53
p21
Bax
PRAS40
β-actin

Figure 4-16. PRAS40 KD increases the protein stability of p53 through a proteasome-dependent mechanism. U2OS cells were transfected with plasmids encoding shRNAs as indicated. Transfected cells were selected by puromycin treatment. Cells were treated with 20 μg/mL cycloheximide in the absence or presence of 20 μM MG132 and lysed at various time points as indicated. Whole-cell lysates were prepared, processed by SDS-PAGE, and analyzed by Western Blotting. Results were quantified by densitometry using ImageJ software.

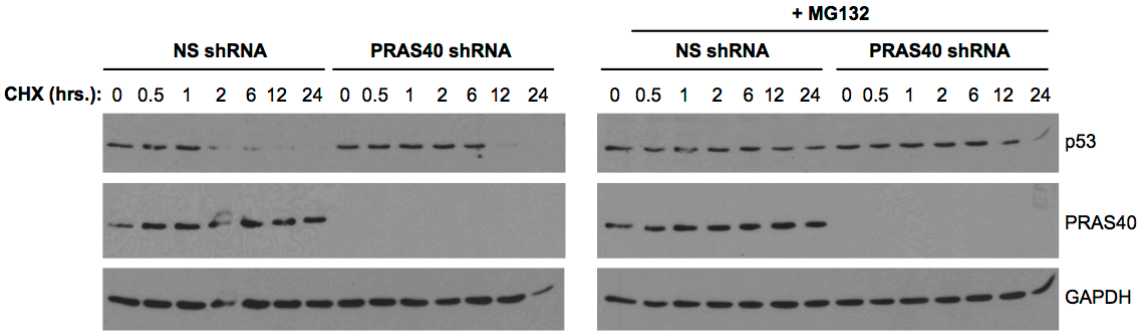
+ MG132
NS shRNA
PRAS40 shRNA
NS shRNA
PRAS40 shRNA
CHX (hrs.): 0 0.5 1 2 6 12 24 0 0.5 1 2 6 12 24
0 0.5 1 2 6 12 24 0 0.5 1 2 6 12 24
p53
PRAS40
GAPDH

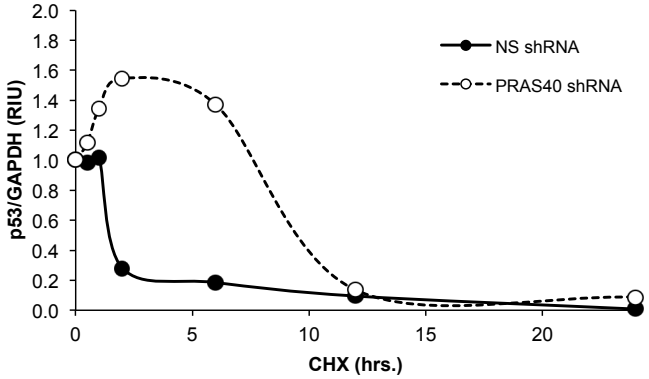
2.0
1.8
1.6
1.4
1.2
1.0
0.8
0.6
0.4
0.2
0.0
p53/GAPDH (RIU)
0
5
10
15
20
CHX (hrs.)
NS shRNA
PRAS40 shRNA

Figure 4-17. PRAS40 KD-induced p53 upregulation is dependent upon RPL11. U2OS cells were transfected with plasmids encoding shRNAs as indicated. The two different RPL11 shRNAs used target different regions of the RPL11 transcript. Transfected cells were selected by puromycin treatment. Whole-cell lysates were prepared, processed by SDS-PAGE, and analyzed by Western Blotting. Blots are representative of three independent experiments. Western Blot bands were quantified by densitometry using ImageJ software. Results are presented as the means of three independent experiments +/- SEM. (*$p < 0.5$, **$p < 0.01$ using the Bonferroni Multiple Comparisons Test)

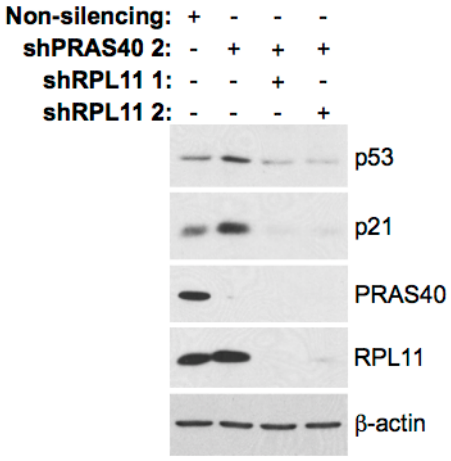
Non-silencing: + - - -
shPRAS40 2: - + + +
shRPL11 1: - - + -
shRPL11 2: - - - +
p53
p21
PRAS40
RPL11
β-actin

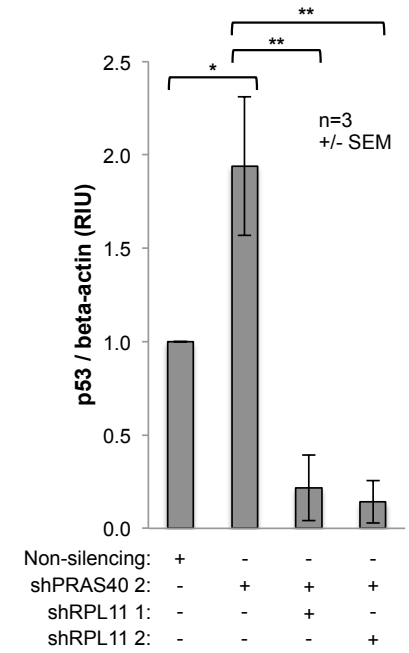
**
**
*
2.5
2.0
1.5
1.0
0.5
0.0
p53 / beta-actin (RIU)
n=3
+/- SEM
Non-silencing: + - - -
shPRAS40 2: - + + +
shRPL11 1: - - + -
shRPL11 2: - - - +

Figure 4-18. PRAS40 KD induces p53 transcriptional activity in an RPL11-dependent manner. U2OS cells were transfected with plasmids encoding PRAS40-, p53-, and RPL11-targeted shRNAs as indicated. The cells were co-transfected with one of two luciferase reporter plasmids in which luciferase transcription is driven by 13 repeats of the consensus p53-binding element (wt) or 15 repeats of a mutated version of the p53-binding element (mut). Whole-cell lysates were prepared and analyzed by the BCA protein concentration assay (Pierce). The lysates were normalized to equal total protein concentrations by adding empty lysis buffer as appropriate. Luiferase activity was measured in triplicate using the Bright-Glo™ Luciferase Assay System from Promega. Luminescence was measured immediately after substrate addition using an Envision® Multilabel plate reader (PerkinElmer) with a 0.1 sec integration time. Results are reported as the means of three independent experiments +/- SEM. (***$p < 0.001$ using the Bonferroni Multiple Comparisons Test)

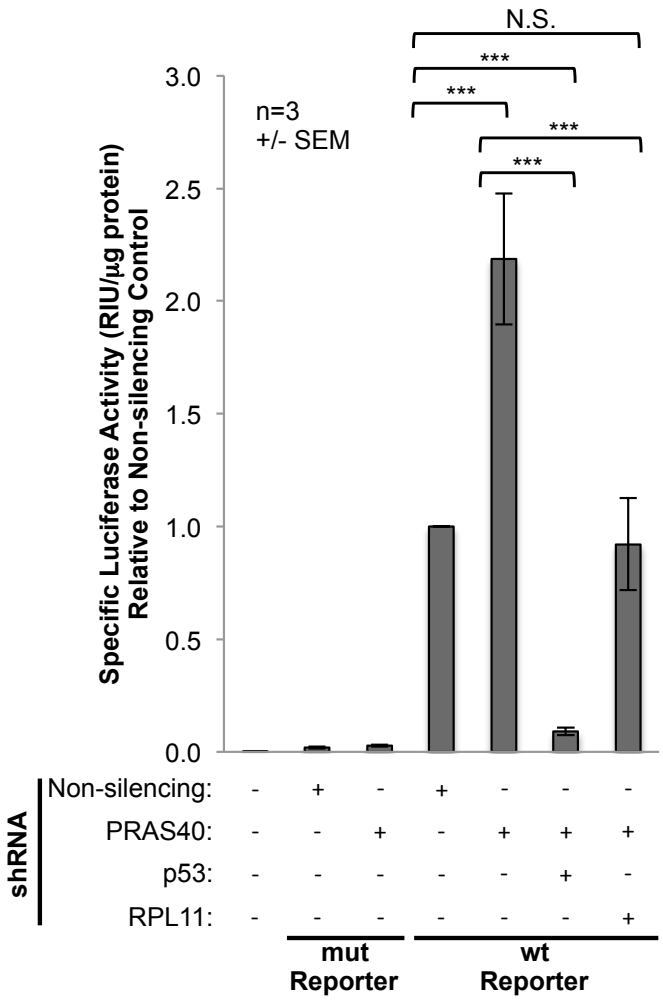
N.S.
***
***
***
***
n=3
+/- SEM
Specific Luciferase Activity (RIU/μg protein)
Relative to Non-silencing Control
3.0
2.5
2.0
1.5
1.0
0.5
0.0
shRNA
Non-silencing: - + - + - - -
PRAS40: - - + - + + +
p53: - - - - - + -
RPL11: - - - - - - +
mut Reporter
wt Reporter

Figure 4-19. PRAS40 KD induces p53 through a mechanism similar to low concentration Actinomycin D. U2OS cells were transfected with plasmids encoding non-silencing or PRAS40-targeted shRNA as indicated. Transfected cells were selected by puromycin treatment. Cells were then treated with various concentrations of Actinomycin D (ActD) as indicated. Whole-cell lysates were prepared, processed by SDS-PAGE, and analyzed by Western Blotting. Western Blot bands were quantified by densitometry using Image J software. Results presented are representative of three independent experiments.

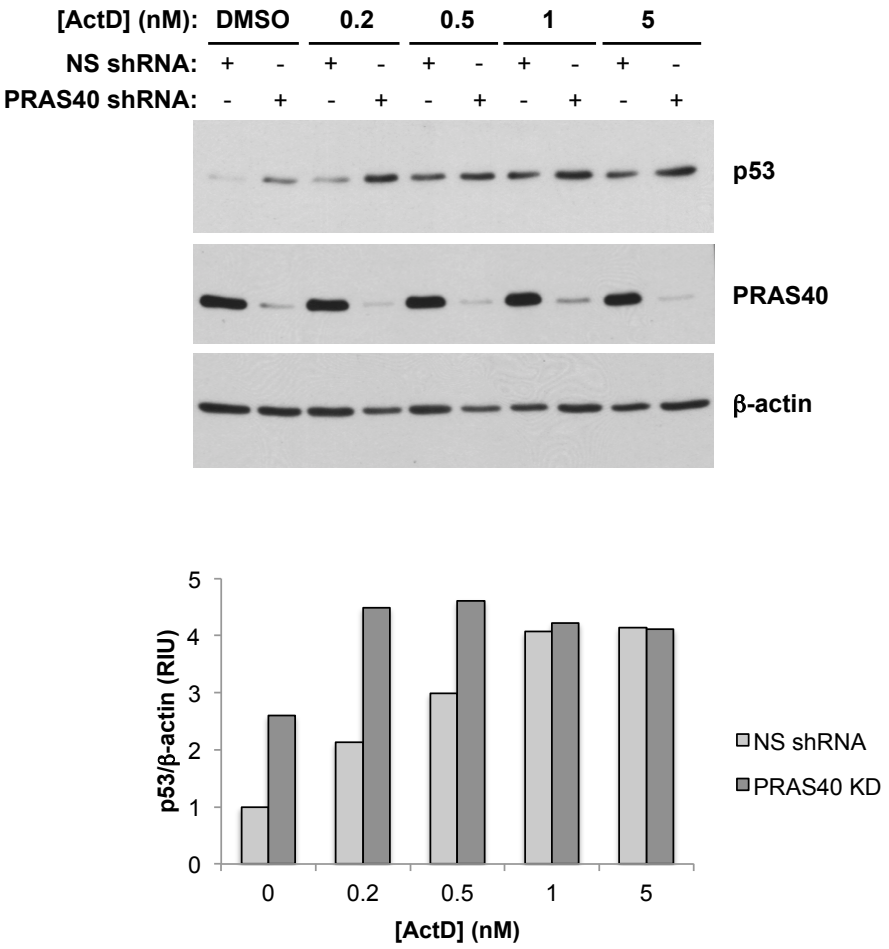
[ActD] (nM): DMSO 0.2 0.5 1 5
NS shRNA: + - + - + - + - + -
PRAS40 shRNA: - + - + - + - + - +
p53
PRAS40
β-actin
p53/β-actin (RIU)
0
1
2
3
4
5
0
0.2
0.5
1
5
[ActD] (nM)
NS shRNA
PRAS40 KD

Figure 4-20. PRAS40 KD induces premature cellular senescence in a p53-dependent manner. U2OS cells were transfected with plasmids encoding various shRNAs as indicated. Transfected cells were selected by treatment with puromycin. Cells were then fixed and stained for senescence-associated β-galactosidase X-gal cleavage activity at pH 6.0 (Senescence β-Galactosidase Staining Kit, Cell Signaling 9860). **A)** Images are representative of three independent experiments. **B)** Cells were counted and scored by two blinded, impartial investigators. Nine sites per well were counted in each experiment. Results are presented as the means of three independent experiments +/- SEM. (***$p<0.001$ using the Bonferroni Multiple Comparisons Test)

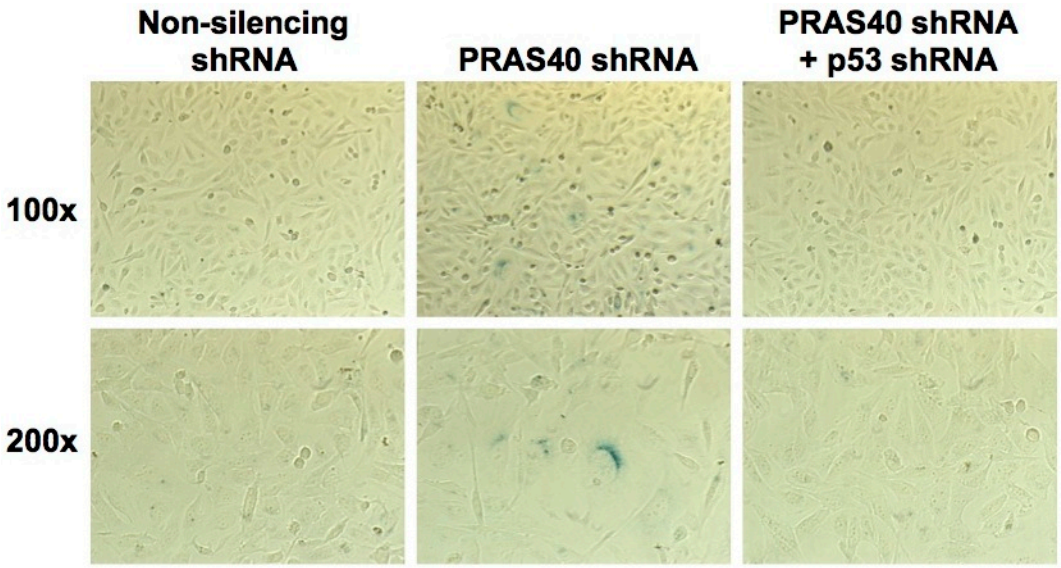
Non-silencing shRNA
PRAS40 shRNA
PRAS40 shRNA + p53 shRNA
100x
200x

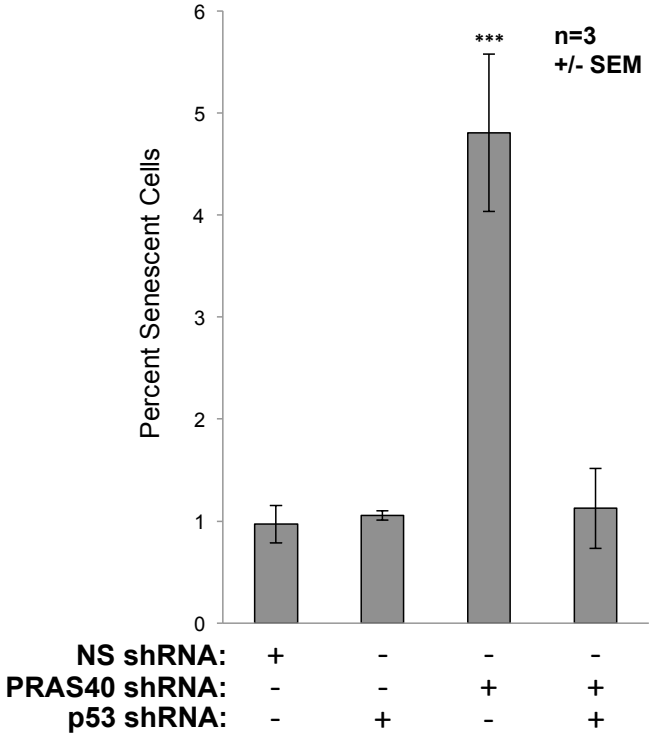
Percent Senescent Cells
0
1
2
3
4
5
6
***
n=3
+/- SEM
NS shRNA: + - - -
PRAS40 shRNA: - - + +
p53 shRNA: - + - +

4.4 Conclusions and Discussion

In this study, I have explored the subcellular localization and interactome of PRAS40. I find that while PRAS40 is a predominantly cytoplasmic protein, it is also present in significant quantities in the nuclei of cancer cells, in agreement with previous reports (100; 101; 120-123). Although it has been suggested by others (129; 130), I demonstrate for the first time that PRAS40 nuclear localization is controlled at least in part by Crm1-dependent active nuclear export directed by a functional NES sequence in the C-terminus of PRAS40 (^{218}IAASMRALVL^{227}). While I also identified a putative nuclear localization signal (NLS) sequence (^{251}KLKRKY^{256}), its deletion has no effect on LMB-induced nuclear accumulation of PRAS40. Proteins equal to or less than 40kDa in size are generally thought to be capable of entering the nucleus via passive diffusion (128). Despite migrating at 40kDa on SDS-PAGE gels, the actual molecular weight of PRAS40 is 27kDa. Therefore, it is possible that PRAS40 nuclear import is accomplished through passive diffusion, although this seems unlikely to be the sole explanation, as Venus- and GST-tagged PRAS40 (~54kDa each) are also able to enter the nucleus. Additionally, the possibility of active nuclear import mediated by an unidentified conformation-dependent NLS in PRAS40 or by an NLS in one of its binding partners cannot be ruled out.

In order to better understand the role of PRAS40 in various sub-cellular compartments, I sought to identify PRAS40-interacting proteins in the cytoplasm and nucleus. Immunoprecipitation from cytoplasmic and nuclear cell fractions followed by mass spectrometry analysis identifies RPL11 as a nuclear-specific PRAS40-associated protein. Size exclusion chromatography reveals that the nuclear PRAS40- and RPL11-

containing complex has a high molecular weight (~300-700kDa) and therefore likely contains other as-of-yet unidentified members. It seems probable that this is the case, because although the mass spectrometry analysis was substantiated through identification of the known PRAS40 interacting protein 14-3-3, it failed to detect another well-established binding partner, Raptor. Subsequent validation experiments revealed via Western Blotting that Raptor was indeed present in the same eluates used for mass spectrometry analysis, indicating that the results of this screen likely underrepresent the full extent of the PRAS40 interactome. Notably, size-exclusion chromatography analysis also indicates that the nuclear PRAS40- and RPL11-containing complex is distinct from mTORC1. Furthermore, it appears unlikely that PRAS40 binds to fully formed ribosomes because 1) the molecular weight of the PRAS40- and RPL11-containing complex (~300-700kDa) is far less than that of a mature ribosome, and 2) no PRAS40-RPL11 co-precipitation occurs in the cytoplasmic fraction despite the vast majority of mature ribosomes being found therein.

I go on to show that the nuclear PRAS40- and RPL11-containing complex is phosphorylation-dependent and requires PRAS40 residues S221 and T246, known mTORC1 and Akt target sites, respectively (57; 58). This complex is responsive to extracellular serum and nutrient conditions and requires the kinase activities of both mTORC1 and Akt. In U2OS cells with a functional RPL11-HDM2-p53 nucleolar stress response pathway and inactive $p14^{ARF}$, PRAS40 KD leads to an RPL11-dependent increase in p53 protein levels and transcriptional activity. This increase in p53 protein level is achieved through a decrease in the rate of p53 proteasomal degradation, resulting in increased p53 protein half-life. Finally, PRAS40 KD sensitizes cells to p53

upregulation in response to ActD-induced nucleolar stress and results in increased levels of premature cellular senescence. Taken together, these data suggest that PRAS40 is a dual-input signal integrator and effector of mTORC1 and Akt kinases that promotes inhibition of the RPL11-HDM2-p53 pathway in the presence of sufficient extracellular growth factors and nutrients (**Figure 4-21**). Further biochemical characterization of the nuclear PRAS40- and RPL11-containing complex, including identification of all its constituent proteins, will likely provide greater insight into its function and the mechanistic details of its relationship to the RPL11-HDM2-p53 pathway. The present data identify PRAS40 as the first known regulatory link between the Akt/mTORC1 signaling axis and the RPL11-HDM2-p53 nucleolar stress response pathway (**Figure 4-21**).

Figure 4-21. A model for PRAS40's role in regulating the RPL11-HDM2-p53 pathway. A) Prior knowledge of PRAS40's molecular function. Previously, it was known that when in its non-phosphorylated state, PRAS40 binds and inhibits mTORC1. In response to growth factors and nutrients, PRAS40 is phosphorylated by Akt and mTORC1, causing it to dissociate from mTORC1. The fate or function of phosphorylated, mTORC1-dissociated PRAS40 was completely unknown. Despite the fact that other mTORC1 inhibitors are known tumor suppressors, PRAS40 displays pro-survival and pro-tumorigenic activity in rodents and humans. Therefore, I hypothesized that phosphorylated, mTORC1-dissociated PRAS40 has a pro-survival function independent of mTORC1 inhibition. **B)** Findings of this dissertation. In response to growth factors and nutrients, Akt and mTORC1 phosphorylate PRAS40 leading to the formation of a nuclear-specific PRAS40- and RPL11-containing complex. PRAS40 suppresses the RPL11-HDM2-p53 pathway and inhibits the induction of cellular senescence under growth conditions. In healthy cells, this may be one mechanism by which mTORC1 and Akt prevent aberrant activation of the RPL11-HDM2 pathway during routine ribosome biogenesis. Cancer cells that overexpress PRAS40 may exploit this mechanism to overcome the tumor suppressive effects of oncogene-induced senescence.

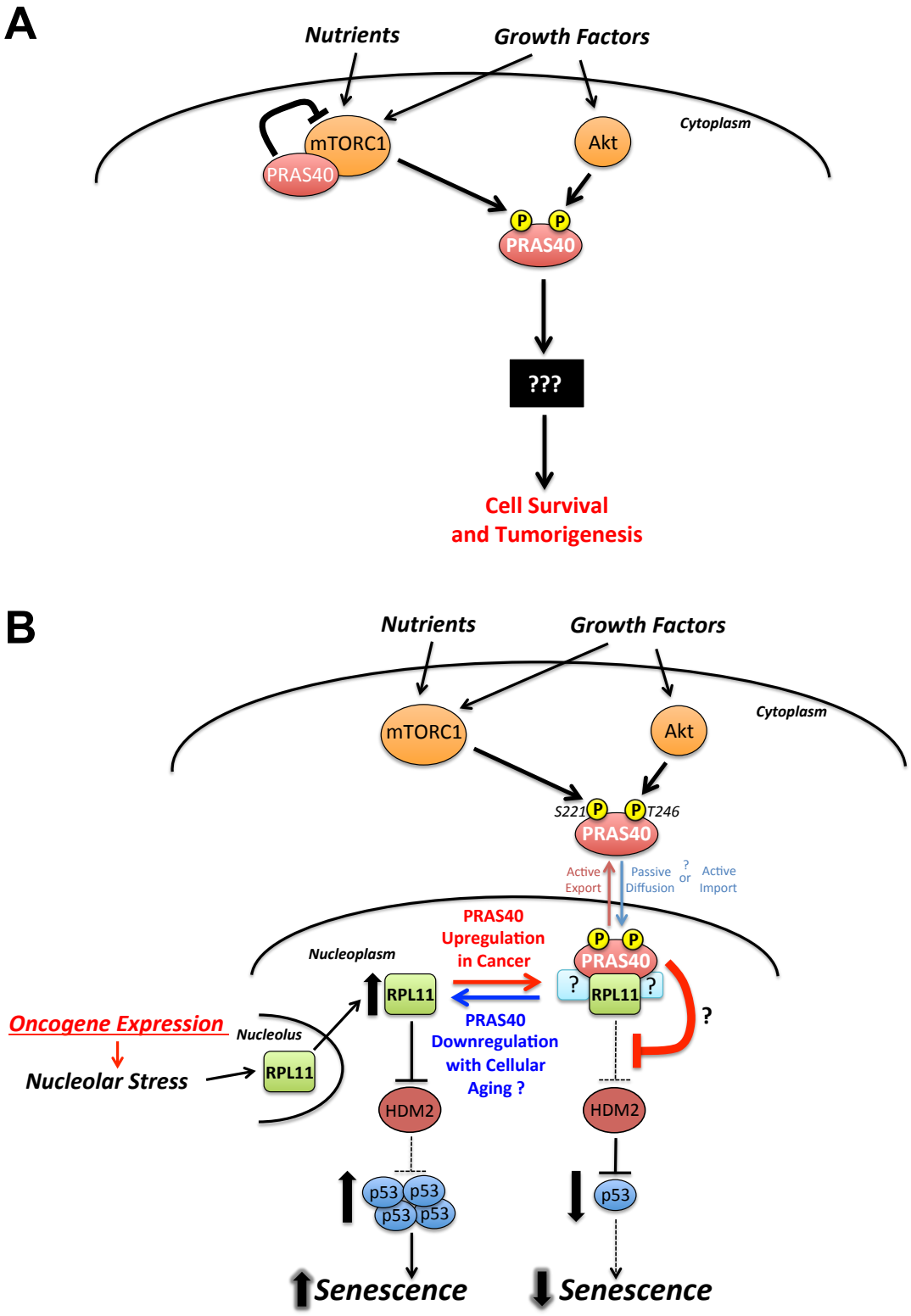
A
Nutrients
Growth Factors
Cytoplasm
mTORC1
PRAS40
Akt
P
P
PRAS40
???
Cell Survival
and Tumorigenesis
B
Nutrients
Growth Factors
Cytoplasm
mTORC1
Akt
S221
P
P
T246
PRAS40
Active
Export
Passive
Diffusion
?
or
Active
Import
PRAS40
Upregulation
in Cancer
Nucleoplasm
P
P
PRAS40
RPL11
?
RPL11
?
?
Oncogene Expression
Nucleolus
RPL11
PRAS40
Downregulation
with Cellular
Aging ?
Nucleolar Stress
HDM2
HDM2
p53
p53
p53
p53
p53
Senescence
Senescence

CHAPTER 5

Discussion

5.1 Implications for the role of PRAS40 in regulation of the RPL11-HDM2-p53 pathway under homeostatic conditions

The data presented in this dissertation identify PRAS40 as the first known regulatory link between the Akt/mTORC1 signaling axis and the RPL11-HDM2-p53 nucleolar stress response pathway (**Figure 4-21**). These findings have important implications for homeostatic and disease-related cellular signaling.

The findings of this dissertation suggest a molecular mechanism by which activation of ribosome biogenesis may be coordinated with suppression of the RPL11-HDM2-p53 nucleolar stress response pathway (**Figure 5-1**). The biosynthesis of ribosomes is one of the most energy-demanding endeavors undertaken by proliferating eukaryotic cells, occupying up to 60% of all transcriptional activity in dividing yeast (139). As such, cells go to great lengths to ensure proper execution of ribosome production. One primary regulator of this process is mTORC1. The growth factor- and nutrient-dependent kinase activity of mTORC1 promotes translation of ribosomal protein (RP) mRNA, as well as activation of all three RNA polymerases involved in rRNA and RP mRNA transcription (140; 141). If ribosome biogenesis is disrupted, the overall biosynthetic capacity of a cell will be greatly diminished and will not be able to meet the demands of cell proliferation. Therefore, these two processes must be tightly regulated and coordinated. It was recently found that RPL11 serves as a critical signal relay molecule linking ribosome biogenesis status to the control of cell proliferation and survival. Specifically, when ribosome biogenesis is disrupted, RPL11 translocates from the nucleolus to the nucleoplasm where it binds and inhibits the E3 ubiquitin-ligase HDM2, thereby stabilizing and activating the tumor suppressor p53. Activated p53

subsequently induces a transcriptional program to promote cell cycle arrest, senescence, or apoptosis (94; 131; 132). While the importance of the RPL11-HDM2-p53 pathway in preventing improper cell division during nucleolar stress is widely appreciated, how this pathway is suppressed during properly executed ribosome biogenesis remains unclear (**Figure 5-1A**) (94). Ribosomal proteins comprise the single most abundant class of proteins in the mammalian proteome (142). During active ribosome biogenesis, newly translated ribosomal proteins undergo high-volume trafficking from the cytoplasm through the nucleoplasm and into the nucleoli. Because the interaction of RPL11 and HDM2 appears to be direct and spontaneous, the law of mass action suggests that the high nucleoplasmic concentrations of RPL11 associated with ribosome biogenesis would trigger activation of the RPL11-HDM2-p53 pathway (**Figure 5-1A**) (94). Such activation would be detrimental to the proliferation and/or survival of healthy, growing cells. Therefore, it seems likely that cells possess a mechanism for suppressing aberrant RPL11-HDM2-p53 pathway activation during properly executed ribosome biogenesis. Recently, PICT1 was identified as a nucleolar protein that helps retain RPL11 in the nucleolus (143). While this finding begins to shed light on regulation of the RPL11-HDM2-p53 pathway under basal conditions, it does not directly address how this pathway is kept in check during ribosome biogenesis-associated nuclear trafficking of RPL11, nor how such regulation may be coordinated with extracellular conditions. Here I demonstrate that in addition to its functions in activating translation and ribosome biogenesis, mTORC1 also promotes formation of a nuclear-specific PRAS40- and RPL11-containing complex through phosphorylation of PRAS40 S221 in a manner dependent upon extracellular conditions. This complex appears to suppress the RPL11-

HDM2-p53 pathway, as KD of PRAS40 induces p53 protein stabilization and transcriptional activation in an RPL11-dependent manner. Thus, these findings suggest a mechanism whereby mTORC1 activity coordinates ribosome biogenesis with suppression of the RPL11-HDM2-p53 pathway through PRAS40 (**Figure 5-1B**). (As an interesting side note, the genes encoding PICT1 and PRAS40 are located within close proximity to one another on chromosome 9. Both are found in the 19q13.33 region.) Furthermore, I show that the nuclear PRAS40- and RPL11-containing complex also requires Akt-mediated phosphorylation of PRAS40 T246, suggesting that both growth factors and nutrients must be present in the extracellular environment to suppress activation of the RPL11-HDM2-p53 pathway during ribosome biogenesis. Importantly, such dual-input regulation would allow for activation of the RPL11-HDM2-p53 pathway as a safeguard when mTORC1 is aberrantly activated in the absence of growth factors, as could potentially occur in cases of tuberous sclerosis complex (TSC) or lung cancer, wherein the negative mTORC1 regulators TSC2 or LKB1, respectively, are inactivated through mutation (96; 97; 99). Thus, these findings suggest that nuclear PRAS40 represents a dual-input signaling checkpoint that coordinates cell proliferation with ribosome biogenesis and microenvironmental conditions (**Figures 4-21** and **5-1**).

Figure 5-1. mTORC1 may coordinate ribosome biogenesis with suppression of the RPL11-HDM2 pathway through PRAS40. A) Nucleoplasmic concentrations of RPL11 are greatly increased during ribosome biogenesis while RPL11 is transported from the cytoplasm through the nucleoplasm and into the nucleoli for ribosome assembly. Because the RPL11-HDM2 interaction is thought to be direct and spontaneous, the law of mass action predicts that the RPL11-HDM2-p53 pathway should be activated during routine ribosome biogenesis. The molecular mechanism preventing this from happening in healthy cells is unknown (94). **B)** A model for PRAS40's potential role in coordinating ribosome biogenesis with suppression of the RPL11-HDM2-p53 pathway.

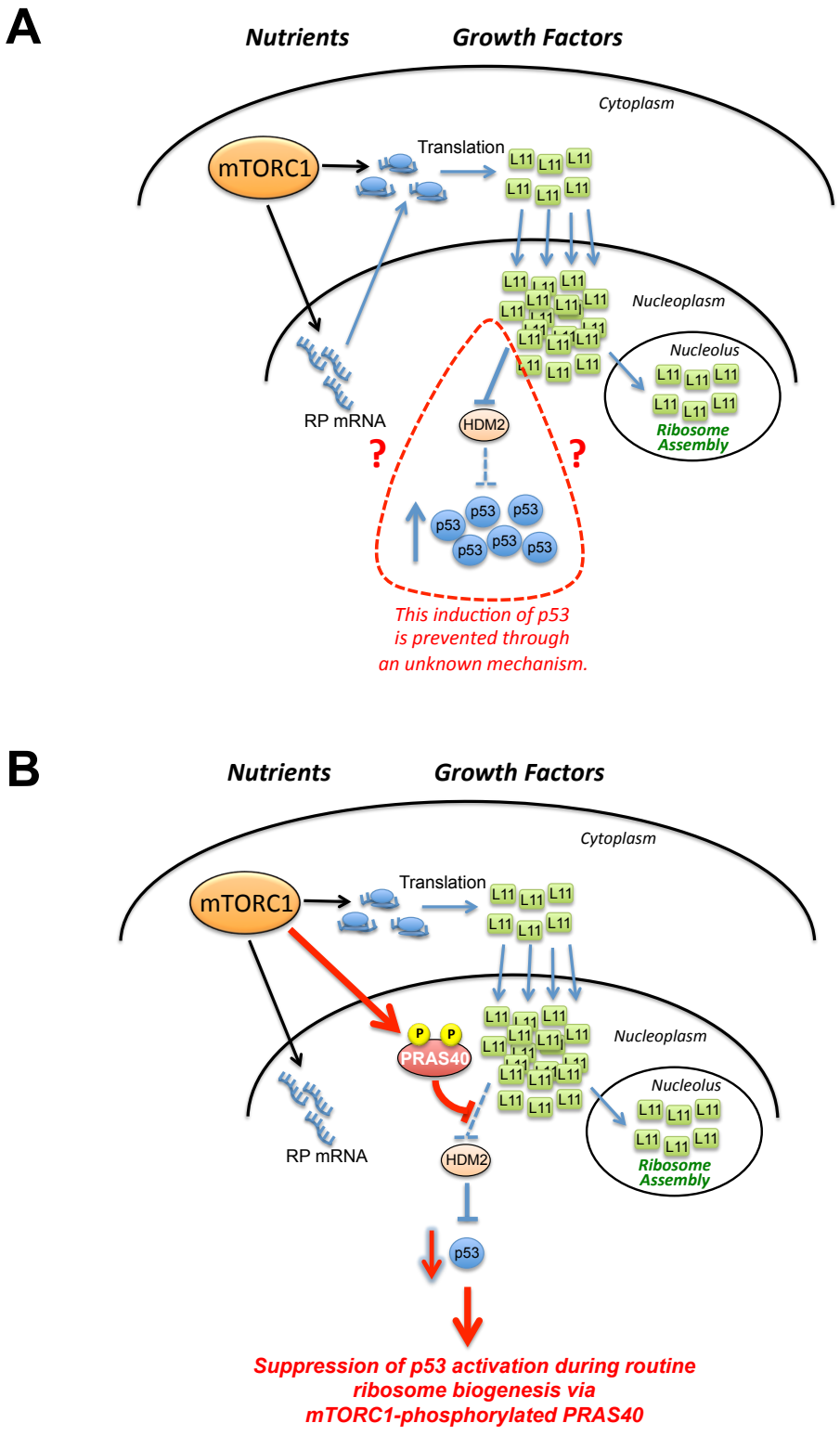
A
Nutrients
Growth Factors
Cytoplasm
mTORC1
Translation
L11
Nucleoplasm
Nucleolus
Ribosome Assembly
RP mRNA
HDM2
?
?
p53
This induction of p53 is prevented through an unknown mechanism.
B
Nutrients
Growth Factors
Cytoplasm
mTORC1
Translation
P
PRAS40
Nucleoplasm
Nucleolus
Ribosome Assembly
RP mRNA
HDM2
p53
Suppression of p53 activation during routine ribosome biogenesis via mTORC1-phosphorylated PRAS40

5.2 A potential molecular mechanism for the observed pro-tumorigenic function of PRAS40

These findings also suggest a mechanism by which aberrant PRAS40 upregulation may support tumorigenesis. Nearly all previous studies of PRAS40's function in cell-based and animal disease models have demonstrated a pro-survival function for PRAS40. It has been shown that PRAS40 is upregulated in Ewing Sarcoma cells (104), and total and phospho-T246 PRAS40 levels are positively correlated with disease progression in melanoma (103). Importantly, PRAS40 KD not only attenuates the pro-proliferative effect of EWS protein disruption in Ewing Sarcoma cells (104), but it also reduces tumorigenesis and increases chemosensitivity in melanoma cells (144). These findings suggest that PRAS40 can play a critical role in tumor formation and progression; however, it is unlikely that PRAS40's known ability to inhibit mTORC1 can fully account for these effects. These findings suggest an mTORC1-independent PRAS40 function for at least two reasons - 1) Although there are some exceptions, inhibition of mTORC1 through other means, such as the use of potent and specific small molecule inhibitors, i.e. the rapalogues, tends to have a cytostatic, *i.e.* not a pro-proliferative, effect on tumor cells (74; 145-148). However, it should be kept in mind that mTORC1 inhibition is also known to induce autophagy, which can play a pro-survival role in cancer cells under certain conditions (41). 2) PRAS40 is thought to bind and inhibit mTORC1 only when in a non-phosphorylated state (52-56). In the Ewing Sarcoma and melanoma cells studied previously, and in many cancer cells in general, the PI3K-Akt pathway is hyperactivated, resulting in hyper-phosphorylation of PRAS40 (103; 104; 149-152). This presumably leads to the dissociation of PRAS40 from

mTORC1, rendering PRAS40 incapable of inhibiting or affecting mTORC1 in any way. Therefore, it seems plausible that phosphorylated, mTORC1-dissociated PRAS40 may serve its own mTORC1-independent pro-survival function. Indeed, others have reported that radiation-induced phosphorylation of PRAS40 promotes formation of a trimeric PRAS40-14-3-3-FOXO3A complex, resulting in cytoplasmic sequestration of FOXO3A and radio-insensitivity in lung cancer cells (122; 123). While this may be one important pro-survival mechanism of PRAS40, it appears to be a specific response to radiation exposure and is dependent upon genetic background. Therefore, it is possible that PRAS40 achieves its pro-tumorigenic function through multiple mechanisms. Here I show that mTORC1- and Akt-mediated phosphorylation of PRAS40 at residues S221 and T246, respectively, promotes formation of a nuclear-specific high molecular weight complex containing PRAS40 and RPL11 that is distinct from mTORC1. This complex appears to suppress activation of the nucleolar stress-triggered RPL11-HDM2-p53 pathway, as PRAS40 KD enhances p53 protein stability and transcriptional activity in an RPL11-dependent manner. As described above, these molecular events may function as a safeguard against inappropriate p53 activation during ribosome biogenesis in healthy cells; however, aberrant PRAS40 upregulation in cancer cells may allow this process to be exploited (**Figure 4-21B**).

Oncogene-induced p53 activation is a major tumor suppressive mechanism in cells (153-155). Recently it has been shown that the RPL11-HDM2-p53 pathway plays a critical role in this process *in vivo* in a genetic mouse model of tumorigenesis. Specifically, Macias *et al.* (2010) show that Eμ-myc-induced p53 stabilization is attenuated and, subsequently, lymphomagenesis is significantly accelerated in mice

expressing an Mdm2 mutant incapable of binding RPL11 but retaining E3 ubiquitin ligase activity towards p53 (90). Importantly, they also show that $p19^{ARF}$ is not required for the p53 response to ribosomal perturbation, and that the RPL11-HDM2 and $p19^{ARF}$-HDM2 pathways function in parallel to mediate oncogene-induced p53 activation. Because my results imply that PRAS40 is a negative regulator of the RPL11-HDM2-p53 pathway, it is plausible that upregulation of PRAS40 may be one mechanism by which cancer cells overcome the tumor suppressive effects of oncogene-induced p53 activation. Importantly, I also show that PRAS40 KD leads to increased levels of p53-dependent premature cellular senescence in cancer cells. It has been shown previously that expression of oncogenes such as RAS, B-RAF, and E2F3 can trigger p53-mediated senescence (153-155). In melanoma for example, progression from benign, oncogene-harboring nevi (or moles) to a malignant phenotype is a multi-step process that depends on the ability of cells to overcome oncogene-induced senescence (156-158). It was recently found that activation of the PI3K-Akt pathway via PTEN deletion or Akt3 upregulation is sufficient to reverse oncogenic $B\text{-}RAF^{V600E}$-induced senescence and cause progression to malignant melanoma (159). However, the exact mechanism by which PI3K-Akt achieves this in not fully understood. Here I show that Akt-mediated phosphorylation of PRAS40 promotes formation of a nuclear-specific PRAS40- and RPL11-containing complex, leading to suppression of the RPL11-HDM2-p53 pathway. As such, it will be interesting to determine whether PRAS40 is a mediator of the PI3K-Akt pathway responsible for overcoming oncogene-induced senescence in melanoma. Indeed, it has already been demonstrated that PRAS40 KD significantly decreases tumorigenicity of melanoma cells in a xenograft mouse model and attenuates the

proliferation of Ewing Sarcoma cells (103; 104). Considering the reported upregulation of PRAS40 in both melanoma and Ewing sarcoma cell lines, it will be interesting to test whether PRAS40 upregulation is a general mechanism used by tumors to overcome oncogene-induced p53 activation.

Interestingly, a number of reports show that activation of both p53 and mTOR is required for induction of cellular senescence (160; 161). Considering this, it is not altogether surprising to observe increased levels of premature cellular senescence in PRAS40-depleted cells, as PRAS40 KD has the effect of activating both p53 and mTOR. Thus, it seems that PRAS40 is well-suited to behave as a regulator of cellular senescence. It will be interesting to monitor PRAS40 levels in proliferating versus naturally-senescent cells to determine if senescence may be physiologically regulated by PRAS40 abundance (**Figure 4-21B**).

5.3 An Alternative Interpretation

While the interpretation that PRAS40 serves as an mTORC1- and Akt-controlled regulator of the RPL11-HDM2-p53 pathway is attractive, an alternative explanation cannot be ruled out. It is also possible that mTORC1- and Akt-phosphorylated nuclear PRAS40 plays an RPL11-dependent role in the execution of ribosome biogenesis. As such, depletion of PRAS40 may in fact be a cause of ribosome biogenesis disruption, and hence trigger activation of the nucleolar stress response pathway. Like its alternative described above, this interpretation also suggests a potential explanation for PRAS40's apparent pro-tumorigenic effects. In this scenario, PRAS40 may serve as a limiting factor for ribosome biogenesis and its upregulation in cancer may support the increased

biosynthetic capacity required of rapidly growing and proliferating cancer cells. Because the association of PRAS40 and RPL11 is regulated by the kinase activities of Akt and mTORC1, this interpretation could suggest a novel mechanism linking Akt and mTORC1 to the control of ribosome biogenesis. Further biochemical characterization of the nuclear PRAS40- and RPL11-containing complex, as well as rigorous assessment of ribosome assembly dynamics may help to distinguish between these two alternative interpretations.

5.4 Therapeutic Implications and Summary

In summary, while PRAS40 was previously thought to function primarily as a binding partner and inhibitor of mTORC1 (**Figure 4-21A**), the findings described herein identify PRAS40 as a novel effector of Akt and mTORC1 that negatively regulates the RPL11-HDM2-p53 nucleolar stress response pathway (either directly or via participation in ribosome biogenesis) to control the induction of cellular senescence (**Figure 4-21B**). These findings suggest a mechanism for suppression of the RPL11-HDM2-p53 pathway during ribosome biogenesis in healthy cells (**Figure 5-1**), and provide a potential explanation for the pro-tumorigenic effects of PRAS40 (**Figures 4-21B**). Importantly, because it requires the kinase activities of both mTORC1 and Akt, the PRAS40- and RPL11-containing complex may form with greater frequency in cancer cells harboring hyperactive mTORC1 and Akt pathways compared to healthy cells. As such, the PRAS40- and RPL11-containing nuclear complex may represent a novel, potentially cancer-specific target for the discovery of p53-restorative anti-cancer therapeutics to treat tumors harboring wild-type p53.

References

1. Datta SR, Brunet A, Greenberg ME. 1999. Cellular survival: a play in three Akts. *Genes & development* 13:2905-27
2. Manning BD, Cantley LC. 2007. AKT/PKB signaling: navigating downstream. *Cell* 129:1261-74
3. Vivanco I, Sawyers CL. 2002. The phosphatidylinositol 3-Kinase AKT pathway in human cancer. *Nature reviews. Cancer* 2:489-501
4. Bellacosa A, Kumar CC, Di Cristofano A, Testa JR. 2005. Activation of AKT kinases in cancer: implications for therapeutic targeting. *Advances in cancer research* 94:29-86
5. Datta SR, Dudek H, Tao X, Masters S, Fu H, et al. 1997. Akt phosphorylation of BAD couples survival signals to the cell-intrinsic death machinery. *Cell* 91:231-41
6. del Peso L, Gonzalez-Garcia M, Page C, Herrera R, Nunez G. 1997. Interleukin-3-induced phosphorylation of BAD through the protein kinase Akt. *Science* 278:687-9
7. Yang E, Zha J, Jockel J, Boise LH, Thompson CB, Korsmeyer SJ. 1995. Bad, a heterodimeric partner for Bcl-XL and Bcl-2, displaces Bax and promotes cell death. *Cell* 80:285-91
8. Gross A, McDonnell JM, Korsmeyer SJ. 1999. BCL-2 family members and the mitochondria in apoptosis. *Genes & development* 13:1899-911
9. Zha J, Harada H, Yang E, Jockel J, Korsmeyer SJ. 1996. Serine phosphorylation of death agonist BAD in response to survival factor results in binding to 14-3-3 not BCL-X(L). *Cell* 87:619-28

10. Datta SR, Katsov A, Hu L, Petros A, Fesik SW, et al. 2000. 14-3-3 proteins and survival kinases cooperate to inactivate BAD by BH3 domain phosphorylation. *Molecular cell* 6:41-51

11. Cardone MH, Roy N, Stennicke HR, Salvesen GS, Franke TF, et al. 1998. Regulation of cell death protease caspase-9 by phosphorylation. *Science* 282:1318-21

12. Brunet A, Bonni A, Zigmond MJ, Lin MZ, Juo P, et al. 1999. Akt promotes cell survival by phosphorylating and inhibiting a Forkhead transcription factor. *Cell* 96:857-68

13. Biggs WH, 3rd, Meisenhelder J, Hunter T, Cavenee WK, Arden KC. 1999. Protein kinase B/Akt-mediated phosphorylation promotes nuclear exclusion of the winged helix transcription factor FKHR1. *Proceedings of the National Academy of Sciences of the United States of America* 96:7421-6

14. Mayo LD, Donner DB. 2001. A phosphatidylinositol 3-kinase/Akt pathway promotes translocation of Mdm2 from the cytoplasm to the nucleus. *Proceedings of the National Academy of Sciences of the United States of America* 98:11598-603

15. Zhou BP, Liao Y, Xia W, Zou Y, Spohn B, Hung MC. 2001. HER-2/neu induces p53 ubiquitination via Akt-mediated MDM2 phosphorylation. *Nature cell biology* 3:973-82

16. Kim AH, Khursigara G, Sun X, Franke TF, Chao MV. 2001. Akt phosphorylates and negatively regulates apoptosis signal-regulating kinase 1. *Molecular and cellular biology* 21:893-901

17. Ozes ON, Mayo LD, Gustin JA, Pfeffer SR, Pfeffer LM, Donner DB. 1999. NF-kappaB activation by tumour necrosis factor requires the Akt serine-threonine kinase. *Nature* 401:82-5

18. Liang J, Zubovitz J, Petrocelli T, Kotchetkov R, Connor MK, et al. 2002. PKB/Akt phosphorylates p27, impairs nuclear import of p27 and opposes p27-mediated G1 arrest. *Nature medicine* 8:1153-60

19. Shin I, Yakes FM, Rojo F, Shin NY, Bakin AV, et al. 2002. PKB/Akt mediates cell-cycle progression by phosphorylation of p27(Kip1) at threonine 157 and modulation of its cellular localization. *Nature medicine* 8:1145-52

20. Viglietto G, Motti ML, Bruni P, Melillo RM, D'Alessio A, et al. 2002. Cytoplasmic relocalization and inhibition of the cyclin-dependent kinase inhibitor p27(Kip1) by PKB/Akt-mediated phosphorylation in breast cancer. *Nature medicine* 8:1136-44

21. Sekimoto T, Fukumoto M, Yoneda Y. 2004. 14-3-3 suppresses the nuclear localization of threonine 157-phosphorylated p27(Kip1). *The EMBO journal* 23:1934-42

22. Zhou BP, Liao Y, Xia W, Spohn B, Lee MH, Hung MC. 2001. Cytoplasmic localization of p21Cip1/WAF1 by Akt-induced phosphorylation in HER-2/neu-overexpressing cells. *Nature cell biology* 3:245-52

23. King FW, Skeen J, Hay N, Shtivelman E. 2004. Inhibition of Chk1 by activated PKB/Akt. *Cell Cycle* 3:634-7

24. Puc J, Keniry M, Li HS, Pandita TK, Choudhury AD, et al. 2005. Lack of PTEN sequesters CHK1 and initiates genetic instability. *Cancer cell* 7:193-204

25. Puc J, Parsons R. 2005. PTEN loss inhibits CHK1 to cause double stranded-DNA breaks in cells. *Cell Cycle* 4:927-9

26. Jones PF, Jakubowicz T, Pitossi FJ, Maurer F, Hemmings BA. 1991. Molecular cloning and identification of a serine/threonine protein kinase of the second-messenger subfamily. *Proceedings of the National Academy of Sciences of the United States of America* 88:4171-5

27. Bellacosa A, Testa JR, Staal SP, Tsichlis PN. 1991. A retroviral oncogene, akt, encoding a serine-threonine kinase containing an SH2-like region. *Science* 254:274-7

28. Staal SP. 1987. Molecular cloning of the akt oncogene and its human homologues AKT1 and AKT2: amplification of AKT1 in a primary human gastric adenocarcinoma. *Proceedings of the National Academy of Sciences of the United States of America* 84:5034-7

29. Al-Saad S, Donnem T, Al-Shibli K, Persson M, Bremnes RM, Busund LT. 2009. Diverse prognostic roles of Akt isoforms, PTEN and PI3K in tumor epithelial cells and stromal compartment in non-small cell lung cancer. *Anticancer research* 29:4175-83

30. Gallay N, Dos Santos C, Cuzin L, Bousquet M, Simmonet Gouy V, et al. 2009. The level of AKT phosphorylation on threonine 308 but not on serine 473 is associated with high-risk cytogenetics and predicts poor overall survival in acute myeloid leukaemia. *Leukemia* 23:1029-38

31. Stambolic V, Suzuki A, de la Pompa JL, Brothers GM, Mirtsos C, et al. 1998. Negative regulation of PKB/Akt-dependent cell survival by the tumor suppressor PTEN. *Cell* 95:29-39

32. Suzuki A, de la Pompa JL, Stambolic V, Elia AJ, Sasaki T, et al. 1998. High cancer susceptibility and embryonic lethality associated with mutation of the PTEN tumor suppressor gene in mice. *Current biology : CB* 8:1169-78

33. Podsypanina K, Ellenson LH, Nemes A, Gu J, Tamura M, et al. 1999. Mutation of Pten/Mmac1 in mice causes neoplasia in multiple organ systems. *Proceedings of the National Academy of Sciences of the United States of America* 96:1563-8

34. Di Cristofano A, Pesce B, Cordon-Cardo C, Pandolfi PP. 1998. Pten is essential for embryonic development and tumour suppression. *Nature genetics* 19:348-55

35. Pal SK, Reckamp K, Yu H, Figlin RA. 2010. Akt inhibitors in clinical development for the treatment of cancer. *Expert opinion on investigational drugs* 19:1355-66

36. Liu P, Cheng H, Roberts TM, Zhao JJ. 2009. Targeting the phosphoinositide 3-kinase pathway in cancer. *Nature reviews. Drug discovery* 8:627-44

37. LoPiccolo J, Blumenthal GM, Bernstein WB, Dennis PA. 2008. Targeting the PI3K/Akt/mTOR pathway: effective combinations and clinical considerations. *Drug resistance updates : reviews and commentaries in antimicrobial and anticancer chemotherapy* 11:32-50

38. Hong DS, Bowles DW, Falchook GS, Messersmith WA, George GC, et al. 2012. A multicenter phase I trial of PX-866, an oral irreversible phosphatidylinositol 3-

kinase inhibitor, in patients with advanced solid tumors. *Clinical cancer research : an official journal of the American Association for Cancer Research* 18:4173-82

39. Guertin DA, Sabatini DM. 2007. Defining the role of mTOR in cancer. *Cancer cell* 12:9-22

40. Sengupta S, Peterson TR, Sabatini DM. 2010. Regulation of the mTOR complex 1 pathway by nutrients, growth factors, and stress. *Molecular cell* 40:310-22

41. Laplante M, Sabatini DM. 2012. mTOR signaling in growth control and disease. *Cell* 149:274-93

42. Zoncu R, Bar-Peled L, Efeyan A, Wang S, Sancak Y, Sabatini DM. 2011. mTORC1 senses lysosomal amino acids through an inside-out mechanism that requires the vacuolar H(+)-ATPase. *Science* 334:678-83

43. Sancak Y, Bar-Peled L, Zoncu R, Markhard AL, Nada S, Sabatini DM. 2010. Ragulator-Rag complex targets mTORC1 to the lysosomal surface and is necessary for its activation by amino acids. *Cell* 141:290-303

44. Bar-Peled L, Schweitzer LD, Zoncu R, Sabatini DM. 2012. Ragulator is a GEF for the rag GTPases that signal amino acid levels to mTORC1. *Cell* 150:1196-208

45. Inoki K, Zhu T, Guan KL. 2003. TSC2 mediates cellular energy response to control cell growth and survival. *Cell* 115:577-90

46. Gwinn DM, Shackelford DB, Egan DF, Mihaylova MM, Mery A, et al. 2008. AMPK phosphorylation of raptor mediates a metabolic checkpoint. *Molecular cell* 30:214-26

47. Woods A, Johnstone SR, Dickerson K, Leiper FC, Fryer LG, et al. 2003. LKB1 is the upstream kinase in the AMP-activated protein kinase cascade. *Current biology : CB* 13:2004-8

48. Kahn BB, Alquier T, Carling D, Hardie DG. 2005. AMP-activated protein kinase: ancient energy gauge provides clues to modern understanding of metabolism. *Cell metabolism* 1:15-25

49. Inoki K, Li Y, Xu T, Guan KL. 2003. Rheb GTPase is a direct target of TSC2 GAP activity and regulates mTOR signaling. *Genes & development* 17:1829-34

50. Potter CJ, Pedraza LG, Xu T. 2002. Akt regulates growth by directly phosphorylating Tsc2. *Nature cell biology* 4:658-65

51. Thedieck K, Polak P, Kim ML, Molle KD, Cohen A, et al. 2007. PRAS40 and PRR5-like protein are new mTOR interactors that regulate apoptosis. *PloS one* 2:e1217

52. Wang L, Harris TE, Roth RA, Lawrence JC, Jr. 2007. PRAS40 regulates mTORC1 kinase activity by functioning as a direct inhibitor of substrate binding. *The Journal of biological chemistry* 282:20036-44

53. Sancak Y, Thoreen CC, Peterson TR, Lindquist RA, Kang SA, et al. 2007. PRAS40 is an insulin-regulated inhibitor of the mTORC1 protein kinase. *Molecular cell* 25:903-15

54. Vander Haar E, Lee SI, Bandhakavi S, Griffin TJ, Kim DH. 2007. Insulin signalling to mTOR mediated by the Akt/PKB substrate PRAS40. *Nature cell biology* 9:316-23

55. Fonseca BD, Smith EM, Lee VH, MacKintosh C, Proud CG. 2007. PRAS40 is a target for mammalian target of rapamycin complex 1 and is required for signaling downstream of this complex. *The Journal of biological chemistry* 282:24514-24

56. Oshiro N, Takahashi R, Yoshino K, Tanimura K, Nakashima A, et al. 2007. The proline-rich Akt substrate of 40 kDa (PRAS40) is a physiological substrate of mammalian target of rapamycin complex 1. *The Journal of biological chemistry* 282:20329-39

57. Wang L, Harris TE, Lawrence JC, Jr. 2008. Regulation of proline-rich Akt substrate of 40 kDa (PRAS40) function by mammalian target of rapamycin complex 1 (mTORC1)-mediated phosphorylation. *The Journal of biological chemistry* 283:15619-27

58. Kovacina KS, Park GY, Bae SS, Guzzetta AW, Schaefer E, et al. 2003. Identification of a proline-rich Akt substrate as a 14-3-3 binding partner. *The Journal of biological chemistry* 278:10189-94

59. Harthill JE, Pozuelo Rubio M, Milne FC, MacKintosh C. 2002. Regulation of the 14-3-3-binding protein p39 by growth factors and nutrients in rat PC12 pheochromocytoma cells. *The Biochemical journal* 368:565-72

60. Hsu PP, Kang SA, Rameseder J, Zhang Y, Ottina KA, et al. 2011. The mTOR-regulated phosphoproteome reveals a mechanism of mTORC1-mediated inhibition of growth factor signaling. *Science* 332:1317-22

61. Yu Y, Yoon SO, Poulogiannis G, Yang Q, Ma XM, et al. 2011. Phosphoproteomic analysis identifies Grb10 as an mTORC1 substrate that negatively regulates insulin signaling. *Science* 332:1322-6

62. Blake JF, Kallan NC, Xiao D, Xu R, Bencsik JR, et al. 2010. Discovery of pyrrolopyrimidine inhibitors of Akt. *Bioorganic & medicinal chemistry letters* 20:5607-12

63. Andersen JN, Sathyanarayanan S, Di Bacco A, Chi A, Zhang T, et al. 2010. Pathway-based identification of biomarkers for targeted therapeutics: personalized oncology with PI3K pathway inhibitors. *Science translational medicine* 2:43ra55

64. Yuan J, Mehta PP, Yin MJ, Sun S, Zou A, et al. 2011. PF-04691502, a potent and selective oral inhibitor of PI3K and mTOR kinases with antitumor activity. *Molecular cancer therapeutics* 10:2189-99

65. Yap TA, Walton MI, Hunter LJ, Valenti M, de Haven Brandon A, et al. 2011. Preclinical pharmacology, antitumor activity, and development of pharmacodynamic markers for the novel, potent AKT inhibitor CCT128930. *Molecular cancer therapeutics* 10:360-71

66. Cassell A, Freilino ML, Lee J, Barr S, Wang L, et al. 2012. Targeting TORC1/2 enhances sensitivity to EGFR inhibitors in head and neck cancer preclinical models. *Neoplasia* 14:1005-14

67. Gokmen-Polar Y, Liu Y, Toroni RA, Sanders KL, Mehta R, et al. 2012. Investigational drug MLN0128, a novel TORC1/2 inhibitor, demonstrates potent oral antitumor activity in human breast cancer xenograft models. *Breast cancer research and treatment* 136:673-82

68. Davies BR, Greenwood H, Dudley P, Crafter C, Yu DH, et al. 2012. Preclinical pharmacology of AZD5363, an inhibitor of AKT: pharmacodynamics, antitumor

activity, and correlation of monotherapy activity with genetic background. *Molecular cancer therapeutics* 11:873-87

69. Kim J, Kundu M, Viollet B, Guan KL. 2011. AMPK and mTOR regulate autophagy through direct phosphorylation of Ulk1. *Nature cell biology* 13:132-41

70. Egan D, Kim J, Shaw RJ, Guan KL. 2011. The autophagy initiating kinase ULK1 is regulated via opposing phosphorylation by AMPK and mTOR. *Autophagy* 7:643-4

71. Yecies JL, Manning BD. 2011. Transcriptional control of cellular metabolism by mTOR signaling. *Cancer research* 71:2815-20

72. Guertin DA, Sabatini DM. 2009. The pharmacology of mTOR inhibition. *Science signaling* 2:pe24

73. Krymskaya VP, Goncharova EA. 2009. PI3K/mTORC1 activation in hamartoma syndromes: therapeutic prospects. *Cell Cycle* 8:403-13

74. Bissler JJ, McCormack FX, Young LR, Elwing JM, Chuck G, et al. 2008. Sirolimus for angiomyolipoma in tuberous sclerosis complex or lymphangioleiomyomatosis. *The New England journal of medicine* 358:140-51

75. Sabatini DM. 2006. mTOR and cancer: insights into a complex relationship. *Nature reviews. Cancer* 6:729-34

76. Campistol JM, Gutierrez-Dalmau A, Torregrosa JV. 2004. Conversion to sirolimus: a successful treatment for posttransplantation Kaposi's sarcoma. *Transplantation* 77:760-2

77. Stallone G, Schena A, Infante B, Di Paolo S, Loverre A, et al. 2005. Sirolimus for Kaposi's sarcoma in renal-transplant recipients. *The New England journal of medicine* 352:1317-23

78. Sun SY, Rosenberg LM, Wang X, Zhou Z, Yue P, et al. 2005. Activation of Akt and eIF4E survival pathways by rapamycin-mediated mammalian target of rapamycin inhibition. *Cancer research* 65:7052-8

79. Wan X, Harkavy B, Shen N, Grohar P, Helman LJ. 2007. Rapamycin induces feedback activation of Akt signaling through an IGF-1R-dependent mechanism. *Oncogene* 26:1932-40

80. Carracedo A, Ma L, Teruya-Feldstein J, Rojo F, Salmena L, et al. 2008. Inhibition of mTORC1 leads to MAPK pathway activation through a PI3K-dependent feedback loop in human cancer. *The Journal of clinical investigation* 118:3065-74

81. Benjamin D, Colombi M, Moroni C, Hall MN. 2011. Rapamycin passes the torch: a new generation of mTOR inhibitors. *Nature reviews. Drug discovery* 10:868-80

82. Levine AJ. 1997. p53, the cellular gatekeeper for growth and division. *Cell* 88:323-31

83. Vousden KH, Lane DP. 2007. p53 in health and disease. *Nature reviews. Molecular cell biology* 8:275-83

84. Oren M. 2003. Decision making by p53: life, death and cancer. *Cell death and differentiation* 10:431-42

85. Kruse JP, Gu W. 2009. Modes of p53 regulation. *Cell* 137:609-22

86. Pestov DG, Strezoska Z, Lau LF. 2001. Evidence of p53-dependent cross-talk between ribosome biogenesis and the cell cycle: effects of nucleolar protein Bop1 on G(1)/S transition. *Molecular and cellular biology* 21:4246-55

87. Lohrum MA, Ludwig RL, Kubbutat MH, Hanlon M, Vousden KH. 2003. Regulation of HDM2 activity by the ribosomal protein L11. *Cancer cell* 3:577-87

88. Zhang Y, Wolf GW, Bhat K, Jin A, Allio T, et al. 2003. Ribosomal protein L11 negatively regulates oncoprotein MDM2 and mediates a p53-dependent ribosomal-stress checkpoint pathway. *Molecular and cellular biology* 23:8902-12

89. Bhat KP, Itahana K, Jin A, Zhang Y. 2004. Essential role of ribosomal protein L11 in mediating growth inhibition-induced p53 activation. *The EMBO journal* 23:2402-12

90. Macias E, Jin A, Deisenroth C, Bhat K, Mao H, et al. 2010. An ARF-independent c-MYC-activated tumor suppression pathway mediated by ribosomal protein-Mdm2 Interaction. *Cancer cell* 18:231-43

91. Dai MS, Zeng SX, Jin Y, Sun XX, David L, Lu H. 2004. Ribosomal protein L23 activates p53 by inhibiting MDM2 function in response to ribosomal perturbation but not to translation inhibition. *Molecular and cellular biology* 24:7654-68

92. Dai MS, Lu H. 2004. Inhibition of MDM2-mediated p53 ubiquitination and degradation by ribosomal protein L5. *The Journal of biological chemistry* 279:44475-82

93. Jin A, Itahana K, O'Keefe K, Zhang Y. 2004. Inhibition of HDM2 and activation of p53 by ribosomal protein L23. *Molecular and cellular biology* 24:7669-80

94. Zhang Y, Lu H. 2009. Signaling to p53: ribosomal proteins find their way. *Cancer cell* 16:369-77

95. Rondinelli RH, Tricoli JV. 1999. CLAR1, a novel gene that exhibits enhanced expression in advanced human prostate cancer. *Clinical cancer research : an official journal of the American Association for Cancer Research* 5:1595-602

96. van Slegtenhorst M, de Hoogt R, Hermans C, Nellist M, Janssen B, et al. 1997. Identification of the tuberous sclerosis gene TSC1 on chromosome 9q34. *Science* 277:805-8

97. Hemminki A, Markie D, Tomlinson I, Avizienyte E, Roth S, et al. 1998. A serine/threonine kinase gene defective in Peutz-Jeghers syndrome. *Nature* 391:184-7

98. Jenne DE, Reimann H, Nezu J, Friedel W, Loff S, et al. 1998. Peutz-Jeghers syndrome is caused by mutations in a novel serine threonine kinase. *Nature genetics* 18:38-43

99. Makowski L, Hayes DN. 2008. Role of LKB1 in lung cancer development. *British journal of cancer* 99:683-8

100. Saito A, Narasimhan P, Hayashi T, Okuno S, Ferrand-Drake M, Chan PH. 2004. Neuroprotective role of a proline-rich Akt substrate in apoptotic neuronal cell death after stroke: relationships with nerve growth factor. *The Journal of neuroscience : the official journal of the Society for Neuroscience* 24:1584-93

101. Saito A, Hayashi T, Okuno S, Nishi T, Chan PH. 2006. Modulation of proline-rich akt substrate survival signaling pathways by oxidative stress in mouse brains

after transient focal cerebral ischemia. *Stroke; a journal of cerebral circulation* 37:513-7

102. Yu F, Narasimhan P, Saito A, Liu J, Chan PH. 2008. Increased expression of a proline-rich Akt substrate (PRAS40) in human copper/zinc-superoxide dismutase transgenic rats protects motor neurons from death after spinal cord injury. *Journal of cerebral blood flow and metabolism : official journal of the International Society of Cerebral Blood Flow and Metabolism* 28:44-52

103. Madhunapantula SV, Sharma A, Robertson GP. 2007. PRAS40 deregulates apoptosis in malignant melanoma. *Cancer research* 67:3626-36

104. Huang L, Nakai Y, Kuwahara I, Matsumoto K. 2012. PRAS40 is a functionally critical target for EWS repression in Ewing sarcoma. *Cancer research* 72:1260-9

105. Kerppola TK. 2008. Bimolecular fluorescence complementation (BiFC) analysis as a probe of protein interactions in living cells. *Annual review of biophysics* 37:465-87

106. Ciruela F. 2008. Fluorescence-based methods in the study of protein-protein interactions in living cells. *Current opinion in biotechnology* 19:338-43

107. Stefan E, Aquin S, Berger N, Landry CR, Nyfeler B, et al. 2007. Quantification of dynamic protein complexes using Renilla luciferase fragment complementation applied to protein kinase A activities in vivo. *Proceedings of the National Academy of Sciences of the United States of America* 104:16916-21

108. Centonze VE, Sun M, Masuda A, Gerritsen H, Herman B. 2003. Fluorescence resonance energy transfer imaging microscopy. *Methods in enzymology* 360:542-60

109. Gandia J, Galino J, Amaral OB, Soriano A, Lluis C, et al. 2008. Detection of higher-order G protein-coupled receptor oligomers by a combined BRET-BiFC technique. *FEBS letters* 582:2979-84

110. Rebois RV, Robitaille M, Petrin D, Zylbergold P, Trieu P, Hebert TE. 2008. Combining protein complementation assays with resonance energy transfer to detect multipartner protein complexes in living cells. *Methods* 45:214-8

111. Truong K, Ikura M. 2001. The use of FRET imaging microscopy to detect protein-protein interactions and protein conformational changes in vivo. *Curr Opin Struct Biol* 11:573-8

112. Wu P, Brand L. 1994. Resonance energy transfer: methods and applications. *Anal Biochem* 218:1-13

113. Bazin H, Preaudat M, Trinquet E, Mathis G. 2001. Homogeneous time resolved fluorescence resonance energy transfer using rare earth cryptates as a tool for probing molecular interactions in biology. *Spectrochim Acta A Mol Biomol Spectrosc* 57:2197-211

114. Hemmila I, Laitala V. 2005. Progress in lanthanides as luminescent probes. *J Fluoresc* 15:529-42

115. Morrison LE. 1988. Time-resolved detection of energy transfer: theory and application to immunoassays. *Anal Biochem* 174:101-20

116. Sarbassov DD, Sabatini DM. 2005. Redox regulation of the nutrient-sensitive raptor-mTOR pathway and complex. *The Journal of biological chemistry* 280:39505-9

117. Guertin DA, Stevens DM, Saitoh M, Kinkel S, Crosby K, et al. 2009. mTOR complex 2 is required for the development of prostate cancer induced by Pten loss in mice. *Cancer cell* 15:148-59

118. Ausubel FM. 1987. *Current protocols in molecular biology*. Brooklyn, N.Y.

Media, Pa.: Greene Pub. Associates ;

J. Wiley, order fulfillment

119. Xu P, Duong DM, Peng J. 2009. Systematical optimization of reverse-phase chromatography for shotgun proteomics. *Journal of proteome research* 8:3944-50

120. Beausoleil SA, Jedrychowski M, Schwartz D, Elias JE, Villen J, et al. 2004. Large-scale characterization of HeLa cell nuclear phosphoproteins. *Proceedings of the National Academy of Sciences of the United States of America* 101:12130-5

121. Nascimento EB, Fodor M, van der Zon GC, Jazet IM, Meinders AE, et al. 2006. Insulin-mediated phosphorylation of the proline-rich Akt substrate PRAS40 is impaired in insulin target tissues of high-fat diet-fed rats. *Diabetes* 55:3221-8

122. Kim W, Youn H, Seong KM, Yang HJ, Yun YJ, et al. 2011. PIM1-activated PRAS40 regulates radioresistance in non-small cell lung cancer cells through interplay with FOXO3a, 14-3-3 and protein phosphatases. *Radiation research* 176:539-52

123. Kim W, Youn H, Kwon T, Kang J, Kim E, et al. 2013. PIM1 kinase inhibitors induce radiosensitization in non-small cell lung cancer cells. *Pharmacological research : the official journal of the Italian Pharmacological Society* 70:90-101

124. Zhang X, Shu L, Hosoi H, Murti KG, Houghton PJ. 2002. Predominant nuclear localization of mammalian target of rapamycin in normal and malignant cells in culture. *The Journal of biological chemistry* 277:28127-34

125. Rosner M, Hengstschlager M. 2008. Cytoplasmic and nuclear distribution of the protein complexes mTORC1 and mTORC2: rapamycin triggers dephosphorylation and delocalization of the mTORC2 components rictor and sin1. *Human molecular genetics* 17:2934-48

126. Li H, Tsang CK, Watkins M, Bertram PG, Zheng XF. 2006. Nutrient regulates Tor1 nuclear localization and association with rDNA promoter. *Nature* 442:1058-61

127. Wei Y, Tsang CK, Zheng XF. 2009. Mechanisms of regulation of RNA polymerase III-dependent transcription by TORC1. *The EMBO journal* 28:2220-30

128. Chahine MN, Pierce GN. 2009. Therapeutic targeting of nuclear protein import in pathological cell conditions. *Pharmacological reviews* 61:358-72

129. Nascimento EB, Ouwens DM. 2009. PRAS40: target or modulator of mTORC1 signalling and insulin action? *Archives of physiology and biochemistry* 115:163-75

130. Wiza C, Nascimento EB, Ouwens DM. 2012. Role of PRAS40 in Akt and mTOR signaling in health and disease. *American journal of physiology. Endocrinology and metabolism* 302:E1453-60

131. Deisenroth C, Zhang Y. 2010. Ribosome biogenesis surveillance: probing the ribosomal protein-Mdm2-p53 pathway. *Oncogene* 29:4253-60

132. Miliani de Marval PL, Zhang Y. 2011. The RP-Mdm2-p53 pathway and tumorigenesis. *Oncotarget* 2:234-8

133. Sun XX, Dai MS, Lu H. 2008. Mycophenolic acid activation of p53 requires ribosomal proteins L5 and L11. *The Journal of biological chemistry* 283:12387-92

134. Gilkes DM, Chen L, Chen J. 2006. MDMX regulation of p53 response to ribosomal stress. *The EMBO journal* 25:5614-25

135. Sun XX, Dai MS, Lu H. 2007. 5-fluorouracil activation of p53 involves an MDM2-ribosomal protein interaction. *The Journal of biological chemistry* 282:8052-9

136. Perry RP, Kelley DE. 1970. Inhibition of RNA synthesis by actinomycin D: characteristic dose-response of different RNA species. *Journal of cellular physiology* 76:127-39

137. Iapalucci-Espinoza S, Franze-Fernandez MT. 1979. Effect of protein synthesis inhibitors and low concentrations of actinomycin D on ribosomal RNA synthesis. *FEBS letters* 107:281-4

138. Perlaky L, Valdez BC, Busch H. 1997. Effects of cytotoxic drugs on translocation of nucleolar RNA helicase RH-II/Gu. *Experimental cell research* 235:413-20

139. Warner JR. 1999. The economics of ribosome biosynthesis in yeast. *Trends in biochemical sciences* 24:437-40

140. Mayer C, Grummt I. 2006. Ribosome biogenesis and cell growth: mTOR coordinates transcription by all three classes of nuclear RNA polymerases. *Oncogene* 25:6384-91

141. Iadevaia V, Huo Y, Zhang Z, Foster LJ, Proud CG. 2012. Roles of the mammalian target of rapamycin, mTOR, in controlling ribosome biogenesis and protein synthesis. *Biochemical Society transactions* 40:168-72

142. Beck M, Schmidt A, Malmstroem J, Claassen M, Ori A, et al. 2011. The quantitative proteome of a human cell line. *Molecular systems biology* 7:549

143. Sasaki M, Kawahara K, Nishio M, Mimori K, Kogo R, et al. 2011. Regulation of the MDM2-P53 pathway and tumor growth by PICT1 via nucleolar RPL11. *Nature medicine* 17:944-51

144. Madhunapantula SV, Mosca PJ, Robertson GP. 2011. The Akt signaling pathway: an emerging therapeutic target in malignant melanoma. *Cancer biology & therapy* 12:1032-49

145. Faivre S, Kroemer G, Raymond E. 2006. Current development of mTOR inhibitors as anticancer agents. *Nature reviews. Drug discovery* 5:671-88

146. Meric-Bernstam F, Gonzalez-Angulo AM. 2009. Targeting the mTOR signaling network for cancer therapy. *Journal of clinical oncology : official journal of the American Society of Clinical Oncology* 27:2278-87

147. Wander SA, Hennessy BT, Slingerland JM. 2011. Next-generation mTOR inhibitors in clinical oncology: how pathway complexity informs therapeutic strategy. *The Journal of clinical investigation* 121:1231-41

148. Wahdan-Alaswad RS, Bane KL, Song K, Shola DT, Garcia JA, Danielpour D. 2012. Inhibition of mTORC1 kinase activates Smads 1 and 5 but not Smad8 in human prostate cancer cells, mediating cytostatic response to rapamycin. *Molecular cancer research : MCR* 10:821-33

149. Benini S, Manara MC, Cerisano V, Perdichizzi S, Strammiello R, et al. 2004. Contribution of MEK/MAPK and PI3-K signaling pathway to the malignant behavior of Ewing's sarcoma cells: therapeutic prospects. *International journal of cancer. Journal international du cancer* 108:358-66

150. Ordonez JL, Osuna D, Herrero D, de Alava E, Madoz-Gurpide J. 2009. Advances in Ewing's sarcoma research: where are we now and what lies ahead? *Cancer research* 69:7140-50

151. Hocker TL, Singh MK, Tsao H. 2008. Melanoma genetics and therapeutic approaches in the 21st century: moving from the benchside to the bedside. *The Journal of investigative dermatology* 128:2575-95

152. Davies MA, Stemke-Hale K, Lin E, Tellez C, Deng W, et al. 2009. Integrated Molecular and Clinical Analysis of AKT Activation in Metastatic Melanoma. *Clinical cancer research : an official journal of the American Association for Cancer Research* 15:7538-46

153. Mooi WJ, Peeper DS. 2006. Oncogene-induced cell senescence--halting on the road to cancer. *The New England journal of medicine* 355:1037-46

154. Schmitt CA. 2007. Cellular senescence and cancer treatment. *Biochimica et biophysica acta* 1775:5-20

155. Kuilman T, Michaloglou C, Mooi WJ, Peeper DS. 2010. The essence of senescence. *Genes & development* 24:2463-79

156. Michaloglou C, Vredeveld LC, Soengas MS, Denoyelle C, Kuilman T, et al. 2005. BRAFE600-associated senescence-like cell cycle arrest of human naevi. *Nature* 436:720-4

157. Patton EE, Widlund HR, Kutok JL, Kopani KR, Amatruda JF, et al. 2005. BRAF mutations are sufficient to promote nevi formation and cooperate with p53 in the genesis of melanoma. *Current biology : CB* 15:249-54

158. Dhomen N, Reis-Filho JS, da Rocha Dias S, Hayward R, Savage K, et al. 2009. Oncogenic Braf induces melanocyte senescence and melanoma in mice. *Cancer cell* 15:294-303

159. Vredeveld LC, Possik PA, Smit MA, Meissl K, Michaloglou C, et al. 2012. Abrogation of BRAFV600E-induced senescence by PI3K pathway activation contributes to melanomagenesis. *Genes & development* 26:1055-69

160. Zhang H, Cicchetti G, Onda H, Koon HB, Asrican K, et al. 2003. Loss of Tsc1/Tsc2 activates mTOR and disrupts PI3K-Akt signaling through downregulation of PDGFR. *The Journal of clinical investigation* 112:1223-33

161. Korotchkina LG, Leontieva OV, Bukreeva EI, Demidenko ZN, Gudkov AV, Blagosklonny MV. 2010. The choice between p53-induced senescence and quiescence is determined in part by the mTOR pathway. *Aging* 2:344-52